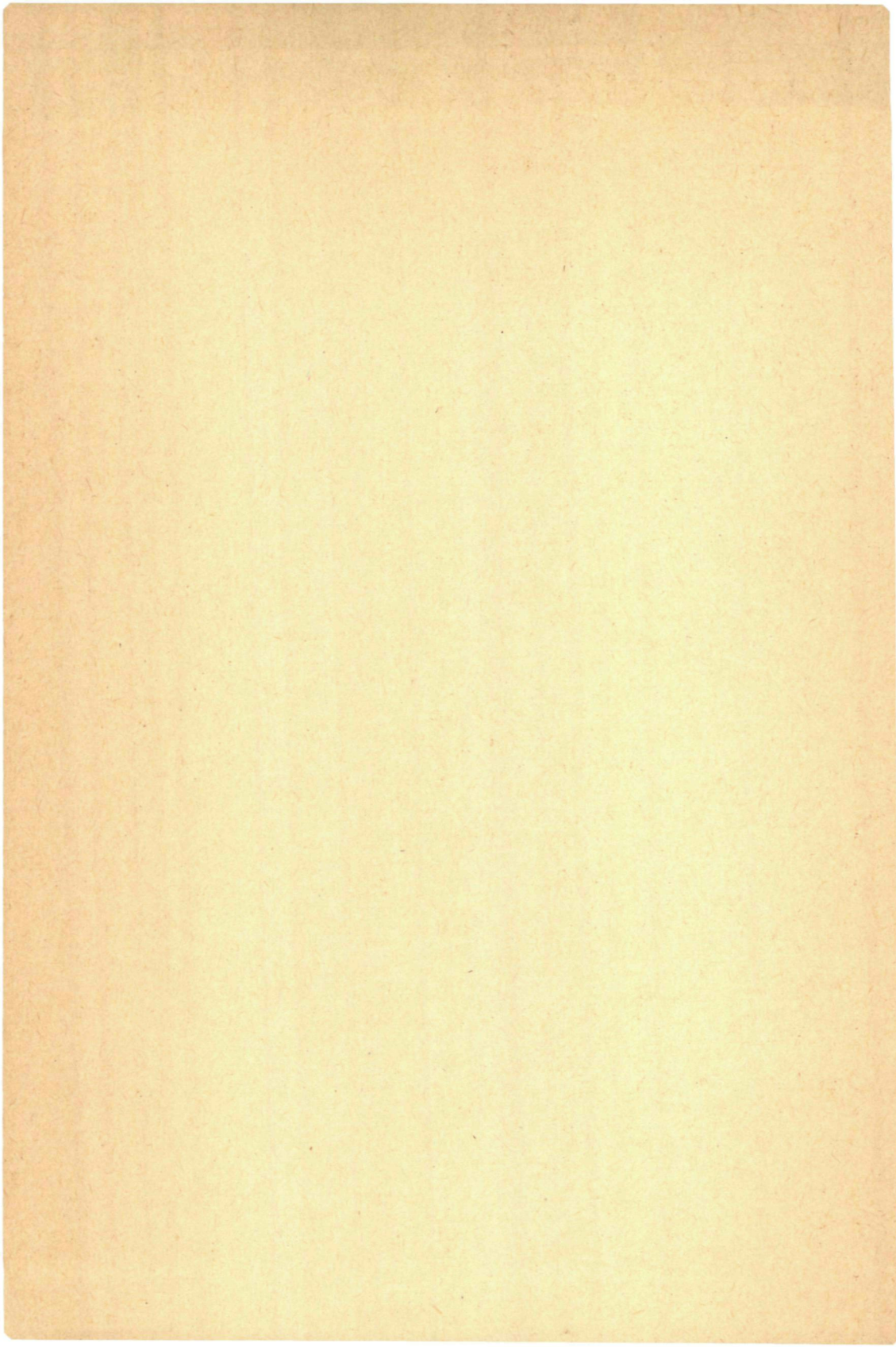


STRANGE  
PARTICLE  
PRODUCTION  
IN 5 GeV/c  $\pi^+p$   
COLLISIONS

D. Z. Toet





# STRANGE PARTICLE PRODUCTION

IN 5 GeV/c  $\pi^+$ p COLLISIONS

**PROMOTOR:**

**PROF. DR. R.T. VAN DE WALLE**

**STRANGE PARTICLE PRODUCTION**

**IN 5 GeV/c  $\pi^+$ p COLLISIONS**

**PROEFSCHRIFT**

**TER VERKRIJGING VAN DE GRAAD VAN DOCTOR  
IN DE WISKUNDE EN NATUURWETENSCHAPPEN  
AAN DE KATHOLIEKE UNIVERSITEIT TE NIJMEGEN, OP GEZAG VAN  
DE RECTOR MAGNIFICUS PROF. MR. F.J.F.M. DUYNSTEE,  
VOLGENS BESLUIT VAN HET COLLEGE VAN DECANEN  
IN HET OPENBAAR TE VERDEDIGEN  
OP VRIJDAG 22 MAART 1974  
TE 14 UUR PRECIES**

**door**

**DIRK ZIER TOET  
geboren te 's Gravenhage**

**Druk: Offsetdrukkerij Faculteit der Wiskunde en Natuurwetenschappen  
Nijmegen**

Gaarne wil ik mijn hartelijke dank betuigen aan allen, die op enigerlei wijze hebben bijgedragen tot het tot stand komen van dit proefschrift. In het bijzonder geldt deze dank

- de scansters/meetsters van de werkgroep Hoge Energie Fysika, van wie vooral mevr. R. Smeets-Van Riswick en mevr. N. Ellenbroek-Schoonderwoerd nauw met mij hebben samengewerkt bij het oplossen van scan- en meetproblemen.
  - Dr.Ir. C.L.A. Pols, Dr.Ir. D.J. Schotanus en Drs. A.A.C. Michielsen voor hun medewerking o.a. bij het verzamelen van de gegevens.
  - de staf en medewerkers van het Universitair Rekencentrum
  - de afdeling Illustratie
  - de afdeling Fotografie
  - de typekamer en de Offsetdrukkerij
- en ten slotte
- mijn vrouw, die met het geduld van een papyrologe de tekst in leesbare vorm heeft gebracht.

I also express my gratitude to all colleagues of the Bonn-Durham-Nijmegen-Paris-Torino collaboration, especially to Dr. A.E. Werbrouck (Torino), Dr. G. Rinaudo (Torino) and Dr. G.G. Winter (Bonn, now at DESY, Hamburg) for cooperation and enlightening discussions. I also thank Dr. W. Metzger for his careful reading of the manuscript. I am indebted to the CERN PS staff and the operating crews of the British National Hydrogen Bubble Chamber. I thank Dr. J. MacNaughton, Prof. P. Zacharias and Mrs. N. Fortmann-Minaylo for translating the summary into Russian.

*Je suis ce vieillard rigoureux  
Qui dedans ce lieu bienheureux  
N'aurait jamais osé paraître  
N'était que .....*

*Louis XIII  
Ballet de la merlaison  
(ouverture)*

*Aan mijn ouders*





# TABLE OF CONTENTS

GENERAL INTRODUCTION	1
CHAPTER I EXPERIMENTAL DETAILS	5
I.1 Introduction	5
I.2 Beam, chamber and pictures	5
I.3 Scan and measurement	8
I.4 Geometrical reconstruction and kinematic fitting	10
I.5 Methods of event identification, Acceptance criteria, Ambiguities	16
I.6 Hypothesis selection for some special channels	20
I.6.1 The channel $pK^+K^-\pi^+$	20
I.6.2 The channels $\Lambda K^+\pi^+$ and $\Sigma^0 K^+\pi^+$	21
I.6.3 The channels with $\Lambda(\Sigma^0)K^0$ production	22
I.7 Summary of Data	26
CHAPTER II ESTIMATION OF CHANNEL CROSS SECTIONS	29
II.1 Introduction	29
II.2 Acceptance criteria	32
II.3 Scanning volume and decay volume	33
II.4 Cross section calculations	47
II.5 Corrections applied to the number of events found experimentally	52
II.5.1 The scanning efficiency correction ( $c_s$ )	52
II.5.2 The correction for unclassified events ( $c_u$ )	53
II.5.3 The correction for $P(\chi^2)$ -cutoff ( $c_p$ )	55
II.5.4 The correction for decays not meeting the length criteria ( $c_l$ )	55
II.5.5 The correction for angular loss ( $c_h$ )	57
II.5.6 The correction for unused decay modes ( $c_d$ )	59
II.5.7 The combined correction factor $c_w$	62
II.6 Channel cross sections	67
II.7 Total strange particle cross section	68
II.8 Results of other experiments	68

CHAPTER III RESONANCE PRODUCTION AND REACTION CROSS

SECTIONS		76
III.1	Introduction	76
III.2	Methods of estimation	77
III.2.1	The estimation of background	77
III.2.2	Estimation of resonance production	79
III.2.3	Significance of the enhancements	82
III.3	Resonance production	82
III.3.1	The channel $p\bar{K}^{\circ}K^{+}$	87
III.3.2	The channel $p\bar{K}^{\circ}K^{+}\pi^{\circ}$	90
III.3.3	The channels $pK^{\circ}\bar{K}^{\circ}\pi^{+}$ and $pK^{+}K^{-}\pi^{+}$	93
III.3.4	The channel $n\bar{K}^{\circ}K^{+}\pi^{+}$	106
III.3.5	The channel $\Lambda K^{\circ}\pi^{+}$	108
III.3.6	The channels $\Lambda K^{+}\pi^{+}\pi^{\circ}$ and $\Lambda K^{\circ}\pi^{+}\pi^{+}$	109
III.3.7	The channels $\Sigma^{+}K^{+}\pi^{\circ}$ and $\Sigma^{+}K^{\circ}\pi^{+}$	114
III.3.8	The channel $\Sigma^{+}K^{+}\pi^{+}\pi^{-}$	119
III.3.9	Search for exotic baryon resonances	121
III.3.10	The $(K\bar{K}\pi)$ spectra	121

CHAPTER IV CHARACTERISTICS OF SOME REACTIONS AND COM-  
PARISON WITH MODELS

IV.1	Introduction	126
IV.2	Mandelstam variables; Differential cross section	127
IV.3	Outline of models used	131
IV.4	The decay angular distribution; spin density matrix elements	138
IV.5	The reaction $\pi^{+}p \rightarrow K^{+}\Sigma^{+}$	144
IV.5.1	Experimental results	144
IV.5.2	Exchange model predictions	148
IV.5.3	SU(3) predictions	150
IV.6	The reaction $\pi^{+}p \rightarrow K^{*+}(890)\Sigma^{+}$	155
IV.6.1	Experimental results	155
IV.6.2	Comparison with theory	157
IV.7	The reaction $\pi^{+}p \rightarrow K^{*+}\Sigma^{+}(1385)$	160
IV.7.1	Experimental results	160
IV.7.2	Comparison with exchange models	165
IV.7.3	SU(3) relations	166
IV.8	The reaction $\pi^{+}p \rightarrow K^{*+}(890)\Sigma^{+}(1385)$	169
IV.8.1	Experimental results	169
IV.8.2	Absorption model calculations	174

IV.8.3	Quark model predictions for the spin density matrix elements	174
IV.8.4	SU(3) relations	175
APPENDIX A	KINEMATIC SOLUTIONS FOR SHORT STRANGE PARTICLE DECAYS	184
APPENDIX B	DETERMINATION OF ANGULAR LOSSES	187
APPENDIX C	LIST OF PARTICLE PROPERTIES	200
SUMMARY		203
<b>Резюме</b>		205
SAMENVATTING		207



## GENERAL INTRODUCTION

This thesis deals with the study of reactions characterized by the fact, that their final states contain particles with strangeness quantum number different from zero. These reactions took place between a beam of  $\pi^+$  mesons of 5 GeV/c and protons in a liquid hydrogen filled bubble chamber. The beam was set up at the CERN Proton Synchrotron and was injected into the British National Hydrogen Bubble Chamber. The reactions (or more strictly speaking: the tracks left by the charged particles before and after the interaction) were photographed in stereo by a set of three cameras. Some 125.000 stereo triplets were available for analysis.

Over a period of several years many different topics were studied. This resulted in the following list of papers:

"Study of the 6-pronged  $\pi^+p$  interactions at 5 GeV/c".(1)

"Test of quark model predictions in double-resonance production by 5 GeV/c  $\pi^+$  mesons or protons".(2)

"Test of absorption model predictions in double-resonance production by 5 GeV/c  $\pi^+$  mesons on protons".(3)

"Decay properties of the 'A<sub>2</sub>(1300)'-meson".(4)

"Study of cross sections and spin density matrix elements for two-body reactions in 5 GeV/c  $\pi^+p$  two-pronged interactions".(5)

"Analysis of  $p\pi^+\pi^-$  enhancements produced in the reaction  $\pi^+p \rightarrow \pi^+p\pi^+\pi^-$  at 5 GeV/c".(6)

"Study of cross-sections and spin-density matrix elements in 5 GeV/c  $\pi^+p$  four-pronged interactions".(7)

"Spin-density analysis of the B-meson produced in  $\pi^+p$  reactions".(8)

"Longitudinal phase space analysis of 5 GeV/c  $\pi^+p$  reactions".(9)

"Analysis of the A<sub>1</sub> and A<sub>2</sub> regions in the reaction  $\pi^+p \rightarrow \pi^+\pi^+\pi^-p$  at 5 GeV/c".(10)

"Evidence for double diffractive dissociation in  $\pi^+p$  reactions at 5 GeV/c".(11)

"Comparison of A<sub>1</sub>-A<sub>2</sub> interference between  $\pi^-p$  and  $\pi^+p$  reactions at 5 GeV/c".(12)

"Strange particle production in 5 GeV/c  $\pi^+p$  collisions".(13)

In addition some 12 contributions, based on this work, were presented at conferences held in Berkeley, Oxford, Heidelberg, Cern, Vienna, Lund and Kiev (ref. 14-20).

In principle all these papers and contributions were prepared and written by a collaboration of five European laboratories:

Physikalisches Institut der Universität Bonn, Federal Republic of Germany.

Department of Physics, University of Durham, United Kingdom.

Fysisch Laboratorium, Universiteit van Nijmegen, the Netherlands.

Ecole Polytechnique, Paris, France.

Istituto di Fisica dell' Università di Torino,

Istituto Nazionale di Fisica nucleare, Sezione di Torino, Italy.

In practice these laboratories cooperated in extracting the data, but agreed to a certain division of tasks in the analysis phase.

The study of the strange particle reactions was mainly done in Bonn ( $V^0$  events) and Nijmegen ( $V^0$  and kink events).

The relatively small cross section for strange particle production ( $\approx 7\%$  of the total  $\pi^+p$  cross section), as well as the fact, that in our experiment only some 50% of the produced strange particle events can be recognized as such, put severe limitations on the statistics that are obtained. As a result, only a few dynamical questions can be discussed meaningfully. In this thesis the dynamical analysis is restricted to the two body reactions  $\pi^+p \rightarrow K^+\Sigma^+$ ,  $\pi^+p \rightarrow K^{*+}(890)\Sigma^+$ ,  $\pi^+p \rightarrow K^+\Sigma^+(1385)$ , and  $\pi^+p \rightarrow K^{*+}(890)\Sigma^+(1385)$ . Much attention is however paid to the determination of channel- and resonance production-cross sections.

## REFERENCES - GENERAL INTRODUCTION

- (1) H. Drevermann, U. Idschok, G. Winter, K. Böckmann, A.J. Apostolakis, G. Briggs, C.A. Kitchen, J.V. Major, C.L. Pols, J. Schotanus, D. Toet, R.T. Van de Walle, R. Lestienne, P. Fleury, C. Grosso, B. Quassiat, G. Rinaudo and A. Werbrouck,  
Phys. Rev. **161**, 1356 (1967).
- (2) Bonn-Durham-Nijmegen-Paris-Strasbourg-Turin Collaboration:  
K. Böckmann, M. Rost, K. Sternberger, G. Winter, Z.I. Bhuyan, H. Halliwell, J.V. Major, T.G. Lim, C.L. Pols, D.J. Schotanus, D.Z. Toet, R.T. Van de Walle, E. Cirba, P. Fleury, G. De Rosny, R. Vanderhaghen, B. Schiby, J. Oudet, R. Strub, B. Quassiat, G. Rinaudo, M. Vigone and A. Werbrouck,  
Phys. Letters **28B**, 72 (1968).

- (3) Bonn-Durham-Nijmegen-Paris-Strasbourg-Turin Collaboration (same authors as ref. (2)),  
Nucl. Phys. **B7**, 681 (1968).
- (4) Bonn-Durham-Nijmegen-Paris(E.P.)-Torino Collaboration:  
K. Böckmann, M. Rost, B. Wagini, G. Winter, J.V. Major, C.L. Pols,  
D.J. Schotanus, D.Z. Toet, R.T. Van de Walle, E. Cirba, R. Vanderhaghen,  
B. Quassati, G. Rinaudo, M. Vigone and A. Werbrouck,  
Nucl. Phys. **B16**, 221 (1970).
- (5) Durham-Nijmegen-Paris-Torino Collaboration:  
D.J. Schotanus, C.L. Pols, D.Z. Toet, R.T. Van de Walle, J.V. Major,  
G.E. Pearson, B. Chaurand, R. Vanderhaghen, G. Rinaudo and A.E.  
Werbrouck,  
Nucl. Phys. **B22**, 45 (1970).
- (6) Bonn-Durham-Nijmegen-Paris(E.P.)-Torino Collaboration:  
E. Cirba, R. Vanderhaghen, H. Drevermann, G. Winter, J.V. Major, R.T.  
Van de Walle, G. Rinaudo and A.E. Werbrouck,  
Nucl. Phys. **B23**, 533 (1970).
- (7) C.L. Pols, D.J. Schotanus, D.Z. Toet, R.T. Van de Walle, K. Böckmann,  
K. Sternberger, B. Wagini, G. Winter, J.V. Major, E. Cirba, R. Vanderhaghen,  
G. Rinaudo and A. Werbrouck,  
Nucl. Phys. **B25**, 109 (1970).
- (8) A. Werbrouck, G. Rinaudo, R.T. Van de Walle, D.J. Schotanus, C.L.  
Pols, N. Stief, G. Gidal and D. Brown,  
Lettere al Nuovo Cimento **4**, 1267 (1970).
- (9) Bonn-Durham-Nijmegen-Paris(E.P.)-Torino Collaboration: G. Rinaudo,  
A.E. Werbrouck, K. Böckmann, H. Drevermann, J.V. Major, C.L. Pols,  
D.J. Schotanus, D.Z. Toet, R.T. Van de Walle, E. Cirba and R. Vanderhaghen,  
Nucl. Phys. **B25**, 351 (1971).
- (10) Bonn-Durham-Nijmegen-Paris(E.P.)-Torino Collaboration:  
G. Rinaudo, A.E. Werbrouck, K. Böckmann, M. Rost, J.V. Major, C.L.  
Pols, R.T. Van de Walle and R. Lestienne,  
Nuovo Cimento **5A**, 239 (1971).



- (11) G. Rinaudo, A.E. Werbrouck, M. Rost, C. Kanazirsky, D.Z. Toet and R. Lestienne,  
Nuovo Cimento **10A**, 1 (1972).
- (12) A.E. Werbrouck, G. Rinaudo, G.J. Bossen, M. Rost, C.L. Pols, R.T. Van de Walle and R. Lestienne,  
Lettere al Nuovo Cimento **3**, 141 (1972).
- (13) D.Z. Toet, C.L.A. Pols, D.J. Schotanus, R.T. Van de Walle, Phu-To Thuan, B. Wessels, G. Winter, J.V. Major, G. Rinaudo and A. Werbrouck,  
Nucl. Phys. **B63**, 248 (1973).
- (14) Bonn-Durham-Nijmegen-Paris(E.P.)-Turin Collaboration,  
Proceedings of the Oxford International Conference on Elementary Particles (1966) Abstract A, p. 72.
- (15) Bonn-Durham-Nijmegen-Ecole Polytechnique-Torino Collaboration,  
Proceedings of the XIII<sup>th</sup> International Conference on High Energy Physics, Berkeley (1966), Session 7a paper 23.
- (16) Bonn-Durham-Nijmegen-Paris(E.P.)-Torino Collaboration,  
Proceedings of the Heidelberg International Conference on Elementary Particles, 1967, papers 65, 178, and 333.
- (17) Bonn-Durham-Nijmegen-Paris(E.P.)-Strasbourg-Turin Collaboration,  
Proceedings of the Topical Conference on High Energy Collisions of Hadrons, CERN, 1968 Vol. II p. 150.
- (18) Bonn-Durham-Nijmegen-Paris(E.P.)-Strasbourg-Turin Collaboration,  
Proceedings of the 14<sup>th</sup> International Conference on High Energy Physics, Vienna, 1968, papers 343 and 344.
- (19) Bonn-Durham-Nijmegen-Paris(E.P.)-Turin Collaboration,  
Proceedings of the Lund International Conference on Elementary Particles 1969, papers 141, 142 and 143.
- (20) Bonn-Durham-Nijmegen-Paris-Turin Collaboration,  
Proceedings of the XV International Conference on High Energy Physics, Kiev (1970), Session 3a, paper 6.

## CHAPTER I

## EXPERIMENTAL DETAILS

*I.1 Introduction*

In this chapter we describe the experimental conditions and the procedures followed in the analysis of the bubble chamber pictures. We also present some details on the beam and the bubble chamber.

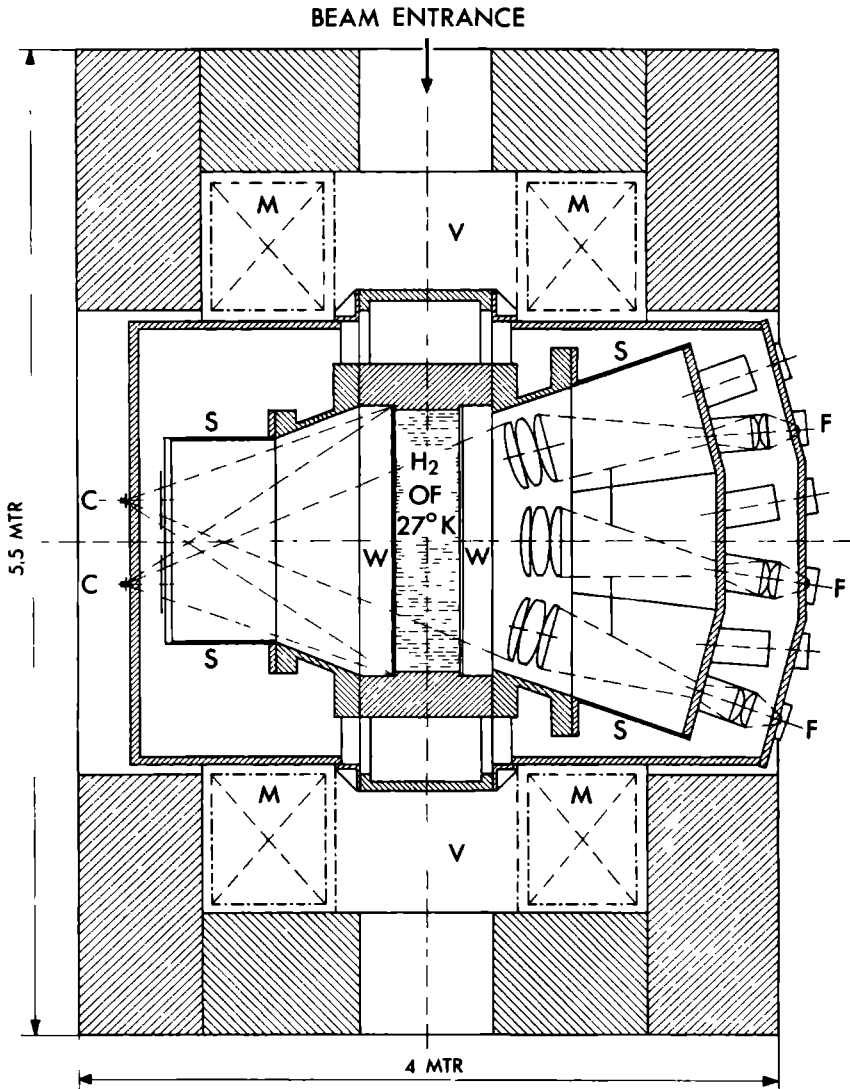
*I.2 Beam, chamber and pictures*

In our experiment an electrostatically separated beam <sup>(12)</sup> of  $\pi^+$  mesons of approximately 5 GeV/c momentum ( $4.997 \pm 0.006$  GeV/c), originating from the CERN Proton Synchrotron, was injected into the British National Hydrogen Bubble Chamber <sup>(13)</sup> (fig. I.1).

The approximate internal dimensions of this chamber are 150 x 50 x 46 cm, where 46 cm is the distance between the two parallel optical glass windows. The liquid hydrogen in this volume was kept at a temperature of 27°K at a pressure of 6.3 kg/cm<sup>2</sup>. The pressure drop required to bring the liquid into a condition sensitive to bubble formation was 3.5 kg/cm<sup>2</sup>.

The expansion and recompression of the liquid was accomplished by means of a piston.

The beam traversed the chamber in the longitudinal direction and was almost parallel to the windows. The strings of vapour bubbles formed along the paths of the charged particles



**C = CAMERA**  
**F = FLASH**  
**M = MAGNET**  
**S = SHIELD OF HYDROGEN**  
**V = VACUUM**  
**W = WINDOW**

Fig. I.1 Plan view of the British National Hydrogen Bubble Chamber.

(tracks) were photographed through the front window by means of three cameras with optical axes perpendicular to the chamber windows. The hydrogen volume was illuminated through the rear window by a set of nine flashes. By means of a condensor system the light was focused in such a way, that the cameras could only receive light scattered by the bubbles (dark-field illumination).

The repetition rate of the expansion-recompression cycle and film exposure was identical to that of the beam injection: approximately once per two seconds.

The bubble chamber was installed inside a Helmholtz type magnet coil system <sup>(14)</sup>. This produced within the chamber a nearly homogeneous magnetic field of approximately 13.5 kGauss perpendicular to the windows. Under the influence of the Lorentzforce, moving charged particles are forced to travel along a helix. Particles with positive or negative electrical charge curve in opposite directions. The radius of curvature of a track, projected onto a plane perpendicular to the field, is proportional to the momentum component in that plane:

$$\rho = p \cos \lambda / (0.3 H) \quad (\text{I.1})$$

where  $\rho$  is the radius of curvature in cm

$p$  is the momentum in MeV/c

$\lambda$  is the dip angle

and  $H$  is the magnetic field expressed in kGauss.

During the exposure some 125.000 picture triplets were taken. They contained an average flux of 12.3 beam tracks within the entrance limits of the fiducial volume defined in section II.1.

### I.3 Scan and measurement

All pictures were scanned at least twice for so-called  $V^0$  and  $V^\pm$  events (fig. I.2).

The  $V^0$  events are interactions showing one or more visibly decaying *neutral* secondary particles:  $\Lambda$  and/or  $K^0$ . They were scanned and measured by the collaborating laboratories in much the same way as the non-strange events <sup>(1)</sup>.

The  $V^\pm$  events - also called kink events - are interactions showing one or more decays of *charged* secondaries:  $\Sigma^\pm$  and/or  $K^\pm$ . The first and second scanning of a large fraction of these events was done in Nijmegen only.

The scanners were instructed to record all events with kinking tracks and/or with associated  $V^0$ 's, provided the primary interaction point (primary vertex) was lying within the limits of a fiducial volume (see sect. II.3). Fig. I.2 shows the most frequently occurring topologies. Charged decays of neutrals showing a zero opening angle and strongly curved tracks with minimum bubble density were excluded; these properties are typical for  $\gamma \rightarrow e^+e^-$  conversions. Separation of scatters from real charged strange particle decays was done by physicists in the output scan stage (see sect. I.5).

The three pictures of each event were measured on conventional film plane digitizers (S.O.M.-ENETRA) using diffraction gratings and Moiré-fringe techniques. The point measuring precision in the film plane was typically of the order of 0.005 mm ( $\approx$  0.05 mm in the chamber).

The measured coordinates of interaction points, points on particle tracks and fiducial marks (see sect. II.3) were punched onto cards for further processing.

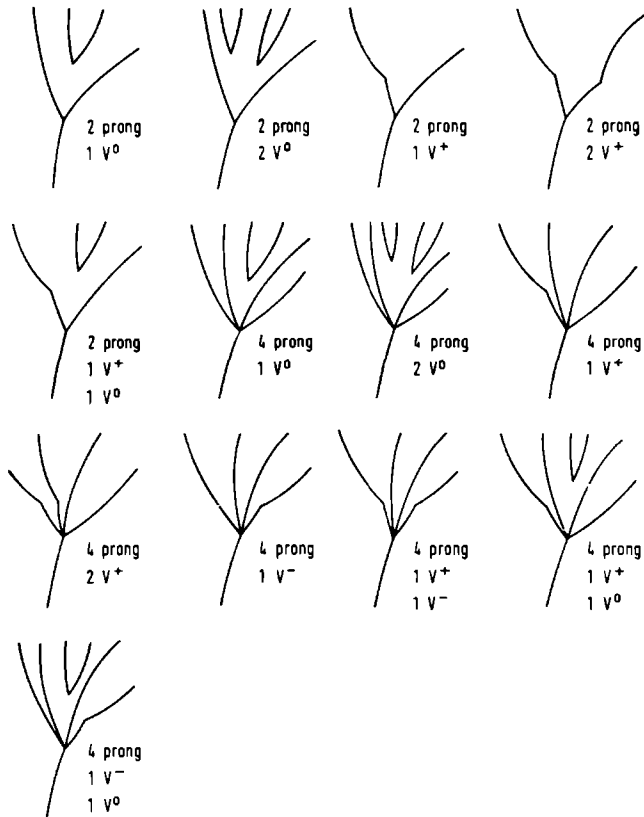


Fig. I.2 Examples of the strange particle topologies found in our experiment.

The measurement of all  $V^+$  events as well as the remeasurement of some 10% of the  $V^0$ -events was done in Nijmegen.

#### *I.4 Geometrical reconstruction and kinematic fitting*

The measurements were first checked for completeness and absence of errors by a computer program called ROOT.

Spatial reconstruction of the events from the coordinates measured on the photographic stereotriplets was done with help of the program THRESH<sup>(2)</sup>. Results obtained from this program are the x, y, z positions of the interaction points (with respect to a bubble chamber reference frame), the curvature, azimuthal- and dip-angle for each measured track, in addition to error estimates for these quantities. For short straight tracks the curvature is left undetermined.

This geometrical information is used in the program GRIND<sup>(2)</sup>. The task of this program is to find which kinematic interpretations out of a list of given hypotheses are compatible with the measurement. Each hypothesis assigns a specific set of particles (masses) to the event-tracks. The momentum of each charged particle is calculated in a straightforward way from the curvature of the track and the magnetic field map of the chamber (Eq. (I.1)). If a particle stops in the liquid the momentum is checked against its range. The program is thus able to test each hypothesis on the basis of compatibility with the laws of conservation of energy and momentum (= 4 constraint equations). The test is performed using constrained least-squares fit techniques. These fits not only lead to probability estimates for the validity of the hypothesis under consideration,



they also result in better (= fitted) values for the measured quantities.

We distinguish the following sequence:

- A. Fitting of decays
- B. Fitting of the primary interaction
- C. Fitting of the complete sequence of interactions

#### A. *Fitting of decays*

a. For a  $V^0$ -decay ( $K^0 \rightarrow \pi^+ \pi^-$ ;  $\Lambda \rightarrow p \pi^-$ ) GRIND first tests if the decaying neutral particle has indeed been created in the visible primary interaction. This is done by checking if the direction of the resultant momentum of the  $V^0$ -decay products passes through the primary vertex under consideration within the error limits. If the test confirms this assumption, the direction of the neutral track is fixed and then there remains only one unknown parameter: the absolute value of its momentum. Using one of the four constraint equations to determine this parameter the program is able to test the hypothesis by submitting the measured quantities to a 3-constraint fit (or 3-C fit).

b. For decays of charged particles, we distinguish between two possibilities:

1. The track between the primary and the decay vertex is sufficiently long to enable a determination of its curvature (momentum). This situation usually occurs for long lived particles ( $K^\pm$ ; mean lifetime  $\tau \sim 10^{-8}$  sec.) and is relatively rare. Occasionally also a  $\Sigma^-$  decay can be treated in this way. Fitting these decays ( $K^\pm \rightarrow \mu^\pm \nu$ ;  $K^\pm \rightarrow \pi^\pm \pi^0$ ;  $\Sigma^- \rightarrow \pi^- n$ ) first requires a determination of the value and direction of the momentum for the neutral decay product (3 unknown quantities).

This leaves us with a 1-C fit.

2. The track between the primary and the decay vertex is too short for curvature measurement. This case applies almost exclusively for decays of short lived particles; e.g. for  $\Sigma^+ \rightarrow \pi^+n$ ,  $\Sigma^+ \rightarrow p\pi^0$  and  $\Sigma^- \rightarrow \pi^-n$ . Only directional information can now be used and we have to evaluate one more unknown quantity, namely the absolute value of the momentum of the decaying particle. This implies that we have no more constraints left. The solutions of the direct (analytic) calculations are by analogy often called 'O-C fits' or 'nofits'.

A complication inherent to a O-C decay fit is the fact that we often find two solutions (see appendix A). Fortunately in many cases one of these solutions (momenta) is incompatible with the momentum balance at the primary interaction.

### *B. Fitting of the primary interaction*

The momentum of any decaying *neutral* particle fitted at its decay vertex is used as such at the production (= primary) vertex. For the decaying *charged* particles the momentum determined at the decay vertex is 'swum back' (i.e. extrapolated applying Coulomb scattering and curvature corrections) to the primary vertex. They are then used together with the momenta of the (semi-) stable secondaries in the identification of the primary interaction.

A hypothesis is tested as follows. For the *charged* (particles) and *visibly decaying neutral* particles the knowledge of their masses, - assigned by the hypothesis - , and their momenta, allows a direct determination of the energy of each of these particles. These energies and momenta are summed,

yielding  $E_V$  and  $\vec{P}_V$  respectively. The so called 'missing' quantities at the primary vertex -  $E_M$  and  $\vec{P}_M$  respectively - are then given by:

$$E_M = E - E_V \quad (\text{I.2})$$

$$\vec{P}_M = \vec{P} - \vec{P}_V \quad (\text{I.3})$$

where  $E$  and  $\vec{P}$  are the total energy and momentum in the initial state. From the above we see that, neglecting 'swim' corrections, only  $E_M$  is a hypothesis-dependent quantity.

The missing mass  $M_M$  is defined as \*):

$$M_M^2 = E_M^2 - (\vec{P}_M)^2 \quad (\text{I.4})$$

If the hypothesis considered is compatible with the measured event,  $M_M$  should be equal (within the errors) to the mass of the eventually *undetected neutral* particle required by this hypothesis. We distinguish between three cases:

1.  $M_M \approx 0$ . If the hypothesis requires no extra neutrals, we will generally have a 4C-fit.

2.  $M_M \approx M_0$ , where  $M_0$  is the mass of a known particle (e.g.  $\pi^0$ ,  $K^0$ ,  $n$ ,  $\Lambda$ ,  $\Sigma^0$ ). If the hypothesis requires a neutral

\*) *Note.* The correct formula reads  $M_M^2 c^4 = E_M^2 - P_M^2 c^2$ . If energy, momentum and mass are measured in units of MeV, MeV/c and MeV/c<sup>2</sup> respectively (as throughout in this thesis), Eq. (I.4) expresses a correct relation between the numerical values of these quantities.

of mass  $M_0$ , 3 constraints are used to calculate the momentum vector of  $M_0$ . This leaves us with a 1-C fit.

$$3. M_M + \Delta M_M \geq M_0 + m_{\pi^0}, \quad (\text{I.5})$$

where  $\Delta M_M$  is the standard deviation of  $M_M$  and  $m_{\pi^0}$  is the mass of the  $\pi^0$  meson. GRIND examines the possibility that the mass assignment to the detected particles is correct but that *more than one* undetected neutral has been created at the primary vertex. It is in any case not possible to determine the individual masses and momenta of these neutrals. GRIND assigns the missing quantities to a single fictitious neutral particle of mass  $M_M$ . The calculation of  $M_M$  effectively uses up the last constraint and we again end up with a 0-C fit.

Sometimes the above cases appear simultaneously. This is one origin of hypothesis ambiguities.

A special case form the events with visible  $\Lambda$  decay ( $\Lambda \rightarrow p\pi^-$ ) fitting a  $\Sigma^0$ . The  $\Sigma^0$  decays into  $\Lambda \gamma$  after a very short lifetime ( $< 10^{-14}$  sec.); for all practical purposes we can consider both the  $\Lambda$  and the  $\gamma$  as created at the primary vertex. The  $\gamma$  has a negligible chance of converting into an  $e^+e^-$ -pair (the conversion length in hydrogen is  $\sim 10$  m). This situation would normally lead to a 1C-primary vertex fit. There is now however an extra constraint equation to be satisfied:

$$(E_{\Lambda} + E_{\gamma})^2 - (\vec{P}_{\Lambda} + \vec{P}_{\gamma})^2 = M_{\Sigma^0}^2, \quad (\text{I.6})$$

The fit for this class of events will thus have 2 constraints.

### *C. Fitting of the complete sequence of interactions*

GRIND finally considers all combinations of successful primary and decay vertex fits that are physically acceptable and performs a multivertex fit. While in the single vertex fits the determination of the best quantities is done at each vertex separately, in a multivertex fit both types of vertices are tested together.

The number of constraints given for the types of fits described above are typical. However, variations may occur, e.g. if one or more of the tracks are difficult to measure. The determination of 'unmeasurable' quantities lowers the number of constraints accordingly.

In reality, as already has been indicated, the fit method used is considerably more sophisticated than described above. All constraints are kept on equal footing using the technique of a constrained least-squares fit with Lagrangian multipliers<sup>(4)</sup>. With this technique the procedures sketched above are actually used to calculate first approximations (= fit starting values). These more refined fit methods however do keep the characteristics (and in particular the constraint class division) of the more simplified methods described.

For hypothesis selection (section I.5) we use the  $\chi^2$ -probability or confidence level  $P_n(\chi^2)$  of the least squares fit. Its value depends on the  $\chi^2$ -value itself and the number of degrees of freedom  $n$ . For the types of fit described here  $n$  is (somewhat surprisingly) equal to the number of con-

straints (\*). (For nofits the confidence level is of course undefined).

The output from GRIND is written onto magnetic tape and printed. It consists of a full description of the successfully fitted hypotheses for each vertex. It gives the initial and fitted values of momenta, angles etc. together with a predicted value for the bubble density of each charged track. The bubble density is an important tool for hypothesis selection. It is statistically proportional to the energy loss of the particle per unit path length, a quantity which in turn depends on the velocity and charge magnitude of the particle considered.

### *1.5 Methods of event identification; Acceptance criteria; Ambiguities*

In view of the limited measurement precision GRIND in many cases finds more than one kinematically successful hypothesis. Selection of 'acceptable' hypotheses was done on the basis of the following additional criteria:

a. The bubble densities of the charged tracks, predicted by GRIND, must be compatible with those visually observed. It is generally possible to distinguish a  $\pi^+$  from a

(\*) *Note.* This is because  $n = (\text{the number of measured quantities}) - (\text{the number of free quantities})$ . In our case the latter term is equal to the difference  $(\text{number of measured quantities}) - (\text{number of constraints})$ .

proton up to momenta of  $\sim 1.3$  GeV/c. For  $\pi$  and K the corresponding limit is  $\sim 0.8$  GeV/c.

b. The confidence level for the primary vertex fit is required to exceed a prescribed minimum. This minimum was chosen as follows:

degrees of freedom (n)	$\chi^2$ max.	$P_n(\chi^2)$ min.
1	6.0	0.014
2	6.0	0.05
4	25.0	0.00005

In many cases these acceptance criteria are not sufficient to completely remove the ambiguities. The problem of resolving these ambiguities in samples with low statistics is known to be difficult. As a first approximation the following rules were used for *event-by-event* decisions:

$\alpha$ . If fits of different constraint classes are present, the fits of the highest constraint class are preferred.

$\beta$ . In cases where we are left with more than one fit within the same constraint class ( $\geq 10$ ) the hypothesis yielding the fit with the highest confidence level is chosen.

Ambiguities of the type OC-OC thus cannot be resolved on an event-by-event basis. A method of handling these will be discussed below.

Some *statistical* methods exist to correct *a posteriori* certain features of the samples selected with the above simple rules. Examples will be treated in section I.6 and mentioned furtheron. For the application of these methods the presence of sufficient statistics is required. Some ambiguous channels, for which this was not the case, were left unseparated.



We first discuss rules  $\alpha$  and  $\beta$  in somewhat more detail.

A. With respect to *rule*  $\alpha$  we can make the following remarks:

(i) 4C fits are always preferred to  $\leq$  1C fits because studies with artificial events<sup>(5)</sup> show that it is unlikely for events involving the production of one or more unseen neutrals to fake energy and momentum conservation without unseen neutrals.

4C-2C ambiguity occurs in events with a visible  $\Lambda$  decay fitting both hypotheses with a  $\Lambda$  and a  $\Sigma^0$ . In section I.6.2 we discuss this type of ambiguity for the channels  $\Lambda K^+ \pi^+$  and  $\Sigma^0 K^+ \pi^+$ .

(ii) 2C-fits ambiguous with 0-C fits seldom occur; the 2C-fit is accepted. The same applies for 2C-1C ambiguities ( $\Sigma^0 \rightarrow \Lambda_{\nu} \gamma$  vs.  $\Lambda_{\nu} \pi^0$  (\*)). Statistics do not allow or justify the use of a special criterion.

(iii) Especially when applied to the frequently occurring 1C-0C ambiguity, rule  $\alpha$  is known to be a far from perfect criterion, but it usually presents the only solution available for an event-by-event decision<sup>(3)</sup>. An example of a correction method is given in sect. I.6.3.

B. Concerning *rule*  $\beta$  the following remarks can be made:

(i) The most frequent use of rule  $\beta$  is to decide 1C-1C ambiguities. Some examples of this type of ambiguity are:

(\*) *Note.* The index  $\nu$  with  $\Lambda$ ,  $\Sigma$  or  $K$  is used to indicate a decay visible within the bubble chamber.  $\Sigma_{\nu}^0$  denotes the decay  $\Sigma^0 \rightarrow \Lambda_{\nu} \gamma$ . The index  $i$  stands for invisible decays.

$\Lambda/\Sigma^{\circ}$  ambiguity:  $\Lambda K_V^{\circ} \pi^+ \pi^+$  vs.  $\Sigma^{\circ} K_V^{\circ} \pi^+ \pi^+$

$K_1^{\pm} \pi^{\circ} / \pi^{\pm} K_1^{\circ}$  ambiguity:  $p K_1^{\pm} K_V^{\circ} \pi^{\circ}$  vs.  $p \pi^{\pm} K_V^{\circ} K_1^{\circ}$

$\Lambda_V K_1^{\pm} \pi^+ \pi^{\circ}$  vs.  $\Lambda_V \pi^+ \pi^{\circ} K_1^{\circ}$

$\Sigma_V^+ K_1^{\pm} \pi^{\circ}$  vs.  $\Sigma_V^+ \pi^+ K_1^{\circ}$

$n K_1^{\pm} / \Lambda_1 \pi^+$  ambiguity:  $n K_1^{\pm} K_V^{\circ} \pi^+$  vs.  $\Lambda_1 \pi^+ K_V^{\circ} \pi^+$

(ii) Rule  $\beta$  is also used for the separation of the few 4C-4C and 2C-2C ambiguities occurring.

The 4C-4C ambiguities in the four-prong-no-kink sample involving a  $p K^+ K^- \pi^+$  fit are an exception. For a detailed discussion we refer to section I.6.1.

(iii) For OC-OC ambiguities an a posteriori repartition of events proportional to the unambiguous events is the only method available.

(iv) At the *decay vertices* distinction between  $\Lambda$  and  $K^{\circ}$ -fits (usually a 3C-3C ambiguity) is almost never a problem. In the case of an ambiguity between a  $K^{\pm}$ - and a  $\Sigma^{\pm}$ -decay (OC-OC) we generally prefer the  $\Sigma$  solution because the lifetime of the K implies that most of the K's will decay outside the chamber volume. Only in cases where the confidence level at the *primary vertex* for the fit with the K is a factor 5 or more higher than that for the other fits, the K-hypothesis is accepted.

Rule  $\beta$  is statistically questionable in situations where the  $\chi^2$ -levels of the ambiguous hypotheses are not sufficiently different. Sometimes alternative strategies are chosen (6,10,11): e.g. one accepts all (N) ambiguous fits for the event, weighting each of them with a factor  $\frac{1}{N}$ . This method clearly gives equal weights to all ambiguous hypotheses, regardless

of the fact, that the corresponding cross sections may be very different. A better statistical method to estimate the population of the ambiguous hypothesis-classes seems to be the method of redistributing a posteriori the ambiguous events proportionally to the number of events having an unambiguous fit to the hypotheses considered (see e.g. ref. 6). For our sample and with regard to channel populations, the results of this latter method are generally fairly compatible with the results obtained using the (a priori) rule  $\beta$ .

In some cases one can statistically check and correct the quality of the hypothesis separation obtained by using rule  $\beta$ . One can for instance inspect the shape of the missing mass distribution of the fitted neutral. Another method is based on the fact, that some channels appear in different topologies. Interactions yielding two neutral strange particles will in general be seen in three different topologies: two topologies characterized by one visible decay and one topology where both particles decay visibly. The ratio between the numbers of events found in these topologies should agree with predictions (see e.g. sect. I.6.3). Analogous cases appear in other topologies. In general this allows a check on the lower constraint class sample (and the way it was affected by rule  $\beta$ ) using the characteristics of the higher constrained sample.

## *I.6 Hypothesis selection for some special channels*

### *I.6.1 The channel $pK^+K^-\pi^+$*

As most of the  $K^\pm$  particles decay outside the chamber,  $pK^+K^-\pi^+$  events mainly show a four-prong-no-kink topology. From

the measurements of the four prong sample we obtained a total of 422 events with a  $pK^+K^-\pi^+$  fit. This sample was composed as follows:

unambiguous $pK^+K^-\pi^+$	: 316 (a)
ambiguous with the same hypothesis, but $\pi^+$ and $K^+$ interchanged (4C-4C)	: 38 (b)
ambiguous $pK^+K^-\pi^+ - p\pi^+\pi^+\pi^-$ (4C-4C)	: 54 (c)
ambiguous $pK^+K^-\pi^+ - p\pi^+\pi^+\pi^-\pi^0$ (4C-1C)	: 14 (d)

These ambiguities have been investigated with artificial events<sup>(7)</sup> generated by the program FAKE<sup>(5)</sup>. As a result we found that we could treat the above ambiguities as follows.

(i) Events in class (b) were assigned to the best fit (= rule  $\beta$ ).

(ii) all events in class (c) were classified as  $p\pi^+\pi^+\pi^-$  because of the much larger cross-section of this channel ( $2.76 \pm 0.04$  mb<sup>(9)</sup>). The FAKE results show that ( $2.5 \pm 1.7$ ) % of the  $pK^+K^-\pi^+$  events are lost in this way.

(iii) all events in class (d) were accepted as  $pK^+K^-\pi^+$  (= rule  $\alpha$ ). The FAKE results show that ( $1 \pm 0.5$ ) % of the  $p\pi^+\pi^+\pi^-\pi^0$  events ( $\sigma = 2.88 \pm 0.04$  mb<sup>(9)</sup>) will give a spurious  $pK^+K^-\pi^+$  fit; this causes a contamination of about 20% in the  $pK^+K^-\pi^+$  channel.

### 1.6.2 The channels $\Lambda K^+\pi^+$ and $\Sigma^0 K^+\pi^+$

Events ambiguous between the hypotheses:

$$\Lambda_{\nu} K^+\pi^+ \text{ (e)}$$

and  $\Sigma_{\nu}^0 K^+\pi^+ \text{ (f)}$

were studied using the decay properties of the  $\Sigma^0 \rightarrow \Lambda\gamma$  decay (see e.g. Butler<sup>(8)</sup>).

Each event ambiguous between (e) and (f) was transformed to the  $\Sigma^0 \rightarrow \Lambda\gamma$  rest system. In this system the  $\Sigma^0 \rightarrow \Lambda\gamma$  decay should show isotropy. Instead, for these ambiguous events we observe a pronounced peaking of the  $\gamma$ -distribution in the direction of the measured tracks at the primary vertex (beam,  $K^+$ ,  $\pi^+$ ). The decay cosine distributions of the  $\gamma$  with respect to the direction of these tracks are given in figs. I.3 (a), I.3 (c) and I.3 (e) respectively. Fig. I.3 (g) shows the  $\cos(\gamma.\pi^+)$  versus  $\cos(\gamma.K^+)$  distribution for the ambiguous events with  $\cos(\gamma.\text{beam}) < 0.8$ . We observe that almost all events lie near the boundaries. This justifies the decision to assign all events ambiguous between (e) and (f) to hypothesis (e). Moreover, for  $\Sigma^0_V K^+ \pi^+$  fits *not* ambiguous with (e) the  $\gamma$ -decay cosine distributions are compatible with isotropy and do not show an important loss in the boundary region - see figs. I.3 (b), I.3 (d) and I.3 (f).

To explain the anisotropy of the ambiguous events we consider a  $\Lambda K^+ \pi^+$  event in the  $\Lambda$  rest frame. If we try to fit a  $\Sigma^0$  instead of a  $\Lambda$ , the energy (momentum) of the incoming particles has to be increased and/or the energy (momentum) of the outgoing charged particles has to be decreased to accommodate the energy (momentum) given to the  $\gamma$ . The fitting process will thus generally find the freedom to fake such a  $\gamma$  near the directions of the charged primary vertex tracks.

### I.6.3 The channels with $\Lambda(\Sigma^0)K^0$ production

The numbers of events found in the samples:

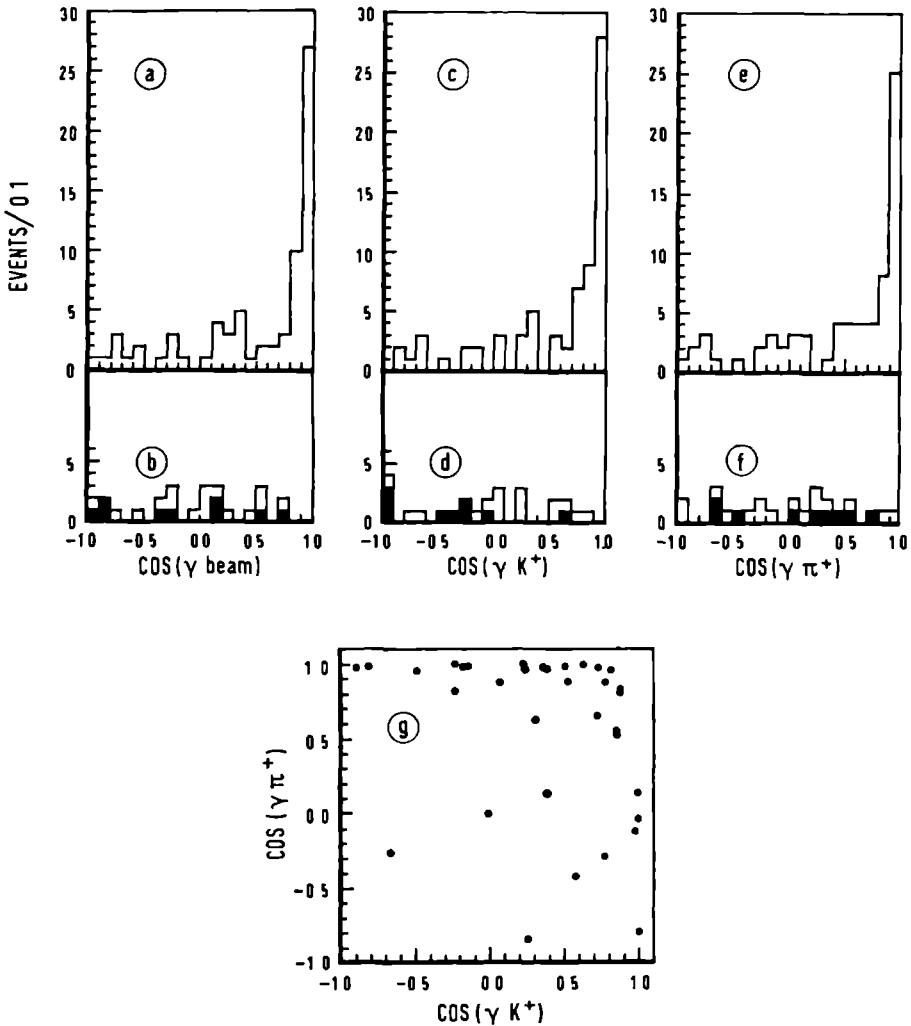


Fig. I.3 Decay cosine distributions of the  $\gamma$  from the decay  $\Sigma^0 \rightarrow \Lambda\gamma$  in the  $\Sigma^0$  rest system. The distributions are from  $\Sigma^0 K^+ \pi^+$  fits ambiguous (a,c,e,g) and not ambiguous (b,d,f) with a  $\Lambda K^+ \pi^+$  fit. Unambiguous  $\Sigma^0 K^+ \pi^+$  events are shaded. The scatter plot (g) is for ambiguous events with  $\cos(\gamma, \text{beam}) < 0.8$ .

$$\Lambda_{\nu} K^{\circ} \pi^{+} \pi^{+} \quad (g)$$

$$\Lambda K_{\nu}^{\circ} \pi^{+} \pi^{+} \quad (h)$$

$$\Lambda_{\nu} K_{\nu}^{\circ} \pi^{+} \pi^{+} \quad (i)$$

do not agree with the known branching ratios for charged  $\Lambda$  and  $K^{\circ}$  decay (modified for bubble chamber geometry, angular loss, etc. - see section II.5.7 for a full discussion). Compared to (h), the number of events in (g) is too high, in (i) too low.

The missing mass squared distribution  $M_M^2(\Lambda)$  from sample (h) is fairly symmetric around the squared mass value of the  $\Lambda$ . However, the  $M_M^2(K^{\circ})$  distribution from sample (g), which should be symmetric around  $M^2(K^{\circ})$  (cf. the distribution of  $M_M^2(K^{\circ})$  from  $pK_{\nu}^{\circ}K^{\circ}\pi^{+}$  in fig. I.4.a), shows a tail towards higher mass.

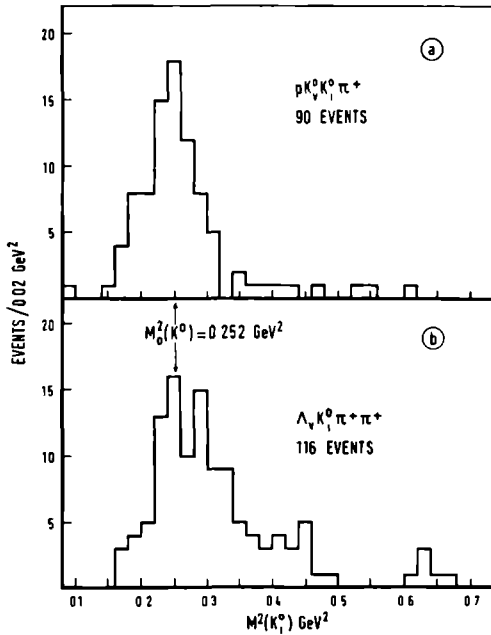


Fig. I.4 Missing mass squared distributions of the invisible  $K^{\circ}$  in the reaction  $pK_{\nu}^{\circ}K^{\circ}\pi^{+}\pi^{+}$  (a) and  $\Lambda_{\nu}K_{\nu}^{\circ}\pi^{+}\pi^{+}$  (b).



values (fig. 1.4.b), indicating contamination by other channels, such as  $\Lambda_V K^0 \pi^+ \pi^+ m \pi^0$  ( $m \geq 1$ ),  $\Sigma_V^0 K^0 \pi^+ \pi^+ m \pi^0$  ( $m \geq 0$ ), etc. We decided to remove all events with  $M_M^2(K^0) > 0.35 \text{ GeV}^2$  from channel (g); these events amount to approximately 1/3 of the channel (g) sample. A fraction of these events was added to the sample

$$\Lambda_V K^+ \pi^+ \pi^0 \quad (j)$$

the fraction required was estimated by redistributing all events ambiguous between (g) and (j) proportionally to the non ambiguous events. After the removal of events from (g) the experimental ratio between (g) and (h) is as required. We observe only  $(73 \pm 10)\%$  of the events predicted for (i) by the sample (h) and the corrected sample (g). It is however plausible that, due to measurement errors, the missing (10) 4C-events have been lost to lower constraint hypotheses (with extra  $\pi^0$  mesons).

Repeating the same analysis for the samples (\*):

$$\Lambda_V(\Sigma_V^0) K^0 \pi^+ \pi^+ (m \pi^0) \quad m \geq 1 \quad (0) \quad (k)$$

$$\Lambda_V(\Sigma_V^0) K_V^0 \pi^+ \pi^+ (m \pi^0) \quad m \geq 1 \quad (0) \quad (l)$$

we find an approximately complementary situation, the number of events in (k) being too low when compared to (l). Adding to sample (k) the remaining events discarded from (g) does not fully compensate this effect. We accept this as an indication that sample (l) is contaminated; the number of contaminating events is compatible with the loss in sample (i).

(\*) *Note.* We do not use the O-C sample with  $K_V^0$  only, because this sample may also include events of the type  $n K_V^0 K^0 \pi^+ \pi^+ (m \pi^0) \quad m \geq 0.$

### *I.7 Summary of Data*

A summary of each accepted hypothesis was written onto a magnetic tape (Data Summary Tape) by the program SLICE (2). Using identification data as input information, this program selected the accepted hypotheses from the GRIND output tape. In addition, other quantities needed for the analysis of the event were calculated from the GRIND data. Details can be found in ref. 2.

*References - Chapter I*

- (1) D.J. Schotanus, Ph.D. Thesis, Nijmegen 1971.
- (2) Descriptions can be found in the CERN program library,  
long write-up no's:  
X201-THRESH  
X601-GRIND  
Y100-SLICE.
- (3) B. Wagini, Diplomarbeit, Bonn 1967.
- (4) R. Böck, CERN 60-30 (1960) and CERN 61-29 (1961).  
B. Ronne, Kinematical Analysis of Bubble Chamber Pictures,  
Proceedings of the 1964 Easter School for Physicists,  
CERN 64-13, Vol.I (1964).
- (5) G. Lynch, UCRL 10335 (1962).
- (6) See for example:  
S.S. Yamamoto, L. Bertanza, G.C. Moneti, D.C. Rahm and  
I.O. Skillicorn,  
Phys. Rev. 134, B383 (1964).
- (7) Phu-Tho-Thuan, Diplomarbeit, Bonn 1968.
- (8) W.R. Butler, D.G. Coyne, G. Goldhaber, J. MacNaughton and  
G.H. Trilling, Phys.Rev. D7, 3177 (1973).
- (9) D.J. Schotanus, C.L. Pols, D.Z. Toet, R.T. Van De Walle,  
K. Böckmann, K. Sternberger, B. Wagini, G. Winter,  
J.V. Major, E. Cirba, R. Vanderhaghen, G. Rinaudo and  
A. Werbrouck,  
Nucl. Phys. B25, 109 (1970).
- (10) M. Aderholz, J. Bartsch, R. Schulte, R. Speth, H.H. Kaufmann,  
S. Nowak, M. Bardadin-Otwinowska, V.T. Cocconi, J.D. Hansen,  
J. Loskiewicz, G. Kellner, A. Mihul, D.R.O. Morrison,  
H. Tøfte, A. Eskreys, K. Juszcak, D. Kisielewska, P. Malecki,  
W. Zielinski, H. Piotrowska and A. Wroblewski,  
Nucl. Phys. B11, 259 (1969).

- (11) W.A. Cooper, W. Manner, B. Musgrave, D. Pollard and L. Voyvodic, Nucl. Phys. B23, 605 (1970).
- (12) E. Keil and W.W. Neale, CERN/TC/02, 63-3 (1963).
- (13) Parameters of the 1.5 m. Hydrogen Bubble Chamber, CERN/TC/NBC, 64-1 (1964).  
W.T. Welford, Applied Optics 2, 981 (1963).
- (14) The Magnetic Field of the British 1.5 m Bubble Chamber, CERN/TC/NBC, 63-2 (1963).

## CHAPTER II

## ESTIMATION OF CHANNEL CROSS SECTIONS

## II.1 Introduction

As the words 'channel' and 'reaction' have different meanings with different authors, we first define their meaning as used in this thesis.

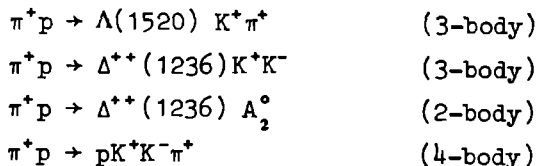
A *channel* will be called the totality of transitions from our initial state to a specific final state characterized in terms of *stable* and/or *semi-stable* particles, irrespective of the intermediate states through which this final state was reached. In general we denote by (semi-)stable particles the particles that (have a mean life long enough to) leave a visible track in the bubble chamber, if charged. The  $\pi^0$  meson and the  $\Sigma^0$  are exceptions or borderline cases. These particles are treated as semi-stable particles, although they really live too short ( $< 10^{-16}$  and  $< 10^{-14}$  sec. respectively) to produce a visible decay path. This can be done without problems in 1-C situations where these particles are the unseen neutrals that are reconstructed from the energy-momentum balance. The treatment of the  $\Sigma^0$  in events with visible  $\Lambda$  decay has been discussed in sect. I.4.

A *reaction* will be called a transition from our initial state to a specific final state characterized in terms of particles *directly produced* by the interaction, whether (semi-) stable or not. In this case the final state may contain short lived (unstable) particles, the so-called *resonances* - usually decaying via strong interactions. Their short mean lifetime

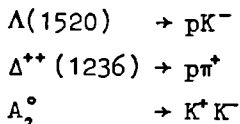
implies, that even if charged they cannot produce a visible track in the bubble chamber. The presence of a specific resonance can be detected by examining the so-called effective mass distribution of the possible decay products of that resonance (see sect. III.2.1).

Knowing the identity (masses) of all (semi-)stable particles, we can in principle classify each individual event into a channel. If no resonances are produced, the channel and reaction classifications coincide and can be performed on an event-by-event basis. If however reactions involving resonance production are present, their contributions can be determined in a statistical way only, e.g. on the basis of the effective mass distributions mentioned above.

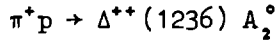
A specific channel thus may contain several reactions. On the other hand, as many resonances have more than one decay mode, one reaction may feed more than one channel. An illustrative example is the *channel*  $pK^+K^-\pi^+$  which contains the *reactions* (section III.3.4):



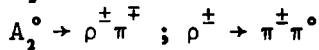
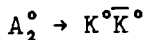
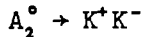
with the following decays of the resonances:



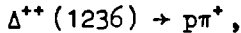
On the other hand, consider for example the above mentioned two body *reaction*:



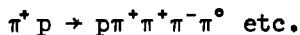
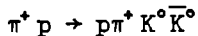
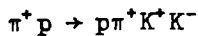
It is known that the resonance  $A_2^0$  can decay into different modes e.g.:



Considering only the decay:



we see that the above mentioned *reaction* may be present in the *channels*:



In this chapter we will calculate the *channel* cross sections. We start with a discussion of the acceptance criteria and continue with a description of the scanning and decay volumes. We next give the formulae and input quantities needed for cross-section calculations. The determination of and correction for losses form the subject of the subsequent sections. The channel cross section results are presented in table II.25

to II.27. At the end of this chapter a review of cross sections obtained in other experiments is given. The reaction cross sections are dealt with in the next chapter.

## II.2 Acceptance criteria

The events used for cross section calculations were selected using the criteria mentioned in section I.5. For decays, we imposed the following additional "length-criteria":

(a) The decay vertex must lie within the decay volume boundaries. (For a description: cf. sect. II.3).

(b) The projected distance between the production - and the decay - vertex must be  $\geq 0.5$  cm. By projected distance we mean the apparent distance in a plane perpendicular to the camera axes.

The purpose of criterion (a) is to eliminate events with a decay close to the chamber boundaries. In these cases the decay tracks are often too short to allow a reliable measurement. Criterion (b) removes events with tracks showing a decay near the vertex. The production angles (azimuth, dip) of such tracks can only be determined with large uncertainty.

Rejecting events using a sharp cut-off has the advantage that the losses due to this procedure are more easily calculable (sect. II.5.4).

The numbers of events ( $N_i$ ' - see section II.4) accepted for cross-section calculation are listed in tables II.1 - II.15. Each table represents a different topology. They generally are arranged in the form of a matrix. The most probable hypothesis determines the *row* where the event is located,



the second most probable hypothesis the *column*. Unambiguous events thus lie on the diagonal. As a consequence of our classification criteria some intersections cannot be populated; we indicate this by a dot in the corresponding squares.

### *II.3 Scanning volume and decay volume*

We did not accept interactions close to the chamber boundaries, because in general one or more of the produced tracks will then be too short to allow a reliable determination of its momentum. A so-called *scanning-volume* was imposed at the beginning of the experiment. Only events with a primary vertex inside this volume were accepted. The shape and position of the scanning-volume were fixed with respect to the so-called fiducial marks. The fiducial marks are crosses of different shapes on the inner (liquid touching) surfaces of the bubble chamber windows. The coordinates of these marks are known with great accuracy. They are visible on the bubble chamber pictures and some of them are measured together with the events in order to serve as reference points during the geometrical reconstruction. If the scanning-volume has been well chosen, one can expect an almost flat distribution of interaction points along the beam direction. We found this to be the case.

Furthermore, for an event involving a decay ( $V^0$ ,  $V^\pm$ ) we also required the decay vertex to be within the so-called *decay-volume*. Its boundary in the "downstream" region of the beam was determined by comparing decay-vertex losses for upstream primary vertices with the losses observed for downstream primary vertices.



TABLE II.2

TOPOLOGY: 2 PRONG + 2 $V^0$									
secondary hypothesis most probable hypothesis	$pK^0\bar{K}^0\pi^+$	$pK^0\bar{K}^0\pi^+\pi^0$	$pK^0\bar{K}^0\pi^+\pi^0$ $m \geq 2$	$nK^0\bar{K}^0\pi^+\pi^+$	$nK^0\bar{K}^0\pi^+\pi^+\pi^0$ $m \geq 1$	$\Lambda K^0\pi^+\pi^+$	$\Sigma^0 K^0\pi^+\pi^+$	$\Lambda K^0\pi^+\pi^+\pi^0$	$\Lambda/\Sigma^0 K^0\pi^+\pi^+\pi^0$ $m \geq 2/1$
$pK^0\bar{K}^0\pi^+$	29								
$pK^0\bar{K}^0\pi^+\pi^0$	.	8	1	1		.			
$pK^0\bar{K}^0\pi^+\pi^0$ $m \geq 2$	.	.		.		.	.	.	
$nK^0\bar{K}^0\pi^+\pi^+$	.			6		.			
$nK^0\bar{K}^0\pi^+\pi^+\pi^0$ $m \geq 1$	.	.		.		.	.	.	
$\Lambda K^0\pi^+\pi^+$						14	6		
$\Sigma^0 K^0\pi^+\pi^+$						7	2	1	
$\Lambda K^0\pi^+\pi^+\pi^0$	.	1				.	1	25	
$\Lambda/\Sigma^0 K^0\pi^+\pi^+\pi^0$ $m \geq 2/1$	.	.		.		.	.	.	6

TABLE II.3

TOPOLOGY: 4 PRONG + 1 $V^0$									
NKK ( $m\pi$ ) HYPOTHESES *)									
secondary hypothesis most probable hypothesis	$pK^+ \bar{K}^0 \pi^+ \pi^-$	$pK^+ \bar{K}^0 \pi^+ \pi^- \pi^0$	$pK^+ \bar{K}^0 \pi^+ \pi^- m\pi^0$ $m \geq 2$	$pK^0 K^- \pi^+ \pi^+$	$pK^0 K^- \pi^+ \pi^+ \pi^0$	$pK^0 K^- \pi^+ \pi^+ \pi^-$	$nK^+ \bar{K}^0 \pi^+ \pi^+ \pi^-$	$nK^+ \bar{K}^0 \pi^+ \pi^+ \pi^- m\pi^0$ $m \geq 1$	$nK^0 K^- \pi^+ \pi^+ \pi^+$
$pK^+ \bar{K}^0 \pi^+ \pi^-$	29	2		4					
$pK^+ \bar{K}^0 \pi^+ \pi^- \pi^0$	.	10		.	2	4			
$pK^+ \bar{K}^0 \pi^+ \pi^- m\pi^0$ $m \geq 2$	.	.		.	.	.	.		.
$pK^0 K^- \pi^+ \pi^+$	3			24					
$pK^0 K^- \pi^+ \pi^+ \pi^0$	.	2		.	4	3			
$pK^0 K^- \pi^+ \pi^+ \pi^-$	.		1	.	1	9			
$nK^+ \bar{K}^0 \pi^+ \pi^+ \pi^-$	.			.			1		
$nK^+ \bar{K}^0 \pi^+ \pi^+ \pi^- m\pi^0$ $m \geq 1$	.	.		.	.	.	.	1	.

\*) non populated channels have been omitted.

TABLE II.4

TOPOLOGY: 4 PRONG + 1 $V^0$										
$Y^0 K$ ( $m\pi$ ) HYPOTHESES										
secondary hypothesis  most probable hypothesis	$\Lambda K^+ \pi^+ \pi^+ \pi^-$	$\Sigma^0 K^+ \pi^+ \pi^+ \pi^-$	$\Lambda K^+ \pi^+ \pi^+ \pi^0$	$\Lambda/\Sigma^0 K^+ \pi^+ \pi^+ \pi^- m\pi^0$ $m \geq 2/1$	$\Lambda_V K^0 \pi^+ \pi^+ \pi^+ \pi^-$	$\Lambda_V K^0 \pi^+ \pi^+ \pi^+ \pi^-$	$\Sigma^0 K_V^0 \pi^+ \pi^+ \pi^+ \pi^-$	$\Lambda_V/\Sigma^0 K_V^0 \pi^+ \pi^+ \pi^+ \pi^- m\pi^0$ $m \geq 1/0$	$\Lambda/\Sigma^0 \left. \begin{matrix} K_V^0 \\ n\bar{K}^0 \end{matrix} \right\} \pi^+ \pi^+ \pi^+ \pi^- m\pi^0$ $m \geq 1/0$	$N\bar{K}K(m\pi)$ hypotheses
$\Lambda K^+ \pi^+ \pi^+ \pi^-$	33	11								
$\Sigma^0 K^+ \pi^+ \pi^+ \pi^-$	7	12	3							
$\Lambda K^+ \pi^+ \pi^+ \pi^- \pi^0$	.	4	54		6					
$\Lambda/\Sigma^0 K^+ \pi^+ \pi^+ \pi^- m\pi^0$ $m \geq 2/1$	.	.	.	1	.	.	.	1		
$\Lambda_V K^0 \pi^+ \pi^+ \pi^+ \pi^-$	.		3	3	11					
$\Lambda K_V^0 \pi^+ \pi^+ \pi^+ \pi^-$	.					5				2*
$\Sigma^0 K_V^0 \pi^+ \pi^+ \pi^+ \pi^-$	.									
$\Lambda_V/\Sigma^0 K_V^0 \pi^+ \pi^+ \pi^+ \pi^- m\pi^0$ $m \geq 1/0$	.	.	.		.	.	.			
$\Lambda/\Sigma^0 \left. \begin{matrix} K_V^0 \\ n\bar{K}^0 \end{matrix} \right\} \pi^+ \pi^+ \pi^+ \pi^- m\pi^0$ $m \geq 1/0$	.	.	.		.	.	.		1	
* ambiguous with $nK^+ \bar{K}^0 \pi^+ \pi^+ \pi^-$										

TABLE II.5

TOPOLOGY: 4 PRONG + 2 $V^0$ *)				
secondary hypothesis most probable hypothesis	$pK^0\bar{K}^0\pi^+\pi^+\pi^-\pi^-$	$pK^0\bar{K}^0\pi^+\pi^+\pi^-\pi^0$	$\Lambda K^0\pi^+\pi^+\pi^-\pi^-$	$\Sigma^0 K^0\pi^+\pi^+\pi^-\pi^-$
$pK^0\bar{K}^0\pi^+\pi^+\pi^-\pi^-$	2			
$pK^0\bar{K}^0\pi^+\pi^+\pi^-\pi^0$	.	1	.	
$\Lambda K^0\pi^+\pi^+\pi^-\pi^-$				1
$\Sigma^0 K^0\pi^+\pi^+\pi^-\pi^-$				
*) non populated channels have been omitted				

TABLE II.6

TOPOLOGY: 2 PRONG, 1 $V^+$										
secondary hypothesis most probable hypothesis	$pK^+ \bar{K}^0$	$pK^+ \bar{K}^0 m\pi^0$ $m \geq 1$	$\Lambda K^+ \pi^+$	$\Sigma^0 K^+ \pi^+$	$\Lambda/\Sigma^0 K^+ \pi^+ m\pi^0$ $m \geq 1$	$\Sigma^+ K^+$	$\Sigma^+ K^+ \pi^0$	$\Sigma^+ K^+ m\pi^0$ $m \geq 2$	$\Sigma^+ K^0 \pi^+$	$\Sigma^+ K^0 \pi^+ m\pi^0$ $m \geq 1$
$pK^+ \bar{K}^0$	6	1	2			.		1		
$pK^+ \bar{K}^0 m\pi^0$ $m \geq 1$	.	3	.	.	2	.	.		.	
$\Lambda K^+ \pi^+$	2			3	1	.				
$\Sigma^0 K^+ \pi^+$			7		3	.				
$\Lambda/\Sigma^0 K^+ \pi^+ m\pi^0$ $m \geq 1$	.	4	.	.	14	.	.		.	
$\Sigma^+ K^+$	2					33	2	1		
$\Sigma^+ K^+ \pi^0$						.	19	3	16	1
$\Sigma^+ K^+ m\pi^0$ $m \geq 2$	.	1	.	.		.	.	6	.	
$\Sigma^+ K^0 \pi^+$						.	19	6	23	4
$\Sigma^+ K^0 \pi^+ m\pi^0$ $m \geq 1$	.		.	.	2	.	.	16	.	31

TABLE II.7

TOPOLOGY: 2 PRONG, 2 $V^+$			
secondary hypothesis most probable hypothesis	$\Sigma^+ K^+$	$\Sigma^+ K^+ \pi^0$	$\Sigma^+ K^+ m\pi^0$ $m \geq 2$
$\Sigma^+ K^+$	2	1	1
$\Sigma^+ K^+ \pi^0$	.	2	2
$\Sigma^+ K^+ m\pi^0$ $m \geq 2$	.	.	1

TABLE II.8

TOPOLOGY: 2 PRONG, 1 $V^+$ + 1 $V^0$										
secondary hypothesis \n most probable hypothesis	$pK^+\bar{K}^0$	$pK^+\bar{K}^0\pi^0$	$pK^+\bar{K}^0m\pi^0$ $m \geq 2$	$nK^+\bar{K}^0\pi^+$	$nK^+\bar{K}^0\pi^+m\pi^0$ $m \geq 1$	$\Lambda K^+\pi^+\pi^0$	$\Lambda/\Sigma^0 K^+\pi^+m\pi^0$ $m \geq 2/1$	$\Sigma^+ K^0\pi^+$	$\Sigma^+ K^0\pi^+\pi^0$	$\Sigma^+ K^0\pi^+m\pi^0$ $m \geq 2$
$pK^+\bar{K}^0$	1									
$pK^+\bar{K}^0\pi^0$	.	2						.		
$pK^+\bar{K}^0m\pi^0$ $m \geq 2$	.	.		.		.		.	.	
$nK^+\bar{K}^0\pi^+$	.		1	1				.		
$nK^+\bar{K}^0\pi^+m\pi^0$ $m \geq 1$	.	.		.		.		.	.	
$\Lambda K^+\pi^+\pi^0$	.					2	1	.		
$\Lambda/\Sigma^0 K^+\pi^+m\pi^0$ $m \geq 2/1$	.	.		.		.	4	.	.	
$\Sigma^+ K^0\pi^+$								8		
$\Sigma^+ K^0\pi^+\pi^0$	.							.	9	1
$\Sigma^0 K^0\pi^+m\pi^0$ $m \geq 2$	.	.		.	1	.		.	.	4

\*) non populated channels have been omitted



TABLE II.9

TOPOLOGY: 4 PRONG, $1 V^+$															
secondary hypothesis most probable hypothesis	$pK^+K^-\pi^+$	$pK^+K^-\pi^+\pi^0$ $m \geq 2$	$pK^+K^-\pi^+\pi^-\pi^0$ $m \geq 2$	$pK^+K^-\pi^+\pi^-\pi^0$ $m \geq 1$	$nK^+K^-\pi^+\pi^+$	$nK^+K^-\pi^+\pi^+\pi^0$ $m \geq 1$	$nK^+K^-\pi^+\pi^+\pi^0$ $m \geq 1$	$\Lambda K^+\pi^+\pi^-\pi^0$	$\Sigma^0 K^+\pi^+\pi^-\pi^0$	$\Lambda/\Sigma^0 \left\{ \begin{array}{l} K^+\pi^+\pi^+\pi^-\pi^0 \\ nK^0 \end{array} \right\}$ $m \geq 1/0$	$\Sigma^+ K^+\pi^+\pi^-\pi^0$	$\Sigma^+ K^+\pi^+\pi^-\pi^0$	$\Sigma^+ K^+\pi^+\pi^-\pi^+\pi^0$ $m \geq 2$	$\Sigma^+ K^+\pi^+\pi^-\pi^+\pi^0$ $m \geq 1$	$\Sigma^+ K^+\pi^+\pi^-\pi^+\pi^+\pi^0$ $m \geq 1$
$pK^+K^-\pi^+$	9														
$pK^+K^-\pi^+\pi^0$	.	4	2	2							.				
$pK^+K^-\pi^+\pi^+\pi^0$ $m \geq 2$	.	.	.	.	1	.	.	.	.	.	.	.	.	.	.
$pK^+K^-\pi^+\pi^-\pi^0$	.	2	1	1	1		1				.	1			
$pK^+K^-\pi^+\pi^-\pi^+\pi^0$ $m \geq 1$	.	.	.	.	5	.	.	.	.	.	.	.	.	.	.
$nK^+K^-\pi^+\pi^+$	.				1		2				.				
$nK^+K^-\pi^+\pi^+\pi^0$ $m \geq 1$	.				.		.	.	.	.	.	.	.	.	.
$\Lambda K^+\pi^+\pi^-\pi^0$	.				1			3							
$\Sigma^0 K^+\pi^+\pi^-\pi^0$	.								2		.				
$\Lambda/\Sigma^0 \left\{ \begin{array}{l} K^+\pi^+\pi^+\pi^-\pi^0 \\ nK^0 \end{array} \right\}$ $m \geq 1/0$	.	.	.	.	.	2	.	.	2	.	.	.	.	.	.
$\Sigma^+ K^+\pi^+\pi^-\pi^0$	.				1						49	2			
$\Sigma^+ K^+\pi^+\pi^-\pi^+\pi^0$	.						1				.	37	1	7	1
$\Sigma^+ K^+\pi^+\pi^-\pi^+\pi^+\pi^0$ $m \geq 2$	.	.	.	.	.	.	.	.	.	.	.	.	3	.	.
$\Sigma^+ K^+\pi^+\pi^+\pi^-\pi^0$	.										.	4	3	4	1
$\Sigma^+ K^+\pi^+\pi^+\pi^-\pi^+\pi^0$ $m \geq 1$	.	.	.	.	.	.	.	.	.	.	.	.	1	.	3

TABLE II.10

TOPOLOGY: 4 PRONG, 1 $V^+$ + 1 $V^0$			*)
$pK^+\bar{K}^0\pi^+\pi^-$		1	} unambiguous
$pK^+\bar{K}^0\pi^+\pi^-\pi\pi^0$	$m \geq 2$	1	
$\Lambda K^+\pi^+\pi^+\pi^-$		1	
$\Sigma^+K^0\pi^+\pi^+\pi^-$		4	
$\Sigma^+K^0\pi^+\pi^+\pi^-\pi^0$		6	
*) non populated channels have been omitted.			



TABLE II.12

TOPOLOGY: 4 PRONG, $1 V^- + 1 V^0$ *)					
secondary hypothesis most probable hypothesis	$pK^0 K^- \pi^+ \pi^+ m\pi^0$ $m \geq 2$	$nK^0 K^- \pi^+ \pi^+ \pi^+$	$\Sigma^- K^0 \pi^+ \pi^+ \pi^+$	$\Sigma^- K^0 \pi^+ \pi^+ \pi^+ \pi^0$	$\Sigma^- K^0 \pi^+ \pi^+ \pi^+ m\pi^0$ $m \geq 2$
$pK^0 K^- \pi^+ \pi^+ m\pi^0$ $m \geq 2$	$\diagdown$	.	.	.	
$nK^0 K^- \pi^+ \pi^+ \pi^+$	1	$\diagdown$	.		
$\Sigma^- K^0 \pi^+ \pi^+ \pi^+$			4		
$\Sigma^- K^0 \pi^+ \pi^+ \pi^+ \pi^0$			.	1	
$\Sigma^- K^0 \pi^+ \pi^+ \pi^+ m\pi^0$ $m \geq 2$		.	.	.	1

\*) non-populated channels have been omitted.

TABLE II.13

TOPOLOGY: 4 PRONG, $2 V^+$			
secondary hypothesis most probable hypothesis	$\Sigma^+ K^+ \pi^+ \pi^-$	$\Sigma^+ K^+ \pi^+ \pi^- \pi^0$	$\Sigma^+ K^+ \pi^+ \pi^- m\pi^0$ $m \geq 2$
$\Sigma^+ K^+ \pi^+ \pi^-$	3	1	
$\Sigma^+ K^+ \pi^+ \pi^- \pi^0$	.	6	1
$\Sigma^+ K^+ \pi^+ \pi^- m\pi^0$ $m \geq 2$	.	.	$\diagdown$

TABLE II.14

TOPOLOGY: 4 PRONG, 1 $V^+$ , 1 $V^-$	
$\Sigma^- K^+ \pi^+ \pi^+ \pi^0$	1 event (unambiguous)

TABLE II.15

TOPOLOGIES FOUND AND NOT FITTED IN GRIND	
TOPOLOGY	CANDIDATES
6 PRONG + 1 $V^0$	5
6 PRONG, 1 $V^+$	5 ( $\Sigma^+$ ), 6 ( $K^+$ ), 4 ( $\Sigma^+$ or $K^+$ )
6 PRONG, 1 $V^-$	7 ( $\Sigma^-$ ), 2 ( $K^-$ ), 5 ( $\Sigma^-$ or $K^-$ )
4 PRONG $\Xi^-$	$3 \pm 1$

The scanning and decay volumes finally accepted are defined by the coordinates in table II.16.

TABLE II.16

SCANNING VOLUME			
z coordinate limits	-20. cm	-29. cm	
Entrance limits	x	-22.7 cm	-23.9 cm
	y	-10.8 cm 11.5 cm	-11.3 cm 12.1 cm
Exit limits	x	45.7 cm	47.5 cm
	y	- 7.6 cm 15.6 cm	- 7.8 cm 16.4 cm
DECAY VOLUME			
Limits for	y	-15.0 cm	17.0 cm
Limits for	z	0. cm	-46.4 cm
Entrance	x	-20.0 cm	-26.2 cm
Exit	x	65.0 cm	77.0 cm

The shapes of the scanning volume and the decay volume as seen by the middle camera are given in fig. II.1.

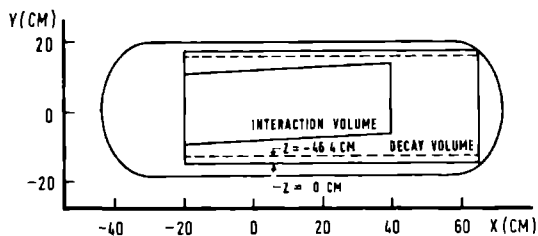


Fig. II.1 The interaction- and decay volume as seen by the middle camera.

## II.4 Cross section calculations

The calculation of the cross section  $\sigma_i$  for a certain final state  $i$  is based on the well known formula:

$$\sigma_i = N_i / \rho L.$$

The definition of the symbols is as follows:

(i)  $\rho$  = proton density in the liquid hydrogen.

In our experiment:

$$\rho = (3.64 \pm 0.03) \cdot 10^{22} \text{ cm}^{-3}.$$

(ii)  $L$  = total incident pion track length:

$$L = P n l c_a c_\mu$$

where:

. $P$  = number of pictures scanned. We found

$$P = (98.8 \pm 1.5) \cdot 10^3 \text{ for } V^\pm \text{ events and}$$

$$P = (121.6 \pm 1.5) \cdot 10^3 \text{ for } V^0 \text{ events.}$$

. $n$  = average number of tracks per picture entering the scanning volume. We found

$$n = 12.35 \pm 0.05.$$

This value was determined from a count of all beam tracks in all scanned frames within a sub-sample of 23 rolls spread evenly over the whole sample.

. $l$  = average track length for non-interacting tracks.

From the length of the scanning volume and the

beam direction we determined:

$$l = 70.1 \pm 0.1 \text{ cm.}$$

Interactions shorten the effective track length. The correction factor  $c_a$  (discussed next), is applied for this effect:

$c_a$  = correction for beam attenuation, given by:

$$c_a = l_c/l, \text{ where}$$

$$l_c = l - \rho\sigma_T \int_0^l \exp(-\rho\sigma_T l')(l-l') dl'.$$

$\sigma_T$  is the total cross section in our experiment. Using  $\sigma_T = (26.60 \pm 0.01) \text{ mb}$ , a value derived by interpolation from counter results <sup>(1,2)</sup>, we found:

$$c_a = 0.968 \pm 0.02.$$

$c_\mu$  = correction for contamination of the beam.

Possible contamination may consist of hadrons (mostly K,p), muons and electrons (from  $\pi$ -decay). The contamination from hadrons is presumably negligible compared to the other contaminations and  $c_\mu$  will therefore essentially only account for non hadronic contamination. From a comparison of our total track length with the one predicted from counter results, we will conclude (see end of this section) that

$$c_\mu = 1.00 \pm 0.01.$$

The resulting values for L are:



$$L = (8.28 \pm 0.31) \cdot 10^7 \text{ cm for } V^\pm \text{ events}$$

$$L = (10.19 \pm 0.34) \cdot 10^7 \text{ cm for } V^0 \text{ events.}$$

(iii)  $N_i$  = total number of events in final state  $i$ . This number is estimated as follows:

$$N_i = N_i^! c_s c_u c_p c_w$$

where:

$N_i^!$  = the number of events *classified* into final state  $i$  (Sect. II.2),

$c_s$  = a correction factor for scanning efficiency (Sect. II.5.1),

$c_u$  = a correction factor for unclassified events (Sect. II.5.2),

$c_p$  = a correction factor for the  $\chi^2$ -probability cut-off (Sect. II.5.3),

$c_w$  = a weight factor accounting for:

- events not meeting the length criteria (Sect. II.5.4),

- events missed due to small decay angles (Sect. II.5.5),

- neutral decay modes, decay modes not fitted and/or ignored in cross section calculation (Sect. II.5.6).

As can be seen from the cross section formula given above, the expression:

$$\sigma_o = (\rho L)^{-1}$$

gives the cross section per corrected event. We can thus write:

$$\sigma_i = N_i \sigma_o$$

Expressed in microbarns ( $1 \mu b = 10^{-30} \text{ cm}^2$ ), the quantity  $\sigma_o$  is called the microbarn-equivalent of the experiment. We found:

$$\sigma_o = (0.332 \pm 0.011) \mu\text{b/event for } V^\pm \text{ events,}$$

$$\sigma_o = (0.269 \pm 0.008) \mu\text{b/event for } V^0 \text{ events.}$$

Another method to determine the  $\mu\text{b}$ -equivalent directly uses the accurately known value of the total cross section  $\sigma_T$  <sup>(1, 2)</sup> (cf. supra):

$$\sigma_T = (26.60 \pm 0.01) \text{ mb}$$

From the sample of rolls processed by the different laboratories, 94 rolls (called sample S) with complete information on the number of interactions, scanning loss, etc. were selected. The corrected <sup>\*</sup>) total number of events in sample S was determined to be:

$$N_T(S) = (78100 \pm 40) \text{ events}$$

This leads to the following value for the microbarn - equivalent in sample S:

$$\sigma_o(S) = \frac{\sigma_T}{N_T(S)} = (0.341 \pm 0.002) \mu\text{b/event.}$$

On the basis of the experimentally determined average number of tracks per picture we calculated for sample S a total effective track length of:

<sup>\*</sup>) *Note.* A correction for lost elastic scattering events was included <sup>(2)</sup>.

$$L(S) = (7.87 \pm 0.25) \cdot 10^7 \text{ cm}$$

On the other hand, using  $\sigma_0(S)$ , we find:

$$L'(S) = [\rho\sigma_0(S)]^{-1} = (8.06 \pm 0.08) \cdot 10^7 \text{ cm}$$

The only possible difference between these two determinations stems from  $c_\mu$ . Non-hadron contamination can only play a role in  $L(S)$  which is essentially based on track counting, while  $L'(S)$  has been determined on the basis of strong interactions only. We found for  $c_\mu$ :

$$c_\mu = \frac{L'(S)}{L(S)} = 1.024 \pm 0.034$$

As values  $c_\mu > 0$  are 'unphysical' we have put:

$$c_\mu = 1.00 \pm 0.01$$

This result indicates that the beam contamination from non-hadron particles is negligible.

Using the  $\sigma_0$  value derived from the S-sample and the ratios between the track lengths found in the S-sample and in our  $V^\pm$  and  $V^0$  samples respectively, we derive:

$$\sigma_0(V^\pm) = (0.325 \pm 0.008) \text{ } \mu\text{b/event}$$

$$\sigma_0(V^0) = (0.264 \pm 0.006) \text{ } \mu\text{b/event}$$

These values again agree very well with the values given earlier, determined from our sample only.

In an analogous way we determined for the  $pK^+K^-\pi^+$  sample:

$$\sigma_0(pK^+K^-\pi^+) = (0.308 \pm 0.010) \text{ } \mu\text{b/event.}$$

Our cross section calculations are based on these latter three values.

### *II.5 Corrections applied to the number of events found experimentally*

These corrections fall into two categories:

a) Sample averaged corrections, like the corrections for scanning efficiency, unclassified events and  $P(\chi^2)$  - cutoff (see subsections II.5.1 - II.5.3).

b) 'Individual' (event-by-event) corrections like the corrections for events eliminated by the length criteria or lost due to a small decay angle configuration (subsections II.5.4 and II.5.5).

Combined weight factors for the various associated strange particle combinations are determined using the known decay branching ratios (subsections II.5.6 and II.5.7).

#### *II.5.1 The scanning efficiency correction ( $c_s$ )*

The probability for an event to be found by the scanners depends on its topology. In addition, the efficiency of the scanning also varies with time and scanning team.

We determine these efficiencies for different topologies under the simplifying assumption that all events within a topology have equal a priori probability to be seen. We use the two scans at our disposal. If we call:

$N_i$  : the number of events found in scan  $i$  ( $i = 1,2$ ),  
 $N_{12}$  : the number of events found twice (i.e. in both scans),  
 $N$  : the unknown total number of events in the topology considered, we can define the scanning efficiency for scan  $i$  by

$$e_i = N_i/N.$$

consequently we have:

$$N_{12} = e_1 e_2 N = e_1 N_2 = e_2 N_1$$

or

$$e_1 = N_{12}/N_2$$

$$e_2 = N_{12}/N_1$$

The total number of events found at least once is:

$$N_T = N_1 + N_2 - N_{12}$$

calling  $e_T = N_T/N$  the overall efficiency (of both scans together) we find:

$$e_T = e_1 + e_2 - e_1 e_2$$

The values  $c_s = (e_T)^{-1}$  for different topologies are listed in table II.17.

### II.5.2 The correction for unclassified events ( $c_u$ )

This correction factor accounts for events that could not be classified because of absence of an acceptable kinematical

TABLE II.17

SCANNING EFFICIENCY CORRECTIONS ( $c_s$ )	
Topology (see fig. I.2)	$c_s$
2 Prong + 1 $V^0$	$1.02 \pm 0.01$
2 Prong + 2 $V^0$	$1.03 \pm 0.01$
4 Prong + 1 $V^0$	$1.03 \pm 0.02$
2 Prong, 1 $V^+$	$1.04 \pm 0.01$
2 Prong, 1 $V^+$ + 1 $V^0$	$1.05 \pm 0.04$
4 Prong, 1 $V^+$	$1.08 \pm 0.04$
4 Prong, 1 $V^-$	$1.05 \pm 0.02$

solution (fit or nofit). In general this is due to the fact that the event, for one reason or another, is difficult to measure. Even in the absence of a (complete) fit, it is often possible to exclude certain interpretations, using topological features, fit information at one of the vertices etc.

Formally distributing the unclassified events over the different possible categories, in ratios proportional to the number of classified events found in each of them, one obtains correction factors  $c_u$  to each of the groups of classified events. They are listed in table II.18. For the  $V^\pm$  topologies the  $c_u$  factor is determined using events with  $\Sigma^\pm$  decay only, because we generally do not use events with  $K^\pm$  decay for cross section determination (see sect. II.5.6).

TABLE II.18

CORRECTIONS FOR UNCLASSIFIED EVENTS ( $c_u$ )	
Topology	$c_u$
2 Prong + 1 $V^0$	$1.36 \pm 0.02$
2 Prong + 2 $V^0$	$1.25 \pm 0.02$
4 Prong + 1 $V^0$	$1.50 \pm 0.02$
2 Prong, 1 $V^+$	$1.33 \pm 0.05$
2 Prong, 1 $V^+$ + 1 $V^0$	$1.58 \pm 0.15$
4 Prong, 1 $V^+$	$1.56 \pm 0.07$
4 Prong, 1 $V^-$	$1.30 \pm 0.10$

### II.5.3 The correction for $P(\chi^2)$ -cutoff ( $c_p$ )

In sect. I.5 we mentioned the  $P_n(\chi^2)$ -cutoff criteria for fits of different degrees of freedom  $n$ . A correction factor  $c_p$  is used to correct for the statistical losses resulting from this procedure:

$$c_p = 1 / [1 - P_n(\chi^2)_{\min}]$$

We list these factors as a function of  $n$  in table II.19.

### II.5.4 The correction for decays not meeting the length criteria ( $c_l$ )

For each accepted event we calculated the probability  $P_1$  for its decay to meet the 'length-criteria' (sect. II.2). We

TABLE II.19

CORRECTIONS FOR $P_n(X^2)$ -CUTOFF ( $c_p$ )	
Number of constraints of primary interaction	$c_p$
1	1.01
2	1.05
4	1.00

define the following quantities:

$m_0, p, \lambda$  - rest mass, laboratory momentum and dip angle of the decaying particle (D),

$t^*(X)$  - time interval - measured in the rest frame of D - between the moment of creation of D and the moment it has travelled a distance X in the lab,

$\tau$  - mean lifetime of D = (decay probability per unit time interval) $^{-1}$ ,

$l_0$  - minimum projected length cutoff in the lab system (= 0.5 cm, see sect. II.2),

L - potential path length of D, i.e. the path length when extrapolated towards the decay volume boundary using range-momentum relations and the magnetic field map.

The probability  $P_1$  for D to decay within the decay volume at a projected distance from the vertex  $\geq l_0$  can now be expressed as:

$$P_1 = \exp [-t^*(l_0)/\tau] - \exp [-t^*(L)/\tau]$$

or:

$$P_1 = \exp \left[ -m_0 \left( \int_0^{l_0} dl/p \right) / (c\tau \cos \lambda) \right] - \exp \left[ -m_0 \left( \int_0^L dl/p \right) / (c\tau) \right]$$



If D is a neutral particle, the integrals in the exponentials are simply equal to  $l_0/p_0$  and  $L/p_0$  resp. ( $p_0$  = the lab momentum of D at production).

If D is charged and range-momentum relations indicate that D cannot leave the decay volume without stopping, we have  $t^*(L) = \infty$  and the second term of  $P_1$  is zero.

The sample-averaged values  $c_1 = P_1^{-1}$  for the different strange particle decays considered are given in table II.20. As indicated, the value for  $c_1(\Sigma^+)$  has been determined using  $n\pi^+$  decays only.

TABLE II.20

CORRECTIONS FOR LENGTH-CUTOFF ( $c_1$ )	
Decay	$\bar{c}_1$
$\Lambda \rightarrow p\pi^-$	$1.11 \pm 0.01$
$K^0 \rightarrow \pi^+\pi^-$	$1.12 \pm 0.01$
$\Sigma^+ \rightarrow n\pi^+$	$1.23 \pm 0.03$
$\Sigma^- \rightarrow n\pi^-$	$1.09 \pm 0.01$

### II.5.5 The correction for angular loss ( $c_h$ )

If the angle between a charged particle and its decay product as seen by the cameras (projected angle) is very small, the decay is liable not to be recognized. This can also be the case for high momentum  $\Lambda$  and  $K^0$  decays lying in a decay plane approximately parallel to the camera axes. The projected opening angle is then small and the  $V^0$  may easily be mistaken for a

$\gamma$ -conversion.

A correction method to account for these losses is described in appendix B. The values of the correction factor  $c_h$  applicable for our  $\Lambda$ ,  $K^0$ ,  $\Sigma^-$  and  $\Sigma^+ \rightarrow n\pi^+$  samples are presented in table II.21.

TABLE II.21

CORRECTIONS FOR SMALL-ANGLE LOSS ( $c_h$ )	
Decay	$\bar{c}_h$
$\Lambda \rightarrow p\pi^-$	$1.03 \pm 0.02$
$K^0 \rightarrow \pi^+\pi^-$	$1.01 \pm 0.01$
$\Sigma^+ \rightarrow n\pi^+$	$1.20 \pm 0.03$
$\Sigma^- \rightarrow n\pi^-$	$1.16 \pm 0.05$

As can be seen in fig. B.2 (appendix B), the experimentally obtained distribution of the projected decay angle for ( $\Sigma^+ \rightarrow p\pi^0$ ) decays is much more concentrated towards small angles than the one for ( $\Sigma^+ \rightarrow n\pi^+$ ) decays. This can be understood from the fact that the velocity of the nucleon in the  $\Sigma$ -rest system is  $\sim 0.3 c$ , whereas for the  $\pi$ -meson this velocity is  $\sim 0.8 c$ . This means that, more than the  $\pi$ -meson, the nucleon will tend to follow the original  $\Sigma$ -direction in the laboratory. Thus a large percentage of ( $\Sigma^+ \rightarrow p\pi^0$ ) will be missed. On the basis of comparison with the ( $\Sigma^+ \rightarrow n\pi^+$ ) sample - which should be almost equally populated - we estimate this loss to be  $\sim 50\%$ . The characteristics of the experimentally observed ( $\Sigma^+ \rightarrow p\pi^0$ ) sample may thus differ considerably from the sample produced. This situation is made worse by the fact that small

angle ( $\Sigma^+ \rightarrow p\pi^0$ ) decays are often indistinguishable from small angle scatters with a very short recoil proton.

As a consequence of these facts we preferred not to 'correct' the ( $\Sigma^+ \rightarrow p\pi^0$ ) events and to use only events with ( $\Sigma^+ \rightarrow n\pi^+$ ) decay.

### II.5.6 The correction for unused decay modes ( $c_d$ )

Only the decaymodes that have a reasonable probability to occur in the bubble chamber are fitted in GRIND. This probability is a function not only of the mean lifetime of the strange particle but also of its branching ratio into the decaymode considered. The decaymodes considered are given in table II.22. As the branching ratios for these modes are known, it is easy to calculate the contribution of the remaining modes. The table presents the factors  $c_d = (\text{branching ratio})^{-1}$ .

In the following we discuss some details concerning these decaymodes:

(i) 'short' charged particle decays usually give a O-C fit and in many cases both  $\Sigma^-$  and K-solutions succeed. Unless a proton can be recognized on one of the primary or secondary tracks, we cannot make a definite choice between these solutions. A short  $K^+$  decay is however a priori much less probable than a  $\Sigma$  decay, because of the difference in mean lifetime between these particles. We therefore decided to accept fits involving short  $K^\pm$  decays only if they are unambiguous or if the  $P(\chi^2)$  for a primary vertex fit with a K on a short track is at least a factor five larger than that for the fit requesting the  $\Sigma$ .

(ii) The same mean lifetime argument also indicates that the sample of events showing a  $K^{\pm}$  decay in the bubble chamber is only a small fraction of the events involving  $K^{\pm}$  production. Each observed K-kink event thus has a large weight. The use of these events for calculation of cross sections is dangerous because a few wrong decisions or losses can lead to large errors. For the channels involving one-K-kink events we therefore base our cross section calculations on events where the "partner"-strange particle (see next section) shows a decay. We run into difficulties with this method if this partner is also a charged K, as is the case for all channels involving  $K^+K^-$  production:  $pK^+K^-\pi^+(m\pi^0)$  and  $nK^+K^-\pi^+\pi^+(m\pi^0)$  ( $m \geq 0$ ). This explains the large errors on the cross sections in these channels. The  $pK^+K^-\pi^+$  hypothesis was included in the hypothesis list for the 4-prong-no-kink events. In principle a comparison of the cross section calculated for this channel on basis of the events with and without K-kinks, would allow a check on the reliability of the kink-method. The four prong-no-kink information however contains a large uncertainty itself, because of contamination by other channels (section I.6.1).

(iii) For the reason why events with  $\Sigma^+ \rightarrow p\pi^0$  decay were not used for cross section calculation we refer to the foregoing section.

(iv) A  $K^0$  can with equal probability behave either as a short lived  $K^0$  ( $K_S^0$ ;  $\tau \approx 0.9 \times 10^{-10}$  sec) or as a long lived  $K^0$  ( $K_L^0$ ;  $\tau \approx 5.2 \times 10^{-8}$  sec). To find the same number of  $K_L^0$  decays as the number of  $K_S^0$  decays would require a  $K_L^0$  - decayvolume whose linear dimension are a factor 650 larger than the one used for  $K_S^0$  decays. As we find  $\sim 570$   $K^0$  decays in the accepted decayvolume we

TABLE II.22

DATA ON STRANGE PARTICLE DECAYS; CORRECTION FACTOR $c_d$							
Particle	Mean life (sec)	Main (charged) decay modes	Branching ratio (%)	Fitted	Used for cross sections	$c_d$	
$K^\pm$	$1.2371 \cdot 10^{-8}$	$\pi^\pm \nu$	$63.77 \pm 0.28$	yes	no *)	-	
		$\pi^\pm \pi^0$	$20.92 \pm 0.29$	yes	no *)	-	
		$\pi^\pm \pi^+ \pi^-$	$5.58 \pm 0.03$	no	-	-	
$K^0$ {	$0.862 \cdot 10^{-10}$	$K_S^0$ (50%)	$\pi^+ \pi^-$	$68.85 \pm 0.31$	yes	yes	$1.452 \pm 0.007$
		$K_L^0$ (50%)	$\pi^+ \pi^- \pi^0$	$12.6 \pm 0.3$	no	-	-
			$\pi^\pm \mu^\mp \nu$	$26.8 \pm 0.6$	no	-	-
			$\pi^\pm e^\mp \nu$	$39.0 \pm 0.6$	no	-	-
$\Lambda$	$2.521 \cdot 10^{-10}$	$p\pi^-$	$64.2 \pm 0.5$	yes	yes	$1.56 \pm 0.01$	
$\Sigma^+$	$0.800 \cdot 10^{-10}$	$p\pi^0$	$51.6 \pm 0.7$	yes	no	-	
		$n\pi^+$	$48.4 \pm 0.7$	yes	yes	$2.07 \pm 0.03$	
$\Sigma^0$	$< 1.0 \cdot 10^{-14}$	$\Lambda\gamma$	$\sim 100$	yes	yes	$1.56 \pm 0.01$	
$\Sigma^-$	$1.484 \cdot 10^{-10}$	$n\pi^-$	$\sim 100$	yes	yes	1.0	

\*) For exceptions: see section II.5.6

may neglect the possibility for the  $K_L^0$  mode to contribute to the  $V^0$ -sample seen in the chamber. Moreover, although the most important charged decay modes of the  $K_L^0$  (see table II.22) show the same charged particle topology as the  $K_S^0$ -decay, they need an additional neutral among the decay products and would thus have a small chance of faking a 3-C  $K_S^0$  decay fit. For all practical purposes we may neglect  $K_S^0$ -decays because of the small branching ratios involved.

### II.5.7 The combined correction factor $c_w$

As the total strangeness of our initial state is zero ( $S = 0$ ) and because strong interactions conserve this quantum number, strange particles ( $S \neq 0$ ) can only be produced in sets of 2 or more (associated production). In our experiment the most important combinations are:

$$\begin{aligned} &K^+\bar{K}^0, K^0\bar{K}^0, K^+K^-, K^0K^- \\ &K^+\Lambda, K^0\Lambda \\ &K^+\Sigma^+, K^0\Sigma^+, K^+\Sigma^0, K^0\Sigma^0, K^+\Sigma^-, K^0\Sigma^- \end{aligned}$$

For each of the particles in the combinations we can calculate the probability  $P_a$  for a decay that will be both *detected* and *acceptable*. We define an '*acceptable*' decay to be a decay that:

- (i) meets the 'length-criteria' (cf. sect. II.2)
- and (ii) is one of the accepted modes (cf. sect. II.5.6).

The probability  $P_a$  can then be expressed as (sect. II.5.4 - II.5.6):

$$P_a = P_l P_d P_h = (C_l C_d C_h)^{-1}$$

The probability that such an acceptable decay will be *detected* - i.e. will not be lost because of a small decay angle - is expressed in this formula by the factor  $P_h = (C_h)^{-1}$ . We list  $P_a$  for several decays in table II.23.

TABLE II.23

THE PROBABILITY $P_a$	
Decay	$\overline{P}_a$
$\Lambda \rightarrow p\pi^-$	$0.57 \pm 0.02$
$K^0 \rightarrow \pi^+\pi^-$	$0.30 \pm 0.01$ *)
$\Sigma^+ \rightarrow n\pi^+$	$0.32 \pm 0.02$
$\Sigma^- \rightarrow n\pi^-$	$0.76 \pm 0.06$
$\Sigma^0 \rightarrow \Lambda\gamma$	see $\Lambda$
*) $P_a(K^0) = \frac{1}{2} P_a(K_S^0)$	

Using the  $P_a$ -values for the individual particles we can now calculate the 'joint' probabilities  $P_w$  for each of the associated productions mentioned above to have one resp. both decays detected and acceptable. If we denote the two partners in a specific combination by  $S_1$  and  $S_2$ , the probability for an acceptable etc. decay of  $S_2$  *only* can be expressed as:

$$P_w(S_1 S_2; S_1, \overline{S}_2) = P_a(S_1)(1 - P_a(S_2))$$

and analogously for  $S_2$  *only*:

$$P_w(S_1 S_2; \overline{S}_1, S_2) = P_a(S_2)(1 - P_a(S_1))$$

For both decays to occur together we find:

$$P_w(S_1 S_2; S_1, S_2) = P_a(S_1)P_a(S_2)$$

The values of  $P_w$  and  $c_w = (P_w)^{-1}$  for the different associated productions considered are given in table II.24.

TABLE II.24

THE COMBINED CORRECTION FACTOR $c_w$			
Combination	Visible decay	$P_w (= c_w^{-1})$	$c_w$
$K^{\pm}K^{\circ}$	$K_S^{\circ}$	$P_a(K^{\circ})$	$3.32 \pm 0.07$
$K_S^{\circ}K_S^{\circ}$	$1K_S^{\circ}$	$2P_a(K_S^{\circ})(1-P_a(K_S^{\circ}))$	$2.09 \pm 0.02$
	$2K_S^{\circ}$	$P_a^2(K_S^{\circ})$	$2.75 \pm 0.12$
$K_S^{\circ}K_L^{\circ}$	$K_S^{\circ}$	$P_a(K_S^{\circ})$	$1.66 \pm 0.04$
$\Lambda K^+$	$\Lambda$	$P_a(\Lambda)$	$1.75 \pm 0.05$
$\Lambda K^{\circ}$	$\Lambda$	$P_a(\Lambda)(1-P_a(K^{\circ}))$	$2.51 \pm 0.08$
	$K_S^{\circ}$	$P_a(K^{\circ})(1-P_a(\Lambda))$	$7.75 \pm 0.36$
	$\Lambda K_S^{\circ}$	$P_a(\Lambda)P_a(K^{\circ})$	$5.81 \pm 0.20$
$\Sigma^+ K^+$	$\Sigma^+ \rightarrow \pi^+ n$	$P_a(\Sigma^+)$	$3.15 \pm 0.17$
$\Sigma^+ K^{\circ}$	$\Sigma^+ \rightarrow \pi^+ n$	$P_a(\Sigma^+)(1-P_a(K^{\circ}))$	$4.50 \pm 0.24$
	$(\Sigma^+ \rightarrow \pi^+ n)K_S^{\circ}$	$P_a(\Sigma^+)P_a(K^{\circ})$	$10.53 \pm 0.56$
$\Sigma^- K^+$	$\Sigma^-$	$P_a(\Sigma^-)$	$1.31 \pm 0.10$
$\Sigma^- K^{\circ}$	$\Sigma^-$	$P_a(\Sigma^-)(1-P_a(K^{\circ}))$	$1.88 \pm 0.15$
	$\Sigma^- K_S^{\circ}$	$P_a(\Sigma^-)P_a(K^{\circ})$	$4.35 \pm 0.36$



TABLE II.25

NK $\bar{K}$ ( $a\pi$ ) CHANNEL CROSS SECTIONS ( $\mu\text{b}$ )							
a = 0	a = 1	a = 2	a = 3	a = 4	a = 5		
$pK^+\bar{K}^0$ 52 ± 8	$pK^+\bar{K}^0\pi^0$ 107±12	$pK^+\bar{K}^0\pi^+\pi^-$ →				3±3	
*	*	$pK^+\bar{K}^0\pi^+\pi^-$ 49±9	$pK^+\bar{K}^0\pi^+\pi^-\pi^0$ 22±6	$pK^+\bar{K}^0\pi^+\pi^-\pi\pi^0$ →		2±2	
*	$pK^+K^-\pi^+$ 99±25	$pK^+K^-\pi^+\pi^0$ 62±20	$pK^+K^-\pi^+\pi\pi^0$ →			15±10	
*	$pK^0\bar{K}^0\pi^+\pi^0$ 87±11	$pK_S^0K_S^0\pi^+\pi^0$ 9±3	$pK_S^0K_S^0\pi^+\pi\pi^0$ →			< 5	
*	*	*	$pK^0\bar{K}^0\pi^+\pi^+\pi^-$ 16±6	$pK_S^0K_S^0\pi^+\pi^+\pi^-\pi^0$ 1± $\frac{2}{1}$	$pK_S^0K_S^0\pi^+\pi^+\pi^-\pi\pi^0$ →		< 3
*	*	$pK^0K^-\pi^+\pi^+$ 36±7	$pK^0K^-\pi^+\pi^+\pi^0$ 12±4	$pK^0K^-\pi^+\pi^+\pi\pi^0$ →			< 5
*	$nK^+\bar{K}^0\pi^+$ 96±12	$nK^+\bar{K}^0\pi^+\pi\pi^0$ →				5±5	
*	*	*	$nK^+\bar{K}^0\pi^+\pi^+\pi^-$ 1± $\frac{2}{1}$	$nK^+\bar{K}^0\pi^+\pi^+\pi^-\pi\pi^0$ →			2±2
*	*	$nK^+K^-\pi^+\pi^+$ 43±25	$nK^+K^-\pi^+\pi^+\pi\pi^0$ →			5± $\frac{20}{5}$	
*	*	$nK_S^0K_S^0\pi^+\pi^+$ 6±2	$nK^0\bar{K}^0\pi^+\pi^+\pi\pi^0$ →			< 5	
*	*	*	*	$nK^0\bar{K}^0\pi^+\pi^+\pi^+\pi^-\pi\pi^0$ →			< 5
*	*	*	$nK^0K^-\pi^+\pi^+\pi^+$ 3±3	$nK^0K^-\pi^+\pi^+\pi^+\pi\pi^0$ →			< 4
*) $pK_S^0K_S^0\pi^+$ : (27±6) $\mu\text{b}$ ; $pK_S^0K_L^0\pi^+$ : (32±7) $\mu\text{b}$							

TABLE II.26

YK ( $a\pi$ ) CHANNEL CROSS SECTIONS ( $\mu\text{b}$ )									
$a = 0$	$a = 1$	$a = 2$	$a = 3$	$a = 4$	$a = 5$				
*	$\Lambda K^+ \pi^+$ $\Sigma^0 K^+ \pi^+$	$65 \pm 9$ $17 \pm 6$	$\Lambda \chi^+ \pi^+ \pi^0$ $\Sigma^0 K^+ \pi^+ m \pi^0$	$139 \pm 11$	$\Lambda \chi^+ \pi^+ m \pi^0$		$39 \pm 4$		
*	*	*	$\Lambda / \Sigma^0 K^+ \pi^+ \pi^+ \pi^-$	$48 \pm 6$	$\Lambda K^+ \pi^+ \pi^+ \pi^- \pi^0$ $\Sigma^0 \chi^+ \pi^+ \pi^+ \pi^- m \pi^0$	$46 \pm 6$	$\Lambda \chi^+ \pi^+ \pi^+ \pi^- m \pi^0$	$2 \pm 2$	
*	*	$\Lambda K^0 \pi^+ \pi^+$ $\Sigma^0 K^0 \pi^+ \pi^+$	$73 \pm 10$ $11 \pm 8$	$\Lambda K^0 \pi^+ \pi^+ m \pi^0$ $\Sigma^0 K^0 \pi^+ \pi^+ m \pi^0$				$76 \pm 12$	
*	*	*	*		$\Lambda / \Sigma^0 K^0 \pi^+ \pi^+ \pi^+ \pi^-$	$12 \pm 10$	$\Lambda / \Sigma^0 K^0 \pi^+ \pi^+ \pi^+ \pi^- m \pi^0$	$4 \pm 4$	
$\Sigma^+ K^+$	$59 \pm 10$	$\Sigma^+ K^+ \pi^0$	$63 \pm 10$	$\Sigma^+ K^+ m \pi^0$				$15 \pm 6$	
*	*	$\Sigma^+ K^+ \pi^+ \pi^-$	$91 \pm 15$	$\Sigma^+ K^+ \pi^+ \pi^- \pi^0$	$90 \pm 15$	$\Sigma^+ K^+ \pi^+ \pi^- m \pi^0$		$7 \pm 4$	
*	$\Sigma^+ K^0 \pi^+$	$77 \pm 25$	$\Sigma^+ K^0 \pi^+ \pi^0$	$58 \pm 21$	$\Sigma^+ K^0 \pi^+ m \pi^0$			$27 \pm 14$	
*	*	*	*	$\Sigma^+ K^0 \pi^+ \pi^+ \pi^-$	$27 \pm 7$	$\Sigma^+ K^0 \pi^+ \pi^+ \pi^- \pi^0$	$14 \pm 10$	$\Sigma^+ K^0 \pi^+ \pi^+ \pi^- m \pi^0$	$< 10$
*	*	$\Sigma^- K^+ \pi^+ \pi^+$	$11 \pm 3$	$\Sigma^- K^+ \pi^+ \pi^+ \pi^0$	$10 \pm 3$	$\Sigma^- K^+ \pi^+ \pi^+ m \pi^0$		$3 \pm 2$	
*	*	*	*	$\Sigma^- K^0 \pi^+ \pi^+ \pi^+$	$9 \pm 3$	$\Sigma^- K^0 \pi^+ \pi^+ \pi^+ \pi^0$	$3 \pm 3$	$\Sigma^- K^0 \pi^+ \pi^+ \pi^+ m \pi^0$	$3 \pm 3$

## II.6 Channel cross sections

The channel cross sections are presented in tables II.25 and II.26. For some channels we are able to calculate the cross-section in more than one way:

(i) For channels with  $\Sigma^\pm K^0$  production we can either use the sample with  $\Sigma^\pm$  decay only or the sample where both particles decay.

(ii) For  $K^0 \bar{K}^0$  events we have in principle an analogous possibility. Here however there is a complication. The  $K_V^0 K_V^0$  sample practically only contains events with two short lived  $K^0$ 's:  $K_S^0 K_S^0$ . The  $K_V^0 K^0$  sample however may contain both events of the type  $K_S^0 K_S^0$  and  $K_S^0 K_L^0$ . We calculate the cross section for  $K_S^0 K_S^0$ -events from the  $K_V^0 K_V^0$  sample and from this we find the contribution of  $K_S^0 K_S^0$  to the  $K_V^0 K^0$  sample. The rest of  $K_V^0 K^0$  is then assumed to be  $K_S^0 K_L^0$ . Finally, because of CP-invariance we can put the cross section of the  $K_L^0 K_L^0$  component equal to that of the  $K_S^0 K_S^0$  component.

(iii) For  $\Lambda K^0$ -channels we have in principle three possibilities to calculate the cross section: from  $\Lambda_V K_V^0$ ,  $\Lambda_V K^0$  or  $\Lambda K_V^0$  (cf. sect. I.6.3).

(iv) For the  $\Sigma^0 K^0$ -channels we use two samples:  $\Lambda_V K_V^0$  ( $\gamma$  fitted) and  $\Sigma^0 K_V^0$  ( $\Sigma^0$  fitted).  $\Sigma^0 K^0$  events with  $\Lambda_V$  only are in the nofit category because of the two missing neutrals:  $\gamma$  and  $K^0$ . We cannot use this sample because it may be contaminated by events with extra  $\pi^0$ 's (cf. sect. I.6.3).

## II.7 Total strange particle cross section

For the total strange particle cross section in  $\pi^+p$  interactions at 5 GeV/c incident momentum we find:

$$\sigma (\pi^+p \rightarrow \text{strange particle channels}) = (1.9 \pm 0.1) \text{ mb}$$

This value contains an estimated  $(30 \pm 10)$   $\mu\text{b}$  contribution from six prong events involving strange particles.

In table II.27 we give a breakdown according to the baryon final state, the pion multiplicity and the prong number.

Table II.27 also presents the fractions of the cross section consisting of extrapolated events, i.e. strange particle events that do not or not clearly show a strange particle decay topology, but that are known to be present (sect. II.5). These events are potential contaminators of the 'bare' 2-prong and 4-prong samples, although many of them might not give a fit to the attempted non-strange 2-prong and 4-prong hypotheses. It is useful to know the a priori size of these sources. We repeat, that the only strange particle hypothesis incorporated in the analysis of our 'bare' 4-prong events was the  $pK^+K^-\pi^+$  hypothesis (sect. I.6.1).

## II.8 Results of other experiments

The total strange particle cross section as well as the cross sections of the more important channels with four bodies or less in the final state are shown in fig. II.2 together with results from some other experiments. The latter are taken from the CERN-HERA tables<sup>(3)</sup> (to which we refer for further details and references) and some other sources<sup>(4,5)</sup>.

TABLE II.27

BREAKDOWN OF THE STRANGE PARTICLE CROSS SECTION IN 2- AND 4-PRONGS									
Channel type	Cross sections ( $\mu\text{b}$ )				Total (mb)	2-prongs		4 prongs	
	a = 0	a = 1	a = 2	a $\geq$ 3		cross section (mb)	non-strange topology	cross section (mb)	non-strange topology
$\text{NK}\bar{\text{K}}$ ( $a\pi$ )	$52 \pm 8$	$390 \pm 30$	$230 \pm 35$	$100 \pm 30$	$0.77 \pm 0.05$	$0.39 \pm 0.02$	} 45%	$0.38 \pm 0.05$	} 72% *)
$\Lambda(\Sigma^0)\text{K}(a\pi)$	-	$82 \pm 11$	$220 \pm 20$	$230 \pm 20$	$0.53 \pm 0.03$	$0.42 \pm 0.02$		$0.11 \pm 0.01$	
$\Sigma^+\text{K}(a\pi)$	$59 \pm 10$	$140 \pm 30$	$160 \pm 30$	$170 \pm 20$	$0.53 \pm 0.05$	$0.30 \pm 0.04$	53%	$0.23 \pm 0.03$	62%
$\Sigma^-\text{K}(a\pi)$	-	-	$11 \pm 3$	$28 \pm 7$	$0.04 \pm 0.01$	-	-	$0.04 \pm 0.01$	32%
					$1.87 \pm 0.08$				

\*) In this percentage are included 4 prong  $p\text{K}^+\text{K}^-\pi^+$  events fitted by GRIND (43%)

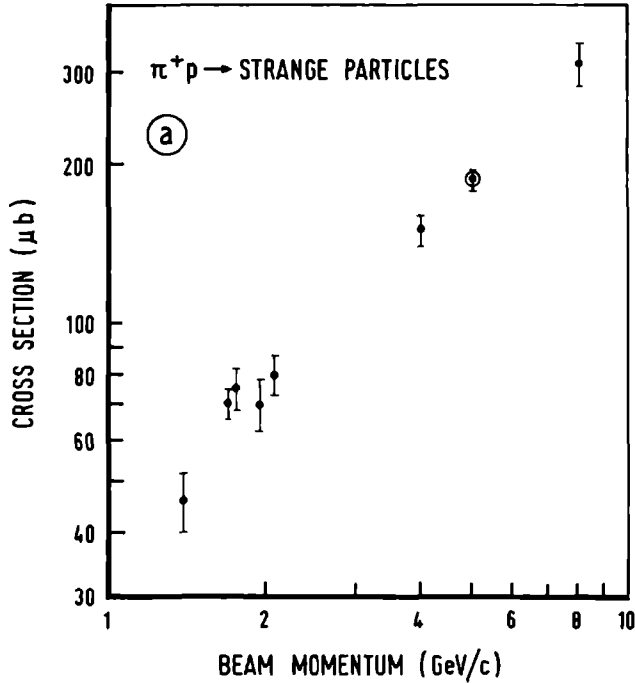


Fig. II.2 Total strange particle production cross sections (a) and cross sections of some strange particle channels (b-1) in  $\pi^+p$  interactions in the range  $1 \text{ GeV/c} < P_{\text{beam}} < 10 \text{ GeV/c}$ .

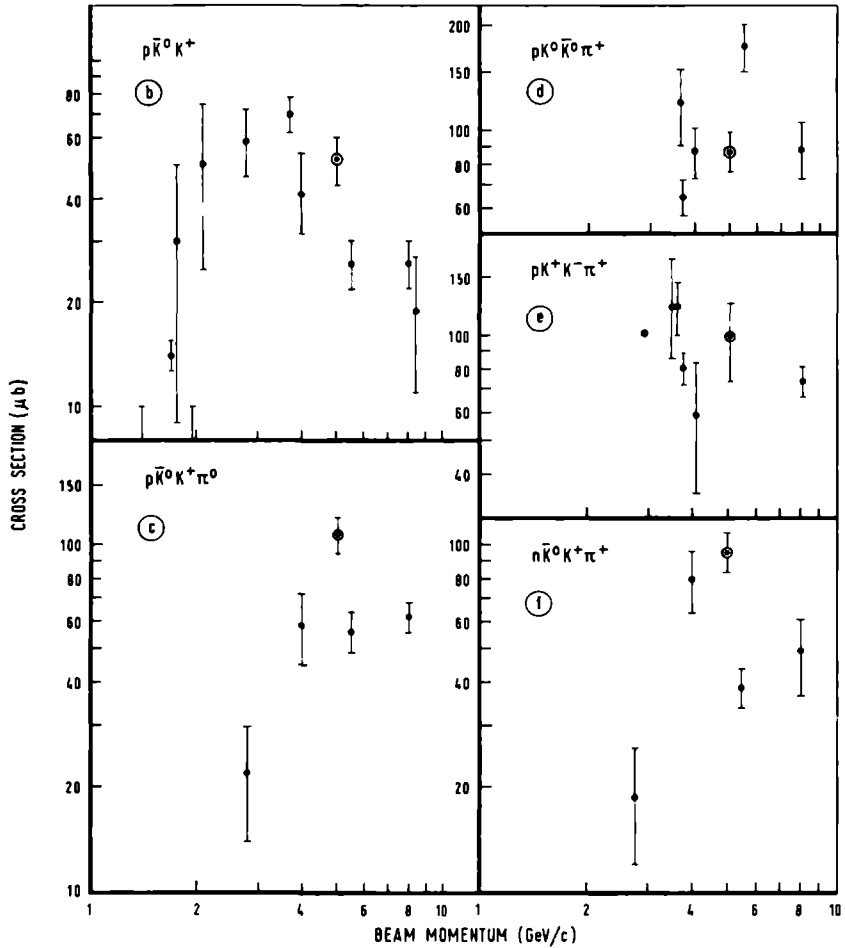


Fig. II.2 (continued)

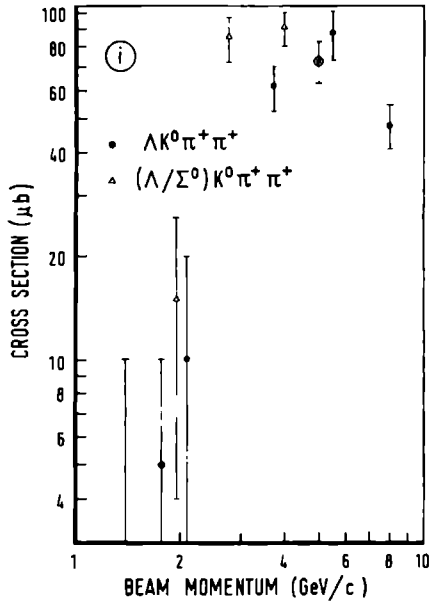
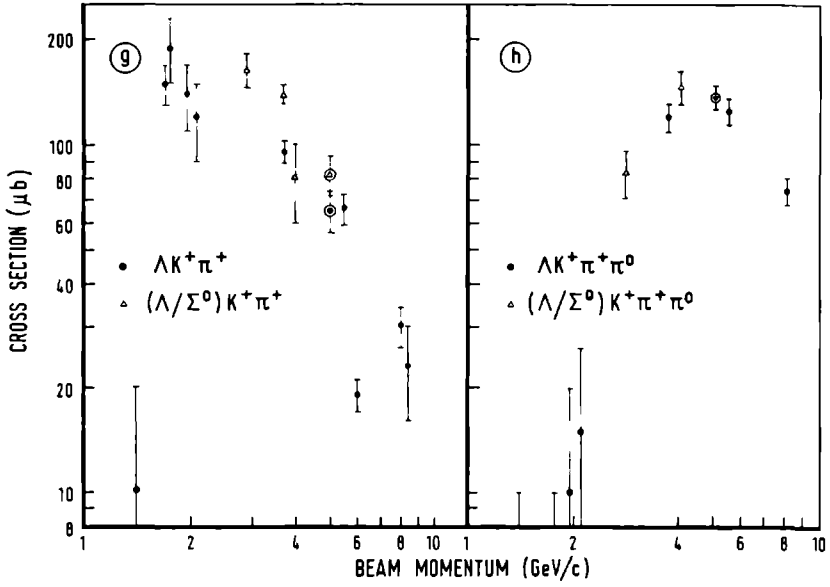


Fig. II.2 (continued)



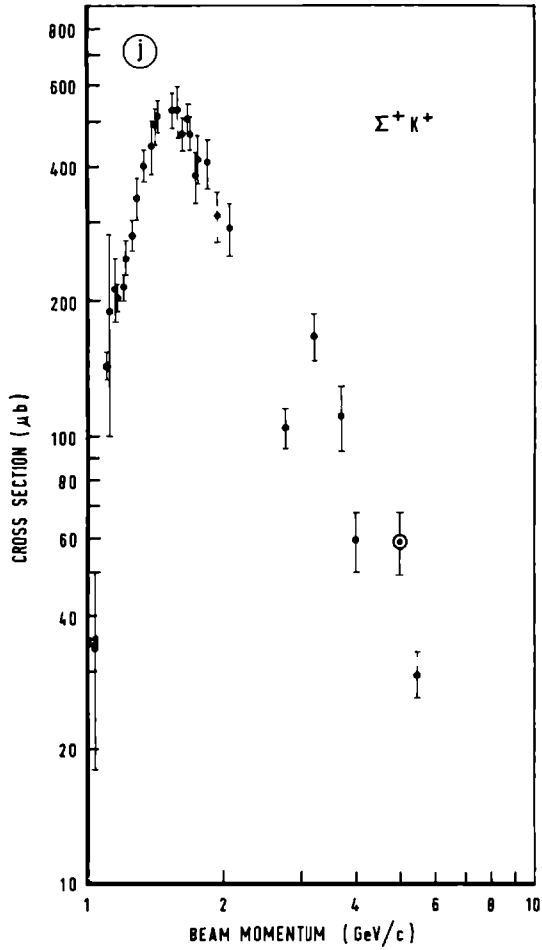


Fig. II.2 (continued)

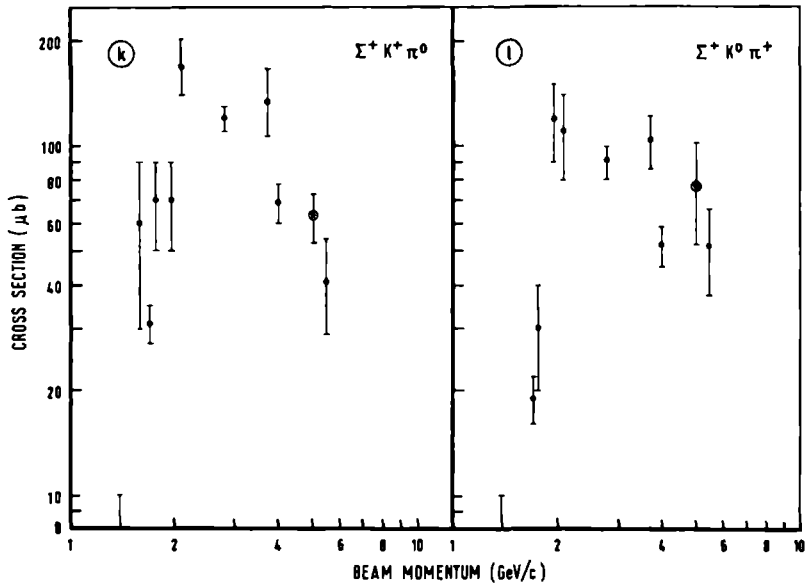


Fig. II.2 (continued)

*References - chapter II*

- (1) A. Citron, W. Galbraith, T.F. Kycia, B.A. Leontic,  
R.H. Phillips, A. Rousset, P.H. Sharp,  
Phys. Rev. 144, 1101 (1966).
- (2) D.J. Schotanus, Ph. D. Thesis, Nijmegen (1971).
- (3) E. Bracci, J.P. Droulez, E. Flaminio, J.D. Hansen and  
D.R.O. Morrison,  
CERN/HERA 72-1 (1972).
- (4) W.A. Cooper, W. Manner, B. Musgrave, D. Pollard and  
L. Voyvodič,  
Nucl. Phys. B 23, 605 (1970).
- (5) W.R. Butler, D.G. Coyne, G. Goldhaber, J. MacNaughton  
and G.H. Trilling,  
Phys. Rev. D7, 3177 (1973).

## CHAPTER III

## RESONANCE PRODUCTION AND REACTION CROSS SECTIONS

## III.1 Introduction

We divide the reactions found in the strange particle sample into two classes:

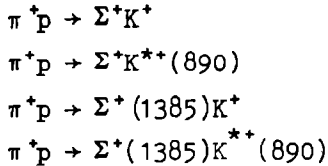
(i) reactions that are only *partially* represented in the strange particle sample.

This class contains the reactions producing particles with strangeness quantum number  $S = 0$ . These reactions lead to strange particle events due to the fact that one or more of the reaction products has a strange particle decay mode. The reaction  $\pi^+p \rightarrow \Delta^{++}(1236)A_2^0$  is an example of this class (see section II.1). If the branching fraction for decay into strange particles is as small as e.g. for the  $A_2$  (which has a branching ratio of  $\sim 5\%$  for decay into  $K\bar{K}$ ), the reaction itself is better studied using non-strange events. The strange particle events are then primarily used for the determination of branching ratios. This situation applies for most  $S = 0$  resonances. A counterexample is the  $\phi(1019)$  resonance which decays mainly into  $K\bar{K}$  (branching ratio  $\sim 82\%$ ).

(ii) reactions that are *exclusively* represented in the strange particle sample.

This class contains reactions producing particles with  $S \neq 0$ , i.e. reactions involving strangeness exchange - mechanisms (see chapter IV).

In our experiment we will be mainly concerned with the reactions:



This chapter starts with a description of the methods used for the estimation of resonance production. We then apply these methods to determine resonance production in some specific channels.

### *III.2 Methods of estimation*

#### *III.2.1 The estimation of background*

The resonances found in our experiment manifest themselves by enhancements (peaks, bumps) in effective mass distributions. The effective mass of a system of  $j$  particles (with masses  $m_j$ , momenta  $\vec{p}_j$  and energies  $E_j$ ) is defined by

$$M_{\text{eff}}^2(m_1, \dots, m_j) = \left( \sum_{i=1}^j E_i \right)^2 - \left( \sum_{i=1}^j \vec{p}_i \right)^2.$$

For a resonance of mass  $M$  decaying into  $j$  particles:

$$M \rightarrow m_1 + m_2 + \dots + m_j$$

one expects  $M_{\text{eff}}(m_1, \dots, m_j)$  to be equal to  $M$ . As a consequence of the uncertainty principle, a very short lifetime of a resonance

is coupled to an appreciable uncertainty in its mass value. The effective mass distribution of the decay products will show a characteristic width symbolized by  $\Gamma$ : the so-called 'full width at half height' (see sect. III.2.2). The resonance is said to cover a 'mass-band'.

If on the other hand the  $j$  particles are produced without forming a resonance, we can predict the distribution of  $M_{\text{eff}}(m_1, \dots, m_j)$  assuming that all kinematical configurations satisfying energy and momentum conservation are equally probable. Such distributions are called phase space (distributions)<sup>(1)</sup>.

In general an experimental effective mass distribution will be a mixture of resonance- and phase space distributions. Thus a fraction of the events with effective mass values within a specific resonance mass band considered, do not really originate from the decay of the resonance. We call these 'background'-events. Separation of these events from the real resonance events can only be done in an overall way and not on an event-by-event basis. The separation of background from the resonance sample is a key problem in the estimation of resonance production. As an approximation for the distribution of the background one either uses the phase-space prediction or an interpolation from neighbouring non-resonant regions (in most cases by a handdrawn curve). The latter method is generally used if statistics are low and the total information about the channel is scarce. The phase space method can further be refined by including the influence ('reflection') of resonance production observed in the other particle combinations.

### III.2.2 Estimation of resonance production

Two methods are used for quantitative determination of resonance production:

*method A: Event counting above background*

If statistics are low we use a method of resonance production estimation which is as simple as our background procedure for this situation, i.e. we just count the events above background within the resonance mass band. A correction for resonance production outside this band (tail correction - see below) is made afterwards.

*method B: Fitting of background + resonance curves to the experimental effective mass plot.*

We denote the experimental effective mass distribution by  $E(M)$ , the background effective mass distribution by  $B(M)$  and the effective mass distribution of the  $i$ -th resonance by  $R_i(M)$ . The normalization is given by the relations:

$$\int_L B(M) dM = \int_L R_i(M) dM = \int_L E(M) dM \quad (\text{III.1})$$

where  $L$  stands for the kinematically accessible region. Neglecting interference effects between different resonances as well as between the resonances and the background<sup>(2) \*</sup>, we can write:

$$E(M) = b B(M) + \sum_{i=1}^{N_R} r_i R_i(M) \equiv F(M) \quad (\text{III.2})$$

\* ) *Note:* An example of a method to deal with resonance - resonance interference effects is described in section III.3.3. Usually however our statistics do not justify the use of such elaborate methods.

where  $N_R$  is the number of resonances and  $b$  and  $r_i$  are the fractions of the total number of events attributed to background and the  $i$ -th resonance respectively

$$(b + \sum_{i=1}^{N_R} r_i = 1).$$

For the effective mass distributions of resonances with *two body decays* we use the so-called Breit-Wigner form<sup>(3)</sup>:

$$R_i(M) = C_i B(M) M p^{-1}(M) \Gamma_i(M) / [(M^2 - M_i^2)^2 + M_i^2 \Gamma_i^2(M)] \quad (\text{III.3})$$

with

$$\Gamma_i(M) = \Gamma_i^\circ [p(M)/p(M_i)]^{2l+1} [\rho_i(M)/\rho_i(M_i)] \quad (\text{III.4})$$

where:  $C_i$  = a normalization constant - cf. equation (III.1).

$p(M)$  = the magnitude of the momentum of each of the decay products in the rest frame of the resonance considered.

$M_i$  = the central mass value of the  $i$ -th resonance (= 'resonance mass'<sup>(10)</sup>).

$\Gamma_i^\circ$  =  $\Gamma_i(M_i)$  - characteristic width of the  $i$ -th resonance<sup>(10)</sup>.

$l$  = relative orbital momentum of the decay products.

$\rho_i(M)$  = a slowly varying function of  $M$  for which in general one uses an empirical expression<sup>(3,4)</sup>.

We use the form  $\rho_i(M) = (p^2(M) + X_i^2)^{-1}$ . The symbol  $X_i$  stands for the so-called inverse interaction radius. We choose  $X_i = 0.11$  GeV for the  $\Delta^{*+}$  (1236) resonance and  $X_i = m_\pi = 0.14$  GeV otherwise.



The best values for the parameters  $r_i$ ,  $M_i$  and  $\Gamma_i^\circ$  are found by fitting the r.h.s. of expression (III.2) to the experimental distribution  $E(M)$ . The fitting method used is the maximum likelihood method. Assuming that for each event the probability distribution, as a function of  $M$ , is proportional to  $F(M)$ , we can express the joint probability  $P$  to find the observed experimental distribution as:

$$P \sim \prod_j^N \{F(M)\}_j$$

where  $N$  is the number of events and  $\{F(M)\}_j$  is the value of  $F(M)$  for the  $j$ -th event.

A program called MINUIT<sup>(5)</sup> was used to find the values for  $r_i$ ,  $M_i$  and  $\Gamma_i^\circ$  maximizing  $P$  or minimizing

$$\mathcal{L}(r_1, M_1, \Gamma_1^\circ, \dots, r_{N_R}, M_{N_R}, \Gamma_{N_R}^\circ) = -\log P.$$

The function  $\mathcal{L}$  is called the likelihood function. In some cases one or more of the masses or widths is kept fixed (e.g. at the nominal value).

Using expression (III.3) one can verify that a substantial fraction of the resonance events is actually produced at effective mass values quite far away from the central mass value, in particular outside the mass band chosen. We therefore always apply 'tail corrections', i.e. corrections accounting for the resonance events outside this band.

In table III.1 we indicate which method was used to determine the contributions of the resonance signals.

### III.2.3 Significance of the enhancements

Having estimated the possible contribution of a resonance signal we must try to ascertain if it is a real effect or possibly just a fluctuation of the background.

To measure the 'strength' of an enhancement we estimate its significance  $s$  by:

$$s = N_r / \sigma_r \quad (\text{III.5})$$

where

$$N_r = N_t - N_b$$

and  $\sigma_r = (N_t + \Delta^2 N_b)^{\frac{1}{2}}$

with

- $N_r$  = number of resonance events,
- $N_t$  = total number of events,
- $N_b$  = number of background events,
- $\Delta N_b$  = estimated error in  $N_b$  events,

all quantities determined in the resonance mass band chosen.

In general we have discarded signals with  $s < 2$ . The values of  $s$  for the 'signals' retained are given in table III.1.

### III.3 Resonance production

We have estimated resonance production in the more populated channels with three or four outgoing particles:

$N\bar{K}(m\pi)$  channels:  $p\bar{K}^{\circ}K^{+}$

$p\bar{K}^{\circ}K^{+}\pi^{\circ}$

$p\bar{K}^{\circ}K^{\circ}\pi^{+}$

$pK^{+}K^{-}\pi^{+}$

$n\bar{K}^{\circ}K^{+}\pi^{+}$

$\Lambda K(m\pi)$  channels :  $\Lambda K^{+}\pi^{+}$

$\Lambda K^{+}\pi^{+}\pi^{\circ}$

$\Lambda K^{\circ}\pi^{+}\pi^{+}$

$\Sigma K(m\pi)$  channels :  $\Sigma^{+}K^{+}\pi^{\circ}$

$\Sigma^{+}K^{\circ}\pi^{+}$

$\Sigma^{+}K^{+}\pi^{+}\pi^{-}$

In view of our statistics we do not attempt to explain all significant enhancements as resonance signals. The primary aim of our analysis is to study the production reactions of known particles and resonances. *We therefore only consider enhancements when near or at the position of known resonances.*

The enhancements found in the above channels can be classified as follows \*):

Mesons  $S \neq 0$  :  $K^{*}(890)$  and  $K^{*}(1420)$ .

Mesons  $S = 0$  :  $A_2, \rho(765), S^{*}$  and possibly  $\phi(1019)$ ,  
 $f^{\circ}(1260)$  and  $A_3$ .

Baryons  $S \neq 0$ :  $\Lambda(1520)$ ,  $\Sigma(1385)$  and possibly  $\Sigma(1670)$ .

Baryons  $S = 0$ :  $\Delta(1236)$ .

\*) *Note.* In appendix C a list of the properties of these particles is given.

For each of the above channels we present all two body effective mass spectra, although not all of them are discussed explicitly. Possible indications for production of the (not well established)  $Z^*$ 's are discussed separately in section III.3.9. None of the three body mass spectra shows clear evidence for resonance production. We nevertheless discuss  $(K\bar{K}\pi)$  because these spectra have been investigated at neighbouring energies (section III.3.10).

A summary of resonance production can be found in table III.1.

*In cases where resonance contributions are either not present or present, but not fitted, the curves in the effective mass plots given in this chapter are the phase-space (effective mass) distributions normalized to the total number of events.* In the remaining cases the curves represent the results of fits as described in the previous section.

We next make a point of notation. We use the shorthand notation (AB....) to denote the effective mass distribution of the particle combination AB.... With a charge index *outside* the parentheses, e.g. (AB.....)<sup>+, -, 0</sup>, we indicate the subset of combinations having the specified net charge.

We also point out, that a notation like

$$\Sigma^+(1385) K^+ \pi^0$$

includes *all* final states and reactions in which the  $\Sigma^+(1385)$  is produced, i.e. in our example:

$$\Sigma^+(1385) K^+ \pi^0 \quad 3\text{-body}$$

$$\Sigma^+(1385) K^{**}(890) \quad 2\text{-body}$$

etc.

TABLE III.1

REACTION CROSS SECTIONS					
Channel	Reaction	%	s	Cross section ( $\mu\text{b}$ )	Method*
$\text{p}\bar{\text{K}}^{\circ}\text{K}^{+}$	$\text{pA}_2^{+}$	$27 \pm 11$	2.5	$14 \pm 6$	A
$\text{p}\bar{\text{K}}^{\circ}\text{K}^{+}\pi^{\circ}$	$\Delta^{+}(1236)\bar{\text{K}}^{\circ}\text{K}^{+}$	$17 \pm 6$	2.5	$19 \pm 7$	A
	$\Sigma^{+}(1670)\text{K}^{+}\pi^{\circ}$	$9 \pm 4$	2	$10 \pm 5$	A
	$\text{p}\bar{\text{K}}^{\circ}\text{K}^{*+}(890)$	$10 \pm 4$	2.5	$11 \pm 4$	A
	$\text{p}\text{K}^{+}\bar{\text{K}}^{*0}(890)$	$10 \pm 4$	2	$10 \pm 4$	A
$\text{p}\bar{\text{K}}^{\circ}\text{K}^{\circ}\pi^{+}$	$\Delta^{*+}(1236)\text{K}^{\circ}\bar{\text{K}}^{\circ}$	$26 \pm 6$	4	$23 \pm 6$	B
	$\text{p}\bar{\text{K}}^{\circ}\text{K}^{*+}(890)$	$26 \pm 9$	3	$23 \pm 9$	B
	$\Delta^{*+}(1236)\text{A}_2^{\circ}/\text{f}^{\circ}$	$16 \pm 5$		$14 \pm 5$	A
$\text{p}\text{K}^{+}\text{K}^{-}\pi^{+}$	$\Delta^{*+}(1236)\text{K}^{+}\text{K}^{-}$	$43 \pm 4$	9.5	$43 \pm 12$	B
	$\Lambda(1520)\text{K}^{+}\pi^{+}$	$8 \pm 2$	3.5	$8 \pm 4$	B
	$\text{p}\text{K}^{+}\bar{\text{K}}^{*0}(890)$	$14 \pm 4$	3	$14 \pm 5$	B
	$\Delta^{*+}(1236)\text{A}_2^{\circ}/\text{f}^{\circ}$	$13 \pm 3$		$13 \pm 4$	A
$\text{p}\pi^{+}(\text{K}\bar{\text{K}})^{\circ}$	$\text{p}\pi^{+}\text{A}_2^{\circ}$	$11 \pm 4$	} 3	$20 \pm 8$	B
	$\text{p}\pi^{+}\text{f}^{\circ}$	$5 \pm 4$		$9 \pm 6$	B
	$\text{p}\pi^{+}\text{S}^{*}$	$11 \pm 4$	2.5	$21 \pm 8$	B
	$\text{p}\pi^{+}\phi(1019)$		< 2	< 9	A
	$\Delta^{*+}(1236)\phi(1019)$			< 5	A
$\text{n}\bar{\text{K}}^{\circ}\text{K}^{+}\pi^{+}$	$\Lambda(1520)\text{K}^{+}\pi^{+}$	$7 \pm 4$	$\leq 2$	$7 \pm 4$	A
	$\text{n}\pi^{+}\text{A}_2^{+}$	$16 \pm 8$	2	$15 \pm 8$	A

TABLE III.1 (cont.)

## REACTION CROSS SECTIONS

Channel	Reaction	%	s	Cross section ( $\mu\text{b}$ )	Method*
$\Lambda K^+ \pi^+$	$\Sigma^+(1385) K^+$	$25 \pm 6$	4.5	$16 \pm 4$	B
$\Lambda K^+ \pi^+ \pi^0$	$\Sigma^+(1385) K^+ \pi^0$	$24 \pm 5$	4.5	$34 \pm 8$	B
	$\Lambda \pi^+ K^{*+}(890)$	$14 \pm 3$	4.5	$20 \pm 4$	B
	$\Lambda \pi^+ K^{*+}(1420)$	$9 \pm 3$	2.5	$12 \pm 5$	B
	$\Lambda K^+ \rho^+(765)$	$19 \pm 5$	3.5	$26 \pm 7$	B
	$\Sigma^+(1385) K^{*+}(890)$	$9 \pm 3$		$13 \pm 4$	B
$\Lambda K^0 \pi^+ \pi^+$	$\Sigma^+(1385) K^0 \pi^+$	$22 \pm 5$	3.5	$16 \pm 5$	B
	$\Lambda \pi^+ K^{*+}(890)$	$39 \pm 5$	5	$29 \pm 6$	B
	$\Lambda \pi^+ K^{*+}(1420)$	$16 \pm 6$	$\lesssim 2$	$11 \pm 5$	B
	$\Sigma^+(1385) K^{*+}(890)$	$14 \pm 4$		$11 \pm 3$	B
$\Sigma^+ K^+ \pi^0$	$\Sigma^+ K^{*+}(890)$	$35 \pm 10$	3.5	$22 \pm 6$	B
$\Sigma^+ K^0 \pi^+$	$\Sigma^+ K^{*+}(890)$	$49 \pm 16$	3	$38 \pm 16$	B
$\Sigma^+(K\pi)^+$	$\Sigma^+ K^{*+}(1420)$		$< 2$	$< 19$	B
$\Sigma^+ K^+ \pi^+ \pi^-$	$\Sigma^+ \pi^+ K^{*0}(890)$	$23 \pm 7$	3	$21 \pm 7$	A
	$\Sigma^+ K^+ \rho^0(765)$	$19 \pm 8$	2	$17 \pm 8$	A

\*) A: method of event counting above estimated background

B: method of fitting Breit-Wigners + phase space

### III.3.1 The channel $p\bar{K}^0K^+$ (44 events)

In this channel we find an  $A_2^+$  signal in the  $(\bar{K}^0K^+)$  distribution (fig. III.1C). We estimate the signal to contain  $(27 \pm 11)\%$  of the channels events ( $s \approx 2.5$ ):

$$\sigma(pA_2^+ \rightarrow p\bar{K}^0K^+) = (14 \pm 6) \mu\text{b}$$

The cross section for  $pA_2^+$  has also been determined using non-strange channels<sup>(6)</sup>. We quote the results<sup>(\*)</sup>:

$$\sigma(pA_2^+ \rightarrow p(\rho\pi)^+) = (208 \pm 53) \mu\text{b}$$

$$\sigma(pA_2^+ \rightarrow p\eta\pi^+) = (46 \pm 16) \mu\text{b}$$

$$\sigma(pA_2^+ \rightarrow pX^0\pi^+) = \left( 5 \begin{array}{c} + \\ - \end{array} \begin{array}{c} 3 \\ 5 \end{array} \right) \mu\text{b}$$

The total cross section thus found is:

$$\sigma(pA_2^+) = (273 \pm 60) \mu\text{b}$$

This leads to a branching fraction:

$$\frac{A_2^+ \rightarrow \bar{K}^0K^+}{A_2^+ \rightarrow \text{all modes}} = 0.05 \pm 0.02$$

in agreement with the world average  $(0.047 \pm 0.006)^{(10)}$ .

The Dalitz-plot  $M^2(p\bar{K}^0)$  versus  $M^2(\bar{K}^0K^+)$  is shown in fig. III.2.

(\*) *Note.* The values quoted here are essentially more refined redeterminations of the values given in ref. 6.

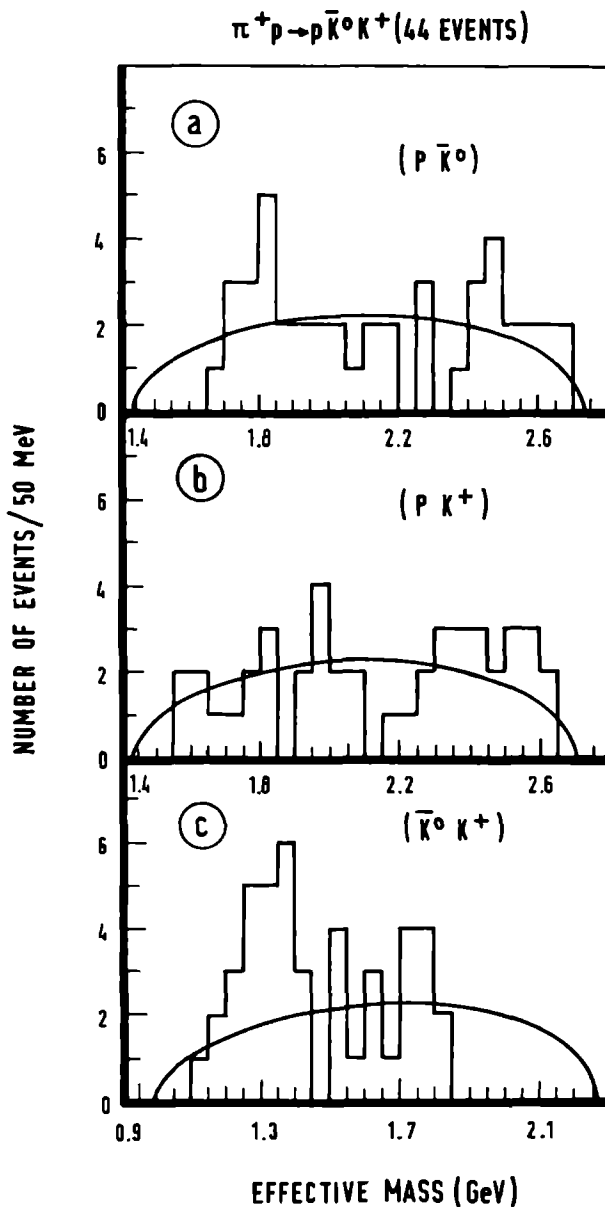


Fig. III.1 Two body effective mass spectra in the channel  $\bar{p}K^0 \pi^+$ . The curves represent the phase space predictions normalized to the total number of events.



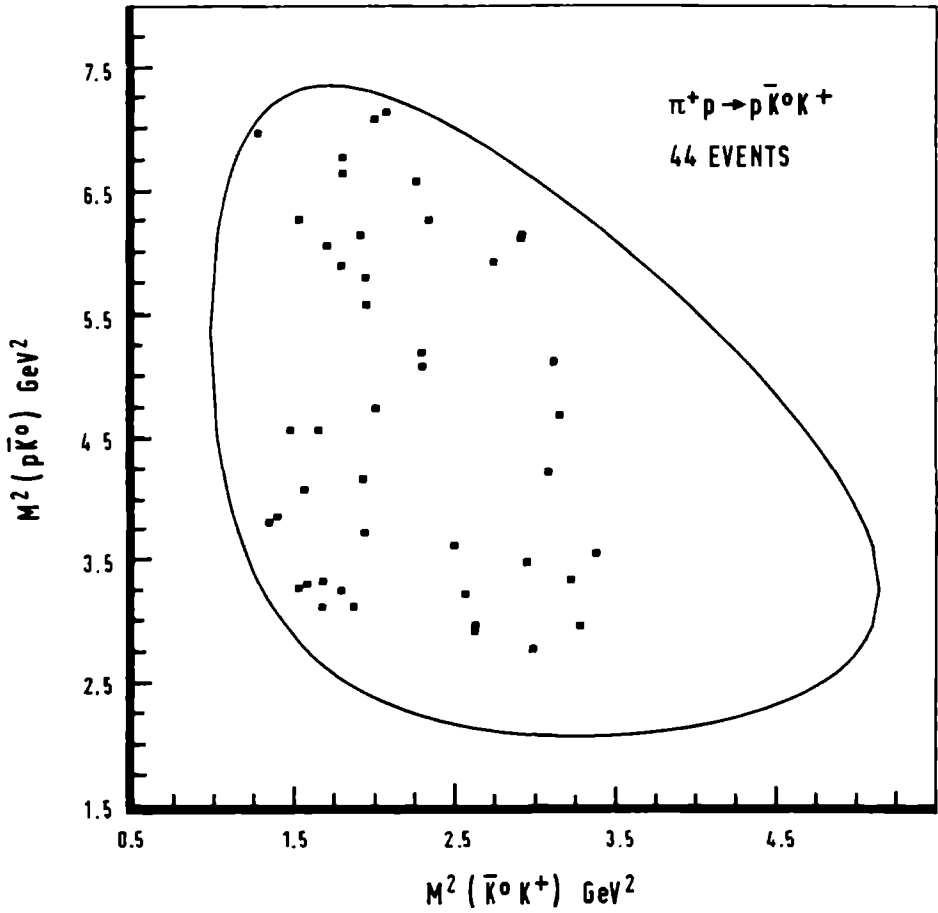


Fig. III.2 Dalitzplot  $M^2(p\bar{K}^0)$  versus  $M^2(\bar{K}^0 K^+)$  in the channel  $p\bar{K}^0 K^+$ .

### III.3.2 The channel $p\bar{K}^0 K^+ \pi^0$ (104 events)

. The ( $p\bar{K}^0$ ) distribution (fig. III.3a) shows an enhancement at the  $\Sigma^+(1670)$  position. The signal is weak ( $s \approx 2$ ) and disappears upon selection of events with the complementary combination ( $K^+ \pi^0$ ) in the  $K^*(890)$  band. We estimate  $(9 \pm 4)\%$   $\Sigma^+(1670)$  production:

$$\sigma(\Sigma^+(1670) K^+ \pi^0 \rightarrow p\bar{K}^0 K^+ \pi^0) = (10 \pm 5) \mu\text{b.}$$

. The ( $p\pi^0$ ) distribution (fig. III.3c) shows an accumulation of events on the low mass side. This is an indication of  $\Delta^+(1236)$  production. The severely distorted signal has a significance of approximately 2.5 and contains  $(17 \pm 6)\%$  of the events:

$$\sigma(\Delta^+(1236) \bar{K}^0 K^+ \rightarrow p\pi^0 \bar{K}^0 K^+) = (19 \pm 7) \mu\text{b}$$

We find no correlation between  $\Delta^+(1236)$  and resonance signals in ( $\bar{K}^0 K^+$ ).

. The ( $\bar{K}^0 \pi^0$ )-spectrum (fig. III.3e) contains a marginally significant ( $s \approx 2$ ) signal indicating  $\bar{K}^{*0}(890)$  production  $((10 \pm 4)\%)$ :

$$\sigma(pK^+ \bar{K}^{*0}(890) \rightarrow pK^+ \bar{K}^0 \pi^0) = (10 \pm 4) \mu\text{b}$$

. In ( $K^+ \pi^0$ ) we find some  $K^{*+}(890)$  production - see fig. III.3f we estimate  $(10 \pm 4)\%$  or:

$$\sigma(p\bar{K}^0 K^{*+}(890) \rightarrow p\bar{K}^0 K^+ \pi^0) = (11 \pm 4) \mu\text{b}$$

As stated above, there is no clear correlation with resonance production in ( $p\bar{K}^0$ ) - see fig. III.3a and fig. III.4.

. The ( $\bar{K}^0 K^+$ )-distribution (fig. III.3d) shows a broad  $s \approx 3$  bump between 1050 and 1200 McV. In this region no established candidate exists for which decay into  $\bar{K}^0 K^+$  ( $IJ^{PG}(\bar{K}^0 K^+) = 10^{+-}, 11^{-+}, 12^{+-}$  etc) is allowed.

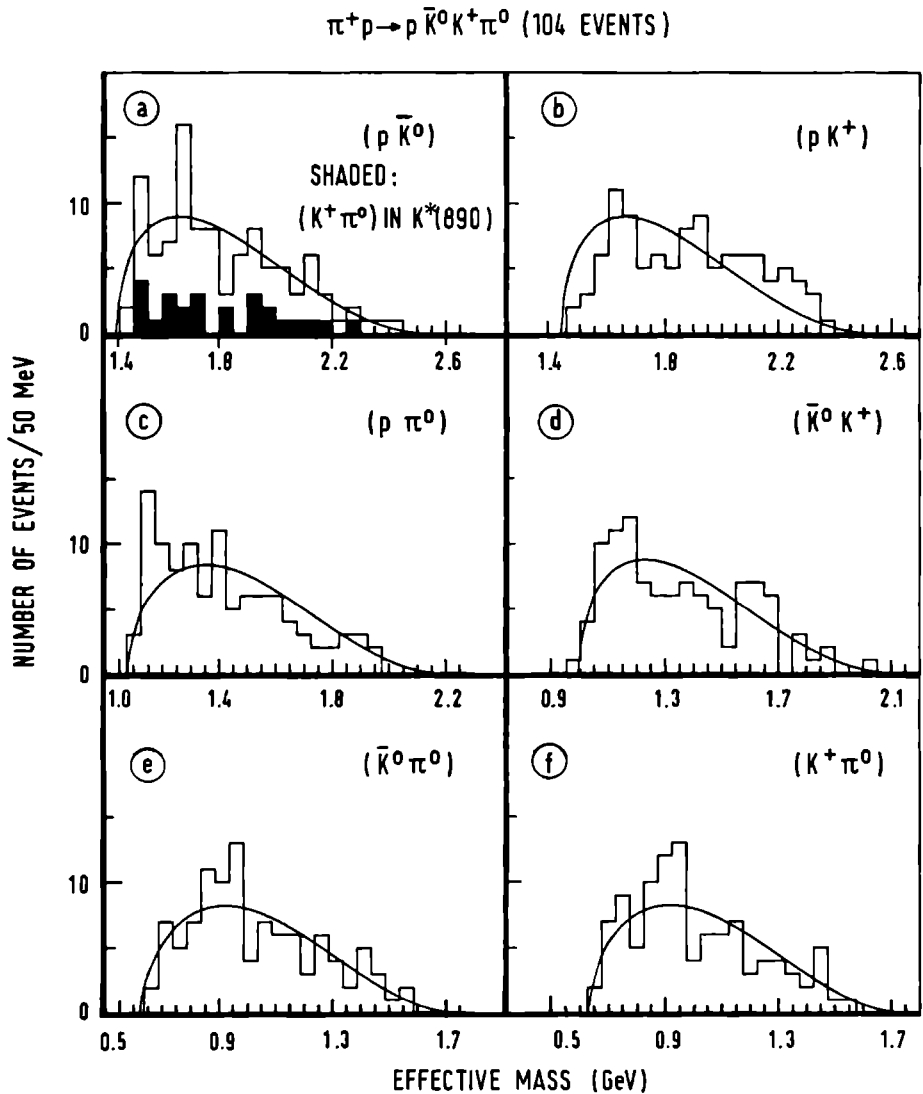


Fig. III.3 Two body effective mass spectra in the channel  $\pi^+\rho \rightarrow \rho \bar{K}^0 K^+ \pi^0$ . The curves represent the phase space predictions normalized to the total number of events. The shaded histogram in (a) represents a selection of events with  $0.84 < M(K^+ \pi^0) (\text{GeV}) < 0.94$  ( $K^*(890)$  band).

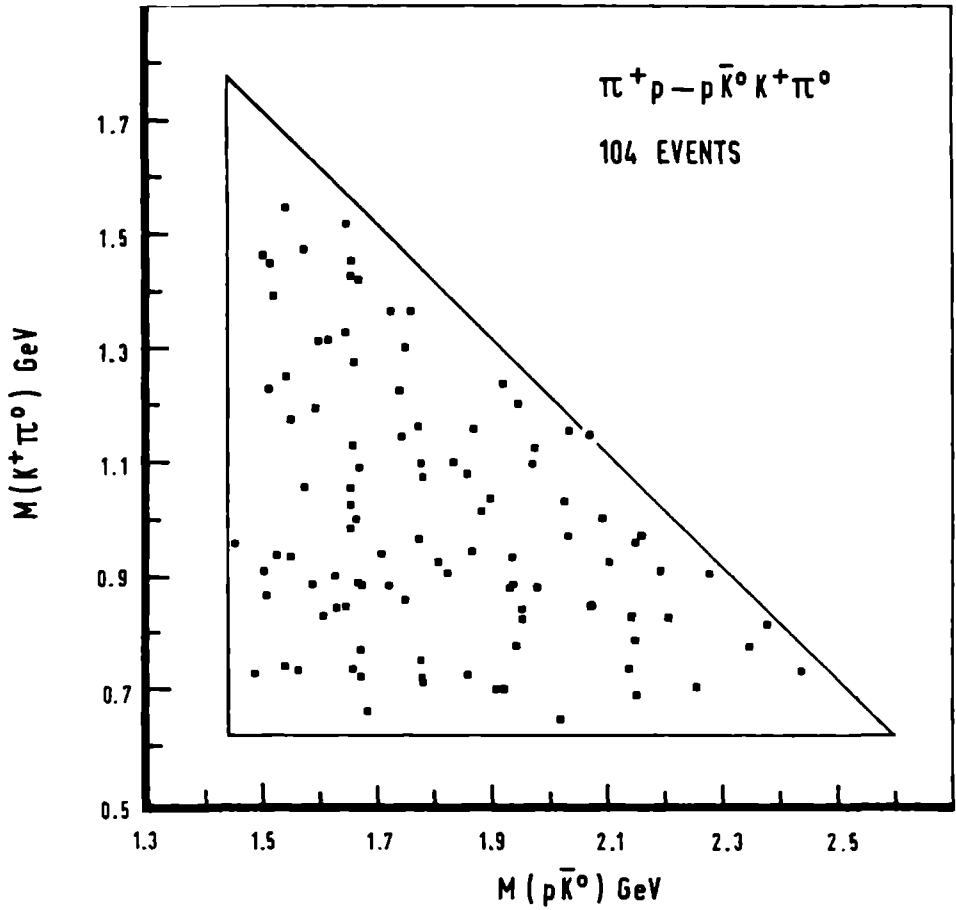


Fig. III.4 Goldhaber plot  $M(K^+ \pi^0)$  versus  $M(p \bar{K}^0)$  in the channel  $p \bar{K}^0 K^+ \pi^0$ .

III.3.3 The channels  $pK^{\circ}\bar{K}^{\circ}\pi^+$  (137 events) and  $pK^+K^-\pi^+$  (376 events)

. The ( $p\pi^+$ ) distributions from  $pK^{\circ}\bar{K}^{\circ}\pi^+$  (fig. III.5b) and  $pK^+K^-\pi^+$  (fig. III.7c) show  $\Delta^{++}(1236)$  production in  $(26 \pm 6)\%$  and  $(43 \pm 4)\%$  of the events respectively. The significances are  $s \approx 4$  and  $s \approx 9.5$  respectively: We find:

$$\sigma(\Delta^{++}(1236) K^{\circ}\bar{K}^{\circ} \rightarrow p\pi^+K^{\circ}\bar{K}^{\circ}) = (23 \pm 6) \mu\text{b},$$

$$\sigma(\Delta^{++}(1236) K^+K^- \rightarrow p\pi^+K^+K^-) = (43 \pm 12) \mu\text{b}.$$

. The ( $pK^-$ ) spectrum (fig. III.7b) shows a clear ( $s \approx 3.5$ ) signal due to the  $\Lambda(1520) \rightarrow pK^-$  decay. We estimate  $(8 \pm 2)\%$  and:

$$\sigma(\Lambda(1520) K^+\pi^+ \rightarrow pK^-K^+\pi^+) = (8 \pm 4) \mu\text{b}.$$

. The ( $K^{\circ}\pi^+ + \bar{K}^{\circ}\pi^+$ ) distribution of fig. III.5d contains two entries per event. The background is thus almost a factor two higher than would have been the case in a one entry plot. We observe an  $s \approx 3$  signal at the  $K^{*+}(890)$  position which must be due to ( $K^{\circ}\pi^+$ ), because ( $\bar{K}^{\circ}\pi^+$ ) has isospin 3/2. We find  $K^{*+}$  production in  $(26 \pm 9)\%$  of the channel and:

$$\sigma(p\bar{K}^{\circ} K^{*+}(890) \rightarrow p\bar{K}^{\circ}K^{\circ}\pi^+) = (23 \pm 9) \mu\text{b}.$$

The ratio 
$$\frac{\sigma(p\bar{K}^{\circ} K^{*+}(890) \rightarrow p\bar{K}^{\circ}K^+\pi^{\circ})}{\sigma(p\bar{K}^{\circ} K^{*+}(890) \rightarrow p\bar{K}^{\circ}K^{\circ}\pi^+)} = 0.48 \pm 0.26$$

is in agreement with the Clebsch-Gordan ratio for the  $K^{*+}(890)$  decay modes involved ( $= 0.5$ ).

. The ( $K^-\pi^+$ ) spectrum (fig. III.7f) shows an  $s \approx 3$  signal for  $\bar{K}^{*0}(890)$ . We estimate  $(14 \pm 4)\%$ :

$$\sigma(pK^+\bar{K}^{*0}(890) \rightarrow pK^+K^-\pi^+) = (14 \pm 5) \mu\text{b}.$$

We find 
$$\frac{\sigma(pK^+\bar{K}^{*0}(890) \rightarrow pK^+\bar{K}^{\circ}\pi^{\circ})}{\sigma(pK^+\bar{K}^{*0}(890) \rightarrow pK^+K^-\pi^+)} = 0.71 \pm 0.38$$

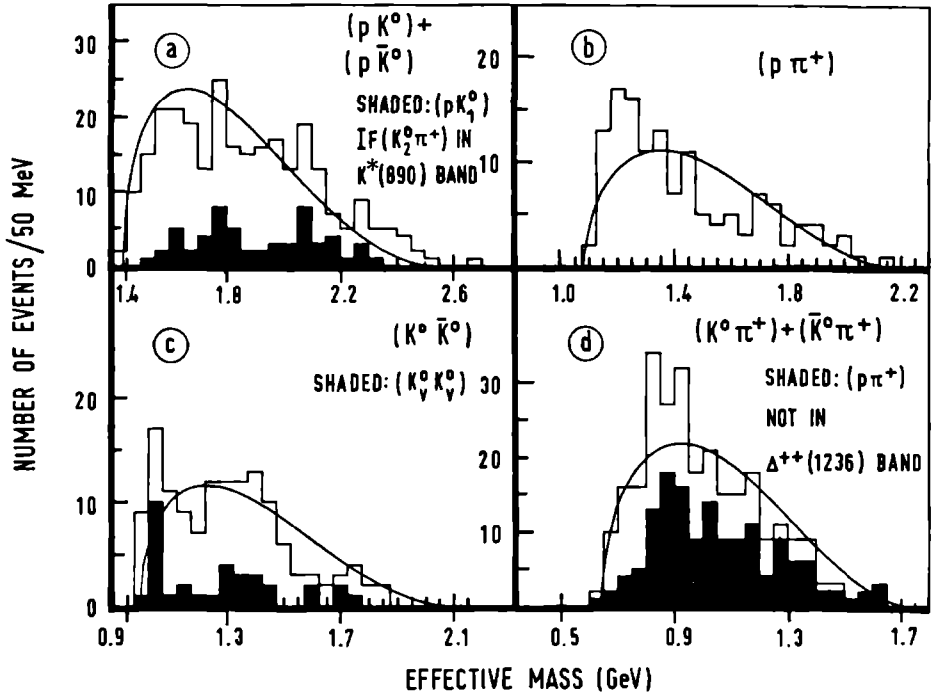
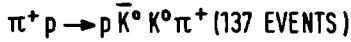


Fig. III.5 Two body effective mass spectra in the channel  $p\bar{K}^0K^0\pi^+$ . The curves represent the phase space predictions normalized to the total number of events. The shaded histogram in (a) represents a selection of events with at least one  $(K^0\pi^+)$  combination having  $0.84 < M(K^0\pi^+)$  (GeV)  $< 0.94$  ( $K^*(890)$  band). The shaded histogram in (c) contains events with two visibly decaying  $K^0$  particles. The shaded histogram in (d) gives the distribution for events with  $M(p\pi^+)$  outside the  $\Delta^{++}(1236)$  band (1.12 - 1.32 GeV).

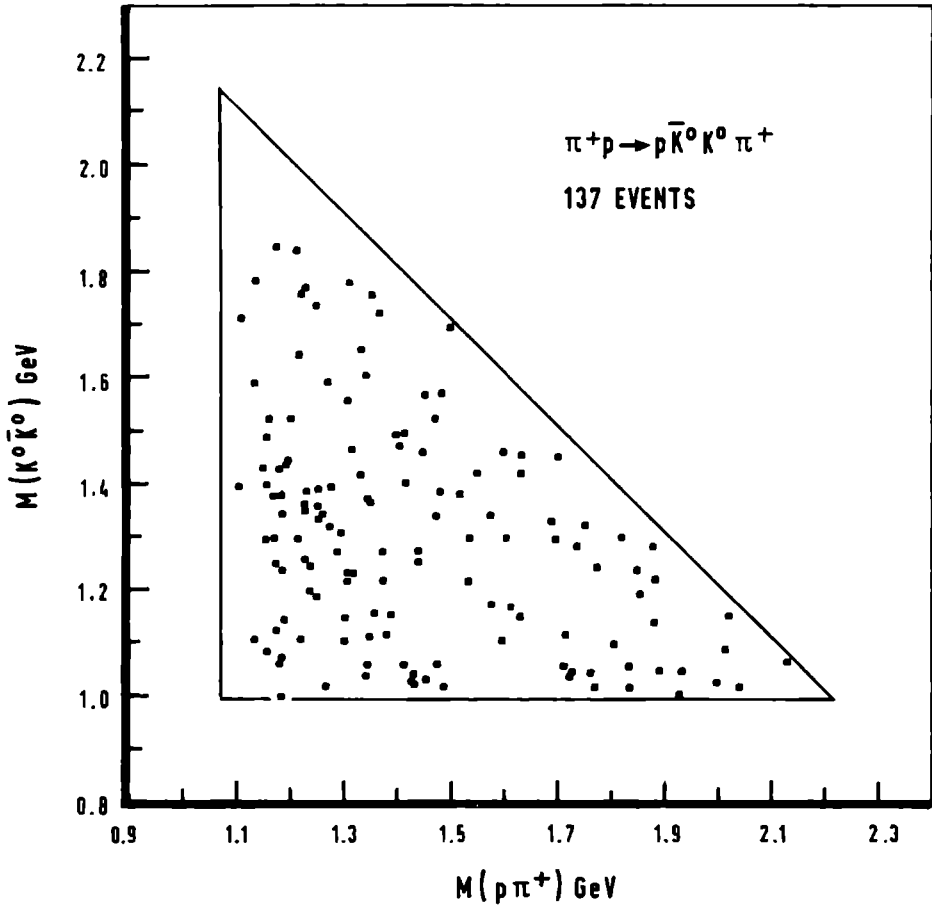


Fig. III.6 Goldhaber plot  $M(K^0 \bar{K}^0)$  versus  $M(p\pi^+)$  in the channel  $p\bar{K}^0 K^0 \pi^+$ .

which is again compatible with the expected C.G. ratio for  $\bar{K}^{*0}$  decay (= 0.5).

The  $(K^0 \bar{K}^0)$  and  $(K^+ K^-)$  distributions - fig. III.5c, fig. III.7d and fig. III.9 show two accumulations: one near threshold and one around 1300 MeV.

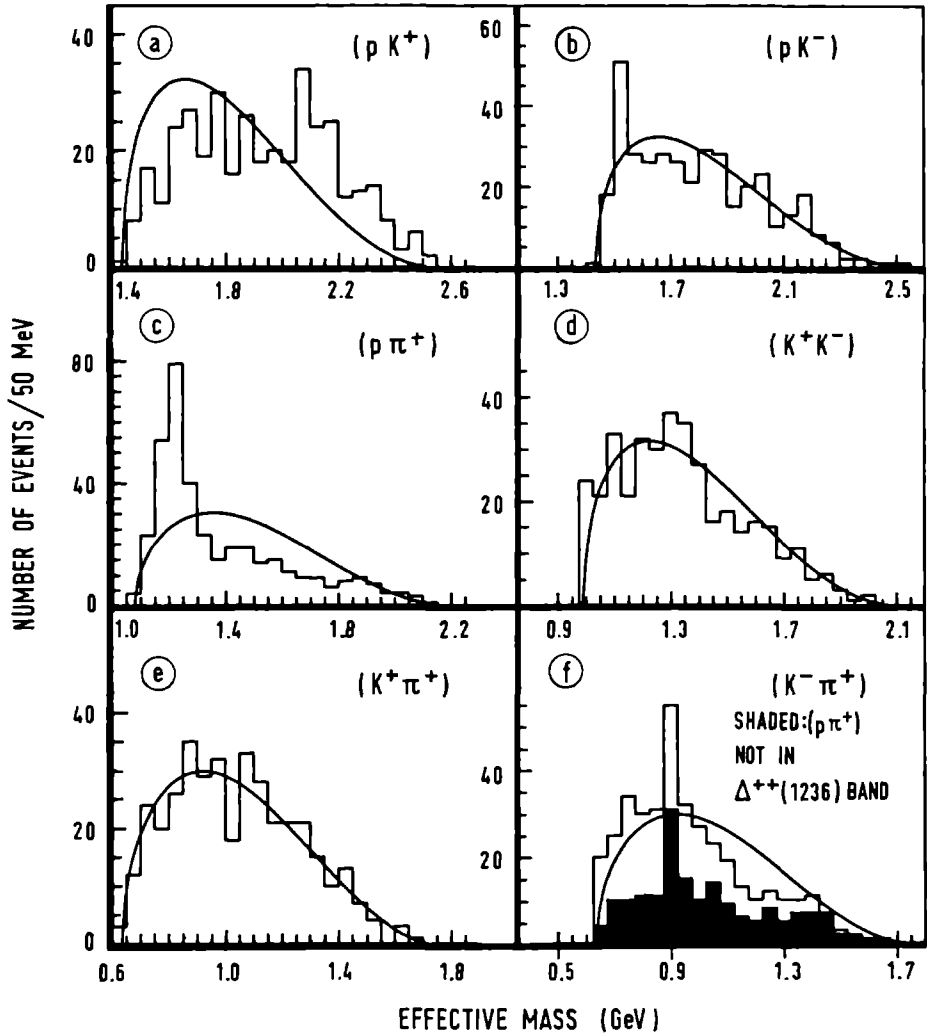
$\pi^+ p \rightarrow p K^+ K^- \pi^+ (376 \text{ EVENTS})$ 


Fig. III.7 Two body effective mass distributions in the channel  $pK^+K^-\pi^+$ . The curves represent the phase space predictions normalized to the total number of events. The shaded histogram in (f) gives the  $(K^-\pi^+)$  distribution of events with  $M(p\pi^+)$  outside the  $\Delta^{++}(1236)$  band (1.12 - 1.32 GeV).



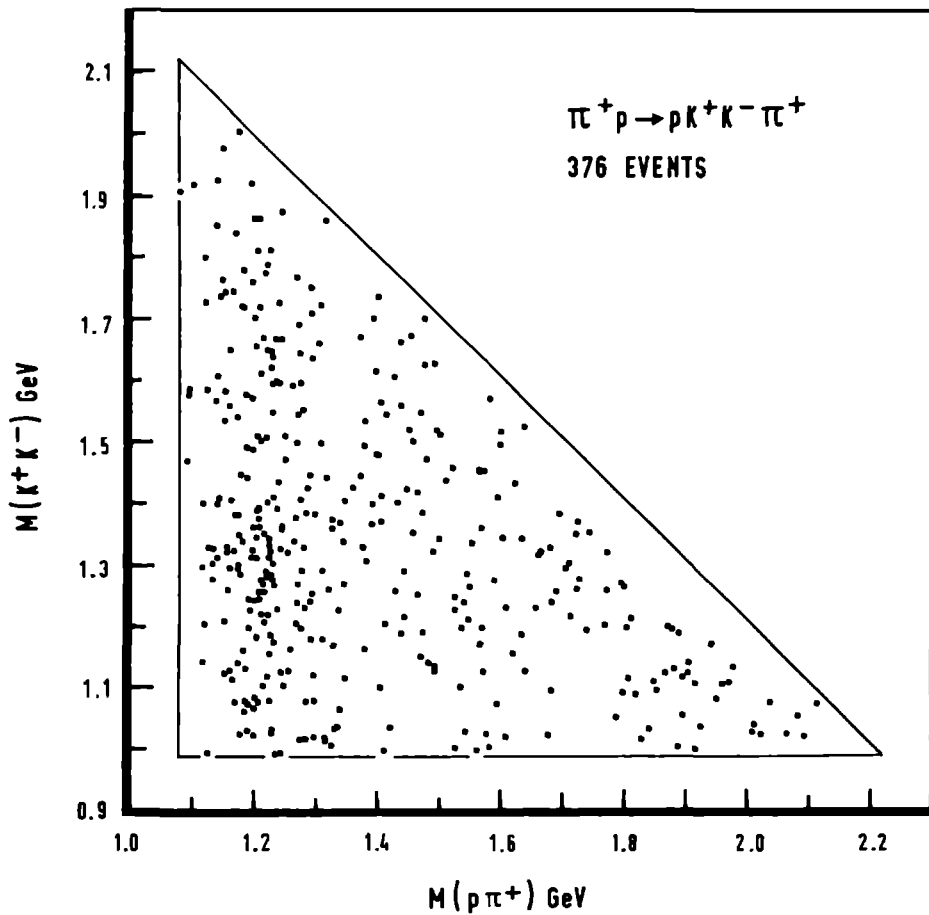


Fig. III.8 Goldhaber plot  $M(K^+ K^-)$  versus  $M(p \pi^+)$  in the channel  $p K^+ K^- \pi^+$ .

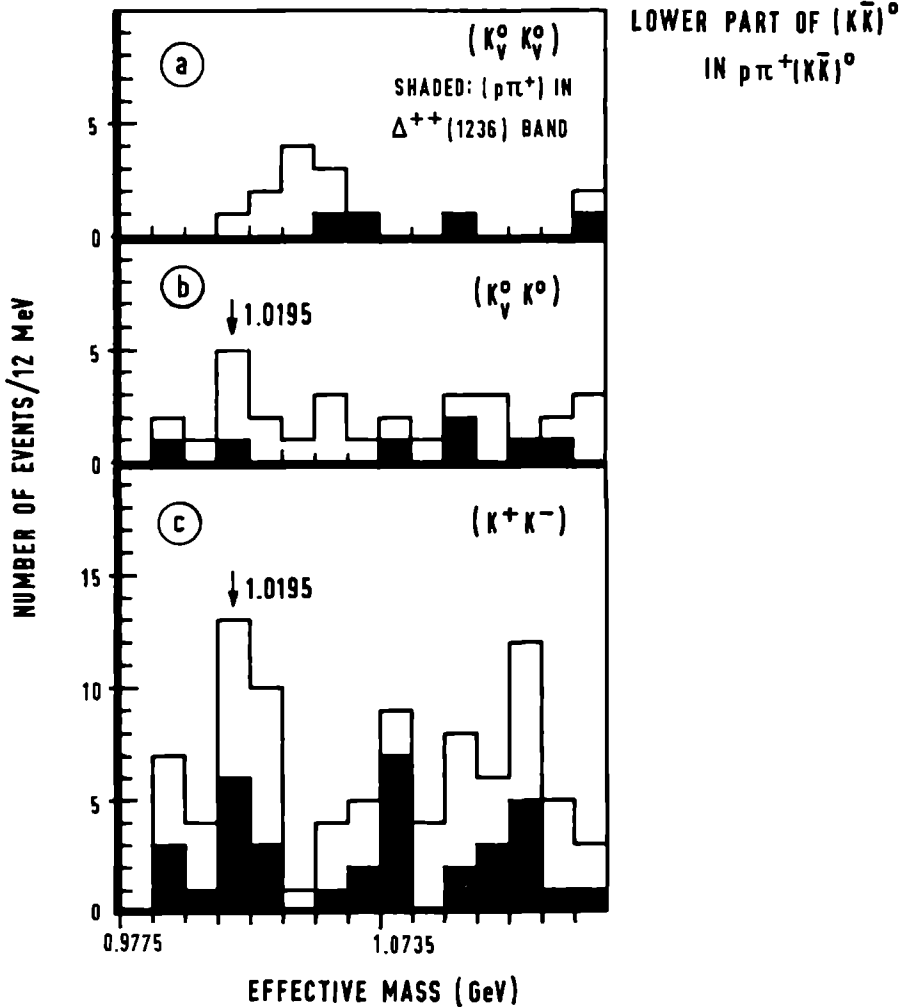


Fig. III.9  $(K\bar{K})^0$  effective mass distributions from the channels  $p\pi^+(K\bar{K})^0$  in the region around  $\phi$  (1019). (a) from  $p\bar{K}^0 K^0 \pi^+$  with two visible  $K^0$  decays and (b) with one visible  $K^0$  decay; (c) from  $pK^+ K^- \pi^+$ . Events with  $M(p\pi^+)$  in the  $\Delta^{++}(1236)$  band (1.12 - 1.32 GeV) are shaded.

If we plot  $(K^0\bar{K}^0)$  and  $(K^+K^-)$  in 12 MeV bins we see enhancements suggestive of  $\phi(1019)$  ( $\Gamma \sim 4.5$  MeV;  $IJ^{PG} = 01^{--}$ ) production in  $K_V^0K^0$  and  $K^+K^-$  (fig. III.9 b,c). In this mass region the experimental effective mass resolution is  $\lesssim 10$  MeV. Background subtraction is very difficult because of the proximity of the  $S^*$  (see below) and the low significance of the signals ( $s \lesssim 2$ ).

The G-parity of the  $\phi(1019)$  permits decay into  $K_S^0K_L^0$  and  $K^+K^-$  while decay into  $K_S^0K_S^0$  and  $K_L^0K_L^0$  is forbidden. We indeed find no excess of events at the  $\phi$  position in  $K_V^0K_V^0$  (fig. III.9a). We estimate the following upper limit for  $\phi$  production (at two standard deviation level):

$$\sigma(p\pi^+ \phi(1019) \rightarrow p\pi^+(K\bar{K})^0) < 9 \mu\text{b}.$$

Likewise we determine (fig. III.9, shaded):

$$\sigma(\Delta^{++}(1236) \phi(1019) \rightarrow p\pi^+(K\bar{K})^0) < 5 \mu\text{b}.$$

The latter quasi two-body reaction is strongly suppressed with respect to the reaction  $\pi^+p \rightarrow \Delta^{++}\omega$ , for which in our experiment a cross-section of  $(280 \pm 10) \mu\text{b}^{(8) *}$  was found.

The broad bump around 1300 MeV in the  $(K\bar{K})^0$  spectra (figs. III.10 a,b,c) may contain both  $f^0$  and  $A_2^0$ . Lipkin has shown<sup>(9)</sup>, that interference between isovector and isoscalar intermediate states like the  $A_2^0$  and  $f^0$  may lead to complications in interpreting the neutral  $(K^0\bar{K}^0)$  and charged  $(K^+K^-)$  spectra. The final states  $(K^0\bar{K}^0)$  and  $(K^+K^-)$ , taken separately, are neither eigenstates of isospin nor of C-parity. Contributions from overlapping resonances like the isoscalar  $f^0$  and the isovector  $A_2^0$  are therefore coherent. Addition of the two spectra however cancels the interference effect, because its

\*) Note. The ratio  $\sigma(\Delta^{++}\phi)/\sigma(\Delta^{++}\omega)$  can be used to determine (limits for) the  $\omega$ - $\phi$  mixing angle<sup>(17)</sup>. Our data are too crude to make the theoretically relevant distinctions.

contributions to both these final states are equal and opposite.

Before adding the  $(K^0\bar{K}^0)$  and  $(K^+K^-)$  spectra, we first have to correct them for the difference in the loss factors (sect. II.5). The method used can be described as follows:

The cross sections for  $p\pi^+\bar{K}^0K^0$  production can be considered to consist of three parts:  $\sigma(K_S^0K_S^0)$ ,  $\sigma(K_S^0K_L^0)$  and  $\sigma(K_L^0K_L^0)$ . Denoting the cross section for  $p\pi^+K^+K^-$  production by  $\sigma(K^+K^-)$  we can write the following expressions for the number of *observed* events  $\Delta N'$  per mass interval  $\Delta M$  in the different spectra:

$$\Delta N'(K_V^0K_i^0) = V_{SS}\Delta\sigma(K_S^0K_S^0) + V_{SL}\Delta\sigma(K_S^0K_L^0) + V_{LL}\Delta\sigma(K_L^0K_L^0)$$

$$\Delta N'(K_V^0K_V^0) = W_{SS}\Delta\sigma(K_S^0K_S^0) + W_{SL}\Delta\sigma(K_S^0K_L^0) + W_{LL}\Delta\sigma(K_L^0K_L^0)$$

$$\Delta N'(K^+K^-) = U \Delta\sigma(K^+K^-)$$

The above conversion factors:  $V_{IJ}$ ,  $W_{IJ}$  and  $U$  are average quantities over the mass region considered, giving the relation between the cross sections and the number of *observed* events in each  $\sigma$ -part, i.e. they are the inverses of microbarn equivalents and thus equal to the expressions  $(\sigma_o C_s C_u C_p C_w)^{-1}$  ( $= N'/\sigma$ ; cf. section II.4). Their values are given in table III.2. As is clear from this table, we exclude the presence of visible  $K_L^0$  decays:  $V_{LL} = W_{SL} = W_{LL} = 0$  (cf. sect. II.5.6). Using these averaged factors, we tacitly assume that the scanning-, classification-, and probability cutoff-corrections (sect. II.5) contained in these factors do not depend on  $M$ . An investigation of the length - and small angle - loss corrections for the mass spectra involved indicates that for these corrections this assumption is fairly well satisfied.

Our objective is now to construct a  $(K^0\bar{K}^0)$  spectrum in which each of the three cross sections  $\sigma(K_S^0K_S^0)$ ,  $\sigma(K_L^0K_L^0)$  and  $\sigma(K_S^0K_L^0)$  is represented by the same number of events per micro-

TABLE III.2

CONVERSION FACTORS IN $p\pi^+(K\bar{K})^\circ$		
Partial cross section	Decays	Conversion factor (observed events/ $\mu\text{b}$ )
$\sigma(K^+K^-)$	No	$U = 3.92 \pm 0.13$
$\sigma(K_S^\circ K_S^\circ)$	1 $K^\circ$	$V_{SS} = 1.27 \pm 0.04$
	2 $K^\circ$	$W_{SS} = 1.02 \pm 0.05$
$\sigma(K_S^\circ K_L^\circ)$	1 $K^\circ$	$V_{SL} = 1.61 \pm 0.06$
	2 $K^\circ$	$W_{SL} = 0.$
$\sigma(K_L^\circ K_L^\circ)$	1 $K^\circ$	$V_{LL} = 0.$
	2 $K^\circ$	$W_{LL} = 0.$

barn as in the  $(K^+K^-)$  spectrum. This objective can be met by multiplying the  $(K_V^\circ K_i^\circ)$  and  $(K_V^\circ K_V^\circ)$  - spectra with factors  $\alpha$  and  $\beta$  respectively and adding them:

$$\begin{aligned} \alpha \Delta N'(K_V^\circ K_i^\circ) + \beta \Delta N'(K_V^\circ K_V^\circ) \\ = U [\Delta\sigma(K_S^\circ K_S^\circ) + \Delta\sigma(K_S^\circ K_L^\circ) + \Delta\sigma(K_L^\circ K_L^\circ)]. \end{aligned} \quad (\text{III.6})$$

Putting  $\Delta\sigma(K_L^\circ K_L^\circ) = \Delta\sigma(K_S^\circ K_S^\circ)$  (CP-invariance), we obtain the relations:

$$\begin{aligned} \alpha V_{SS} + \beta W_{SS} &= 2U \\ \alpha V_{SL} &= U \end{aligned} \quad (\text{III.7})$$

from which  $\alpha$  and  $\beta$  can be evaluated. We find

$$\begin{aligned} \alpha &= 2.4 \pm 0.1 \\ \beta &= 4.6 \pm 0.4 \end{aligned}$$

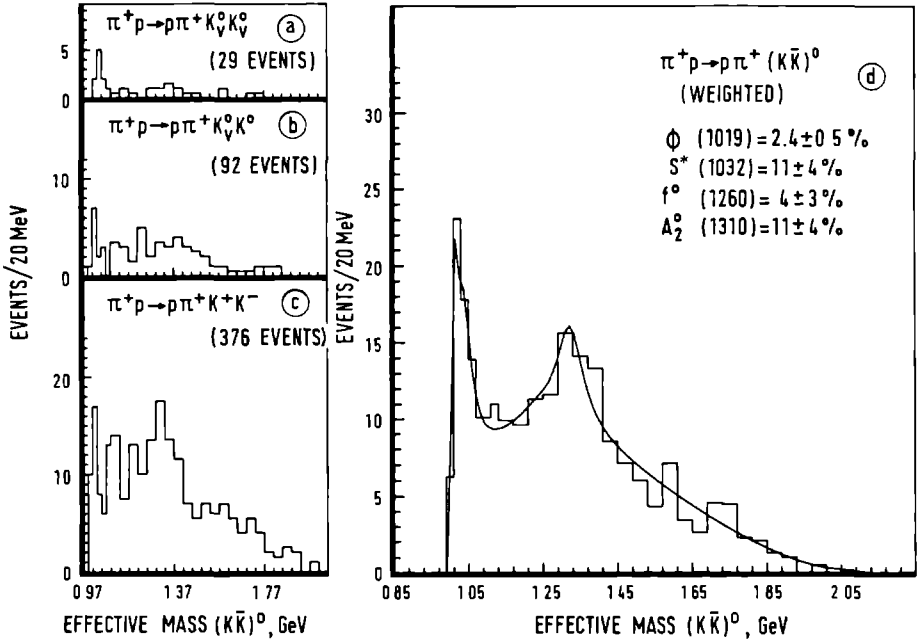


Fig. III.10 Unweighted  $(K\bar{K})^0$  mass spectra from the channels  $\pi^+ p \rightarrow \rho \pi^+ K_V^0 K_V^0$  (a),  $\pi^+ p \rightarrow \rho \pi^+ K_V^0 K_0$  (b) and  $\pi^+ p \rightarrow \rho \pi^+ K^+ K^-$  (c) and the weighted  $(K\bar{K})^0$  spectrum from the combined channels (d). The vertical scale in all plots is (events/20 MeV) for the whole spectrum. The bandwidth is 20 MeV for  $M(K\bar{K})^0 < 1.09$  GeV and 40 MeV for  $M(K\bar{K})^0 > 1.09$  GeV. The curve in (d) represents the result of a fit to 4 Breit-Wigners + phase space (see table III.3 for other fit results).

Adding the  $(K^0 \bar{K}^0)$  spectrum given by  $\alpha \Delta N'(K_V^0 K_V^0) + \beta \Delta N'(K_V^0 K_0)$  to the  $(K^+ K^-)$  spectrum results in a distribution for  $(K\bar{K})^0$  in which possible  $A_2^0/f^0$  interference effects are eliminated.

TABLE III.3

FIT RESULTS FOR THE WEIGHTED $(K\bar{K})^0$ SPECTRUM									
Fit interval	$M_{\text{eff}} > 1.15 \text{ GeV}$			$M_{\text{eff}} > 1.15 \text{ GeV}$			Complete spectrum *)		
Resonance	M (GeV)	$\Gamma$ (GeV)	%	M (GeV)	$\Gamma$ (GeV)	%	M (GeV)	$\Gamma$ (GeV)	%
$A_2^0$	1.344	0.120	$14 \pm 5$	1.360	0.076	$9 \pm 4$	1.330	0.090	$11 \pm 4$
$f^0$	-	-	-	1.273	0.103	$6 \pm 3$	1.279	0.219	$4 \pm 3$
$S^*$	-	-	-	-	-	-	1.032	0.058	$11 \pm 4$
$\phi$	-	-	-	-	-	-	1.019	0.005	$2.4 \pm 0.5$
$\chi^2/\text{ND}$	111/169			115/166			154/191		
<p>*) In this fit the <math>A_2</math> mass and width have been allowed to vary in intervals covered by the published<sup>(10)</sup> values for the <math>(K\bar{K})^0</math>-mode: 1.280 - 1.330 GeV and 0.090 - 0.125 GeV respectively. The <math>\phi(1019)</math> central mass value and width have been fixed, while the percentage is based on an estimation from fig. III.9.</p>									

The spectrum obtained is shown in fig. III.10d. We fitted this spectrum for  $M(K\bar{K})^\circ > 1.15$  GeV to one ( $A_2^\circ$ ) and two ( $A_2^\circ + f^\circ$ ) independent Breit-Wigner curves + phase space. We also fitted the whole spectrum with four Breit-Wigner resonances ( $\phi(1019)$ ,  $S^*$ ,  $f^\circ$ ,  $A_2^\circ$ ) + phase space. The curve in fig. III.10d represents the result of the latter fit. The results of the different fits can be found in table III.3.

We summarize our conclusions as follows:

$$\sigma(p\pi^+ A_2^\circ \rightarrow p\pi^+(K\bar{K})^\circ) = (20 \pm 8) \mu\text{b}$$

$$\sigma(p\pi^+ f^\circ \rightarrow p\pi^+(K\bar{K})^\circ) = (9 \pm 6) \mu\text{b}$$

$$\sigma(p\pi^+ S^* \rightarrow p\pi^+(K\bar{K})^\circ) = (21 \pm 8) \mu\text{b}.$$

The difference between the  $(K^+K^-)$  spectrum and the  $(K\bar{K})^\circ$  spectrum constructed above in principle shows the effect of the interference term. This difference (not shown) is compatible with zero in the  $A_2^\circ/f^\circ$  region.

For the joint production of  $\Delta^{++}$  and  $A_2^\circ/f^\circ$  (fig. III.11) we estimate:

$$\sigma(\Delta^{++}(1236)(A_2^\circ + f^\circ) \rightarrow p\pi^+(K\bar{K})^\circ) = (27 \pm 7) \mu\text{b},$$

indicating a very strong correlation between the production of these resonances (see also fig. III.6 and fig. III.8). Previously, our collaboration has observed this strong correlation for  $\Delta^{++}A_2^\circ$  in the channel  $\pi^+p \rightarrow \pi^+p\pi^+\pi^-\pi^0$ <sup>(11)</sup> and for  $\Delta^{++}f^\circ$  in the channel  $\pi^+p \rightarrow \pi^+p\pi^+\pi^-$ <sup>(12)</sup>. The cross sections determined from these non-strange channels were:

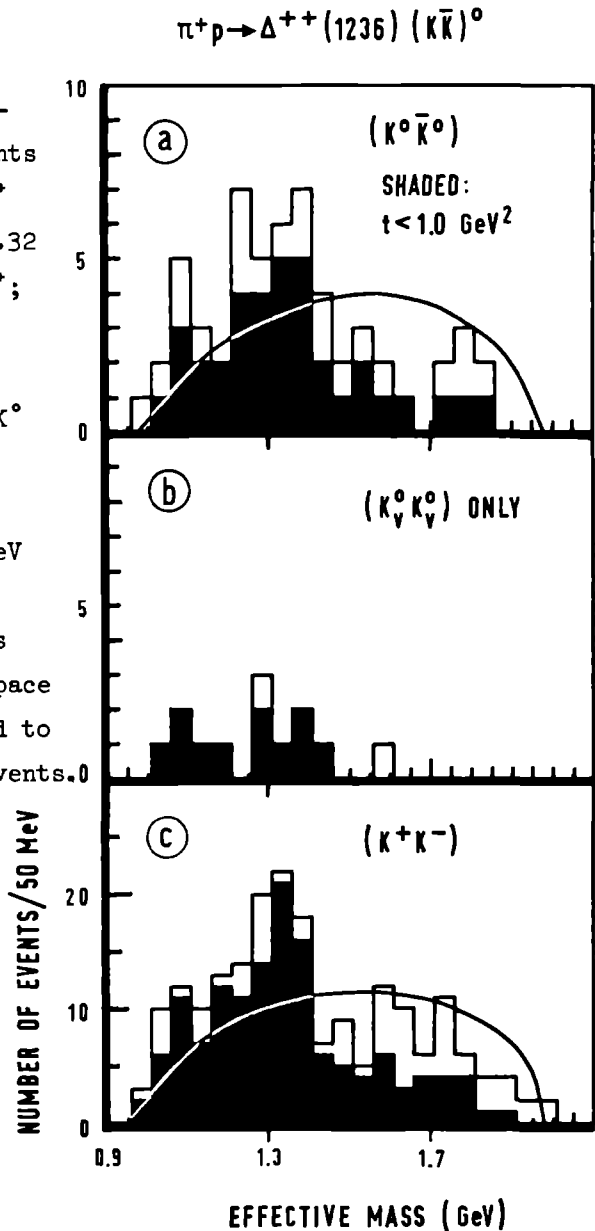
$$\sigma(\Delta^{++}A_2^\circ; A_2^\circ \rightarrow \text{all modes}) = (220 \pm 30) \mu\text{b}^{(8)(11)}$$

$$\text{and } \sigma(\Delta^{++}f^\circ; f^\circ \rightarrow \text{all modes}) = (340 \pm 70) \mu\text{b}^{(8)(12)}$$



Fig. III.11

$(K\bar{K})^0$  effective mass spectra from the channels  $p\pi^+(K\bar{K})^0$  for events with  $M(p\pi^+)$  in the  $\Delta^{++}$  (1236) band (1.12 - 1.32 GeV). (a) from  $p\bar{K}^0K^0\pi^+$ ; (b) from  $p\bar{K}^0K^0\pi^+$  upon selecting events with two visibly decaying  $K^0$  particles; (c) from  $pK^+K^-\pi^+$ . Selection of events with  $t < 1.0$  GeV results in the shaded histograms. The curves represent the phase space predictions normalized to the total number of events.



Using these results, we derive the branching ratios:

$$\frac{A_2^{\circ} \rightarrow (K\bar{K})^{\circ}}{A_2^{\circ} \rightarrow \text{all modes}} = 0.09 \pm 0.04$$

and

$$\frac{f^{\circ} \rightarrow (K\bar{K})^{\circ}}{f^{\circ} \rightarrow \text{all modes}} = 0.03 \pm 0.02$$

Our  $A_2^{\circ}$  branching ratio is higher than the world average  $(0.047 \pm 0.006)^{(10)}$ ; our  $f^{\circ}$  branching ratio agrees with the literature value  $(0.05 \pm 0.03)^{(10)}$  within the errors.

### III.3.4 The channel $n\bar{K}^{\circ}K^+\pi^+$ (86 events)

. In the  $(n\bar{K}^{\circ})$  spectrum (fig. III.12a) we find a weak indication ( $s \lesssim 2$ ) for  $\Lambda(1520)$  production. The signal contains  $(7 \pm 4)\%$  of the events:

$$\sigma(\Lambda(1520) K^+\pi^+ \rightarrow n\bar{K}^{\circ}K^+\pi^+) = (7 \pm 4) \mu\text{b}$$

The ratio 
$$\frac{\sigma(\Lambda(1520) K^+\pi^+ \rightarrow p\bar{K}^{\circ}K^+\pi^+)}{\sigma(\Lambda(1520) K^+\pi^+ \rightarrow n\bar{K}^{\circ}K^+\pi^+)} = 1.1 \pm 0.9$$

is in agreement with the C.G. prediction for  $\Lambda(1520)$  decay ( $= 1$ ).

. In the  $(\bar{K}^{\circ}K^+)$ -distribution (fig. III.12d) an  $s \approx 2$  indication for  $A_2^+$  production is present. We estimate  $(16 \pm 8)\%$  or

$$\sigma(n\pi^+A_2^+ \rightarrow n\pi^+\bar{K}^{\circ}K^+) = (15 \pm 8) \mu\text{b}.$$

We find no clear indication for correlated  $\Delta^+A_2^+$  production.

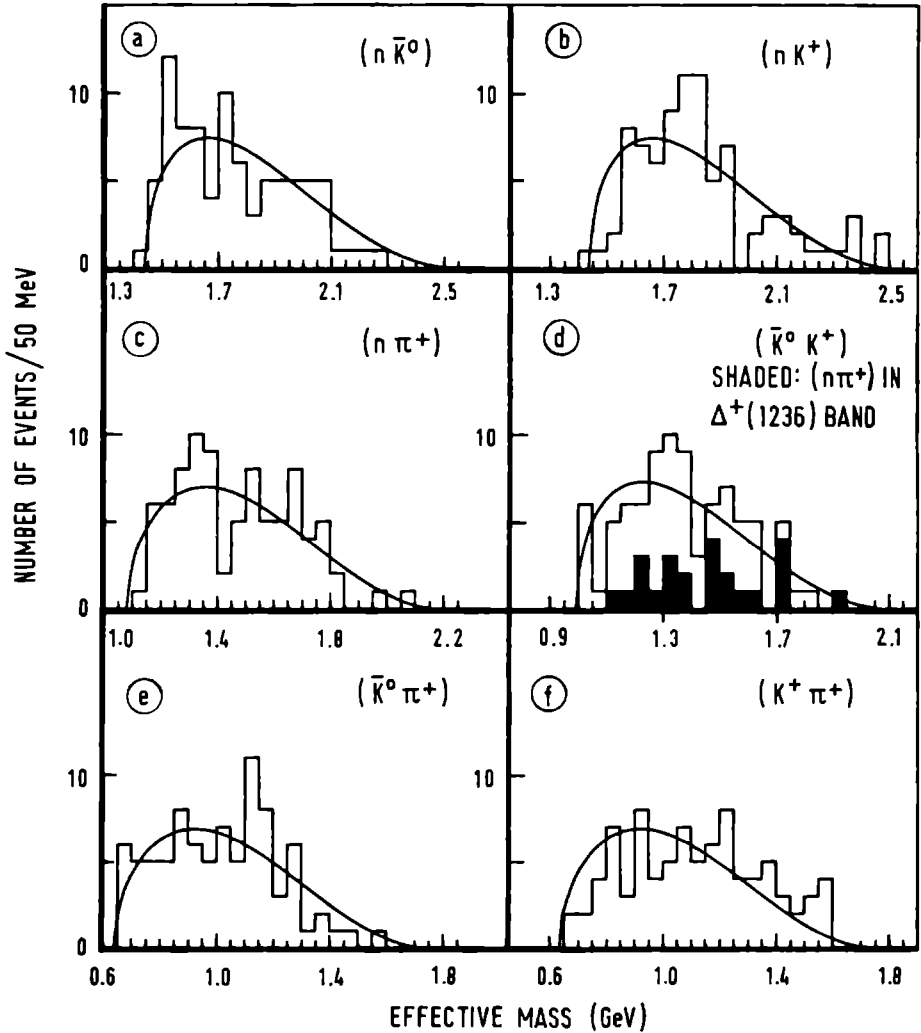
$$\pi^+ p \rightarrow n \bar{K}^0 K^+ \pi^+ \text{ (86 EVENTS)}$$


Fig. III.12 Two body effective mass spectra from the channel  $n\bar{K}^0 K^+ \pi^+$ . The curves represent the phase space predictions normalized to the total number of events. The shaded histogram in (d) gives  $M(\bar{K}^0 K^+)$  for events with  $M(n\pi^+)$  in the  $\Delta^+(1236)$  band (1.12 - 1.32 GeV).

### III.3.5 The channel $\Lambda K^+ \pi^+$ (104 events)

In this channel the only prominent feature is the strong  $\Sigma^+(1385)$  signal ( $s \approx 4.5$ ) in  $(\Lambda\pi^+)$  (fig. III.13c) containing  $(25 \pm 6)\%$  of the events. By fitting we find:

$$\sigma(\Sigma^+(1385) K^+ \rightarrow \Lambda\pi^+ K^+) = (16 \pm 4) \mu\text{b}$$

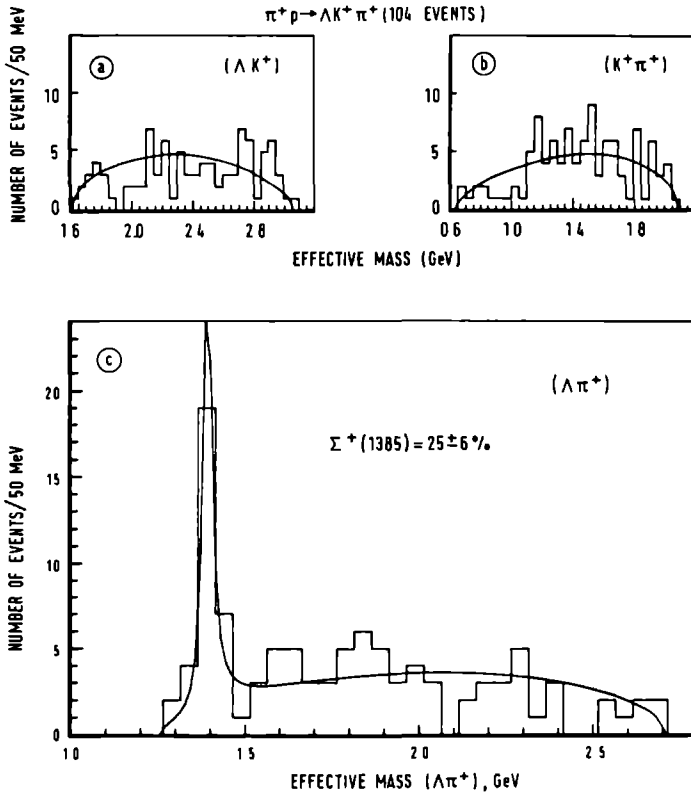


Fig. III.13 Two body spectra in  $\Lambda K^+ \pi^+$ . The curves in (a) and (b) represent normalized phase space. The curve in (c) represents a fit to a  $\Sigma^+(1385)$  Breit-Wigner + phase space.

The Dalitzplot  $M^2(\Lambda K^+)$  versus  $M^2(\Lambda \pi^+)$  is presented in fig. III.14.

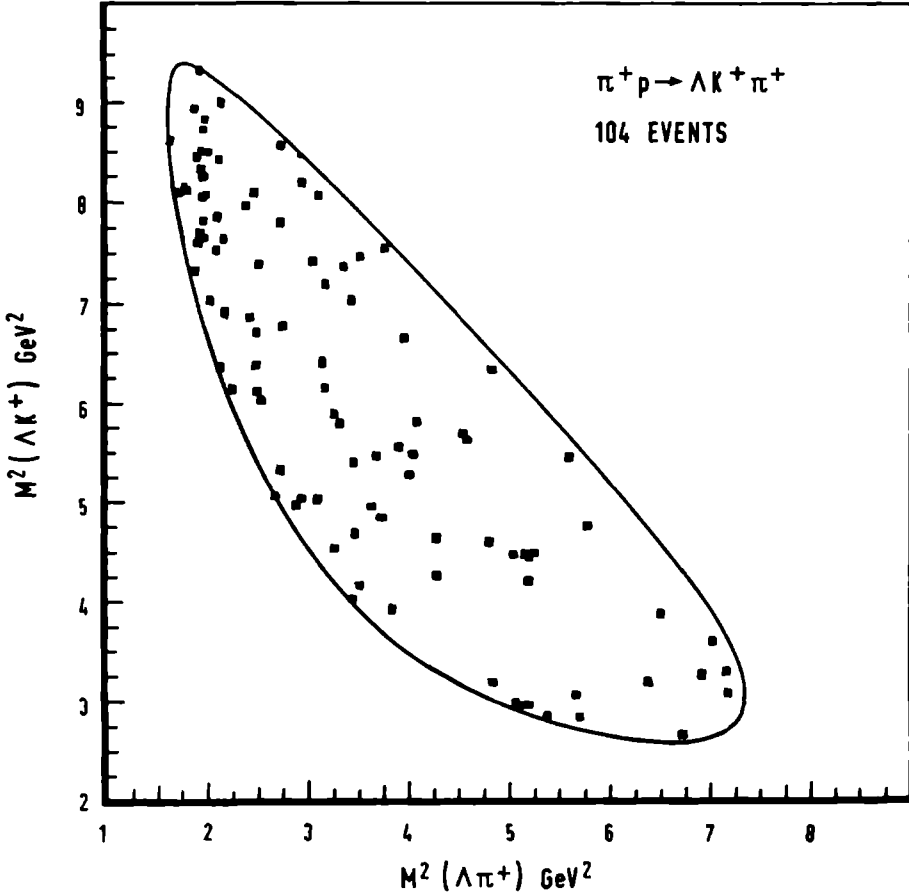


Fig. III.14 Dalitzplot  $M^2(\Lambda K^+)$  versus  $M^2(\Lambda \pi^+)$  in the channel  $\Lambda K^+ \pi^+$ .

### III.3.6 The channel $\Lambda K^+ \pi^+ \pi^0$ (236 events) and $\Lambda K^0 \pi^+ \pi^+$ (151 events)

The  $(\Lambda \pi^+)$  spectra (fig. III.15a, III.16a) show clear  $\Sigma^+(1385)$  signals, containing  $(24 \pm 5)\%$  and  $(22 \pm 5)\%$  of the events and having a significance of 4.5 and 3.5 respectively.

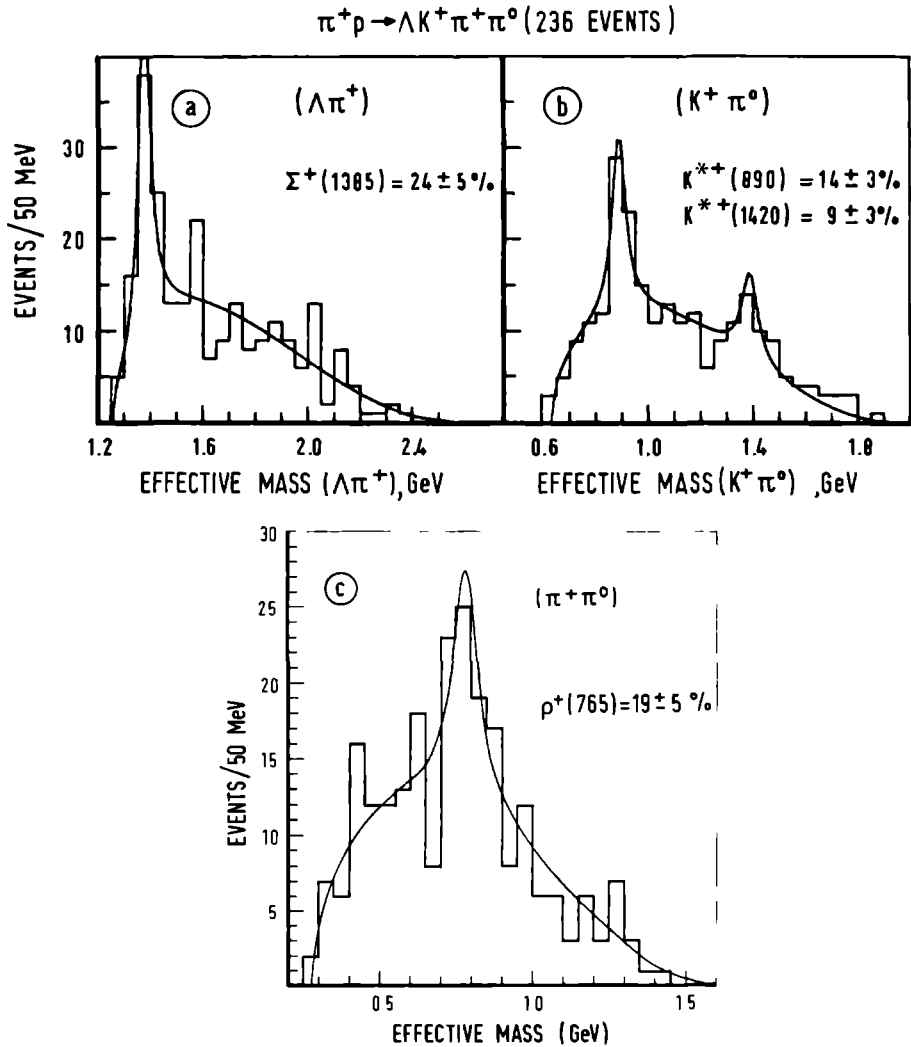
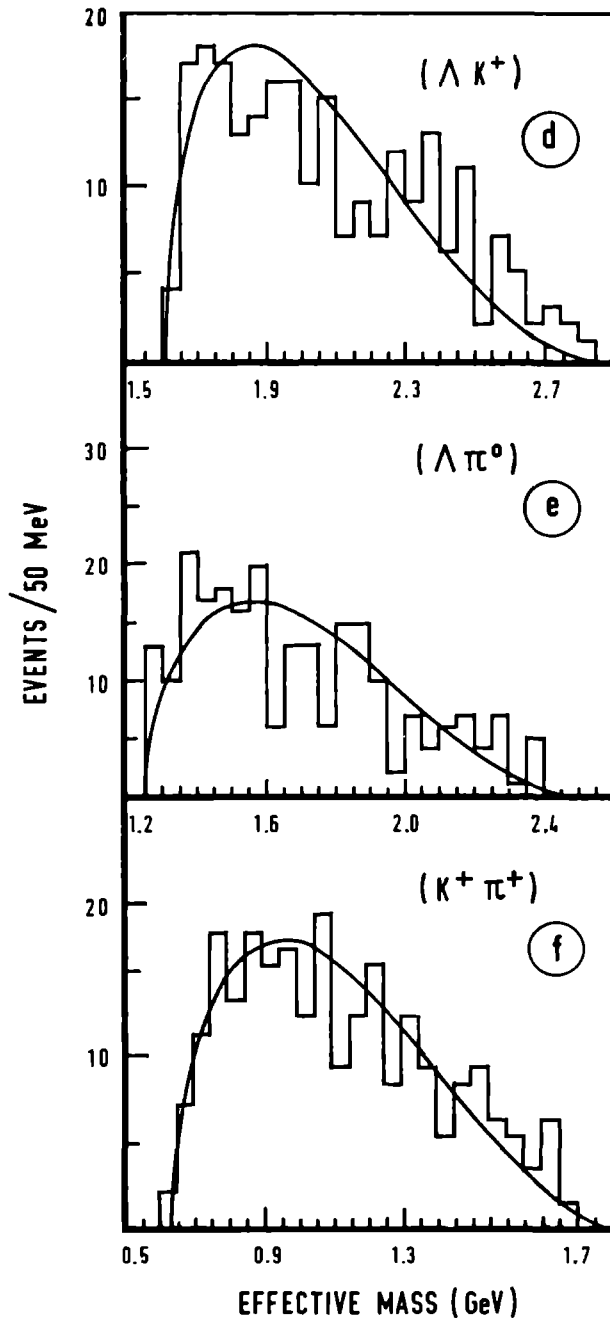


Fig. III.15 Two body effective mass plots in the channel  $\Lambda K^+ \pi^+ \pi^0$ . The curves in (a), (b) and (c) are the results of fitting Breit-Wigner(s) + phase space. The curves in (d), (e) and (f) give the phase space distributions normalized to the total number of events.

$\pi^+ p \rightarrow \Lambda K^+ \pi^+ \pi^0$  (236 EVENTS)

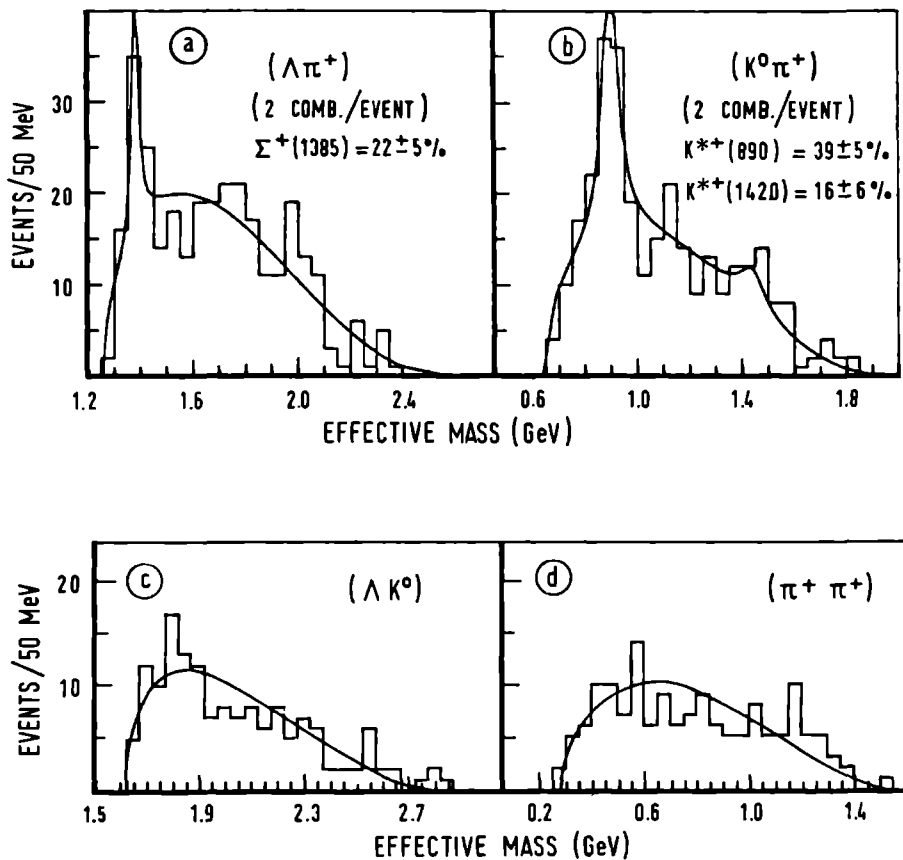
$\pi^+p \rightarrow \Lambda K^0 \pi^+ \pi^+ (151 \text{ EVENTS})$ 


Fig. III.16 Two body effective mass spectra in the channel  $\Lambda K^0 \pi^+ \pi^+$ . The curves in (a) and (b) are the results of fitting Breit-Wigner(s) + phase space. These plots contain 2 entries per event. The curves in (c) and (d) are phase space predictions.



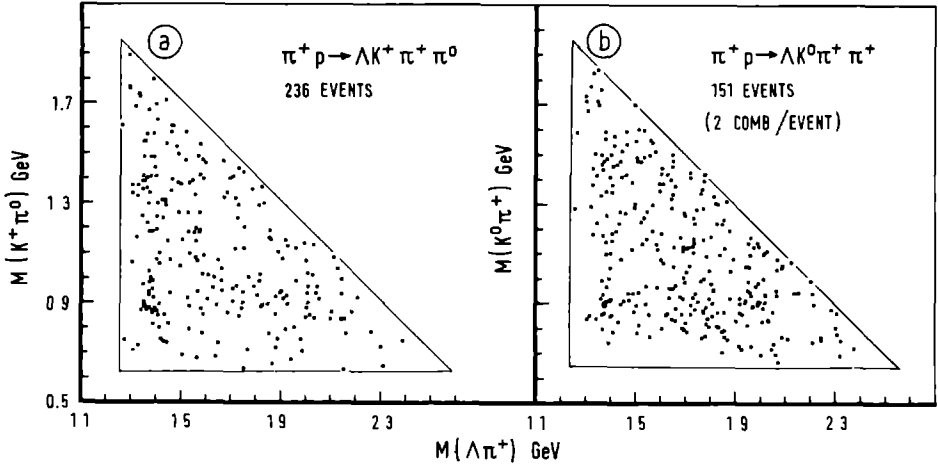


Fig. III.17 Goldhaber plots in the channels  $\Lambda K^+ \pi^+ \pi^0$  and  $\Lambda K^0 \pi^+ \pi^+$ .  
 (a)  $M(K^+ \pi^0)$  versus  $M(\Lambda \pi^+)$  in  $\Lambda K^+ \pi^+ \pi^0$  and (b)  $M(K^0 \pi^+)$  versus  $M(\Lambda \pi^+)$  in  $\Lambda K^0 \pi^+ \pi^+$ .

$$\sigma(\Sigma^+(1385) K^+ \pi^0 \rightarrow \Lambda \pi^+ K^+ \pi^0) = (34 \pm 8) \mu\text{b}$$

$$\sigma(\Sigma^+(1385) K^0 \pi^+ \rightarrow \Lambda \pi^+ K^0 \pi^+) = (16 \pm 5) \mu\text{b}$$

. In the  $(K^+ \pi^0)$  and  $(K^0 \pi^+)$  distributions (fig. III.15b, III.16b) we observe  $K^{**}(890)$  production ( $s \approx 4.5$  and  $5$  respectively) and in  $(K^+ \pi^0)$  an indication for  $K^{**}(1420)$ . The contributions of  $K^{**}(890)$  are  $(14 \pm 3)\%$  and  $(39 \pm 5)\%$  respectively:

$$\sigma(\Lambda \pi^+ K^{**}(890) \rightarrow \Lambda \pi^+ K^+ \pi^0) = (20 \pm 4) \mu\text{b}$$

$$\sigma(\Lambda \pi^+ K^{**}(890) \rightarrow \Lambda \pi^+ K^0 \pi^+) = (29 \pm 6) \mu\text{b}$$

From the C.G. ratio for  $K^{**}$  decay we expect a ratio between these cross sections of  $1/2$ . We find  $0.69 \pm 0.20$ .

The  $K^{**}(1420)$  signals are weak ( $s \approx 2.5$  and  $\lesssim 2$  respectively); the corresponding contributions are  $(9 \pm 3)\%$  and  $(16 \pm 6)\%$  respectively:

$$\sigma(\Lambda\pi K^{**}(1420) \rightarrow \Lambda\pi^+K^+\pi^0) = (12 \pm 5) \mu\text{b}$$

$$\sigma(\Lambda\pi K^{**}(1420) \rightarrow \Lambda\pi^+K^0\pi^+) = (11 \pm 5) \mu\text{b}$$

For the ratio between these cross sections, expected to be 1/2, we find  $\frac{12 \pm 5}{11 \pm 5} = 1.1 \pm 0.7$ .

The cross section for associated production of  $\Sigma^+(1385)$  and  $K^{**}(890)$  was determined using a program written by Pöls<sup>(12)</sup>.

This program calculated the fractional contributions of the different *reactions* - ( $\Sigma^+(1385) K^{**}(890)$ ,  $\Sigma^+(1385)(K\pi)^+$ ,  $\Lambda\pi^+K^{**}(890)$ ,  $\Lambda\pi^+K^{**}(890)$ ,  $\Lambda\pi^+K^{**}(1420)$  and  $\Lambda\pi^+(K\pi)^+$ ) - to the *channels*  $\Lambda\pi^+(K\pi)^+$  by performing a maximum likelihood fit of the contributions from phase space and Breit Wigner distributions to the so-called Goldhaber-plots  $M(K\pi)^+$  versus  $M(\Lambda\pi^+)$  (see fig. III.17a and b). We found the following cross sections:

$$\sigma(\Sigma^+(1385) K^{**}(890) \rightarrow \Lambda\pi^+K^+\pi^0) = (13 \pm 4) \mu\text{b}$$

$$\sigma(\Sigma^+(1385) K^{**}(890) \rightarrow \Lambda\pi K \pi) = (11 \pm 3) \mu\text{b}$$

The results for the other (3- and 4-body) reactions obtained from this program are in very good agreement with the values already quoted in this section.

A rather strong  $\rho^+(765)$  signal ( $s \approx 3.5$ ) is visible in the  $(\pi^+\pi^0)$ -spectrum (fig. III.15c). We estimate a contribution of  $(19 \pm 5)\%$  or:

$$\sigma(\Lambda K^+ \rho^+(765) \rightarrow \Lambda K^+ \pi^+ \pi^0) = (26 \pm 7) \mu\text{b}$$

### III.3.7 The channels $\Sigma^+K^+\pi^0$ (62 events) and $\Sigma^+K^0\pi^+$ (89 events)

In these channels the only clear signal stems from  $K^{**}(890)$ . The significance of the signals is 3.5 and  $\sim 3$  respectively (fig. III.18c and fig. III.19c). Fitting the combined mass plot

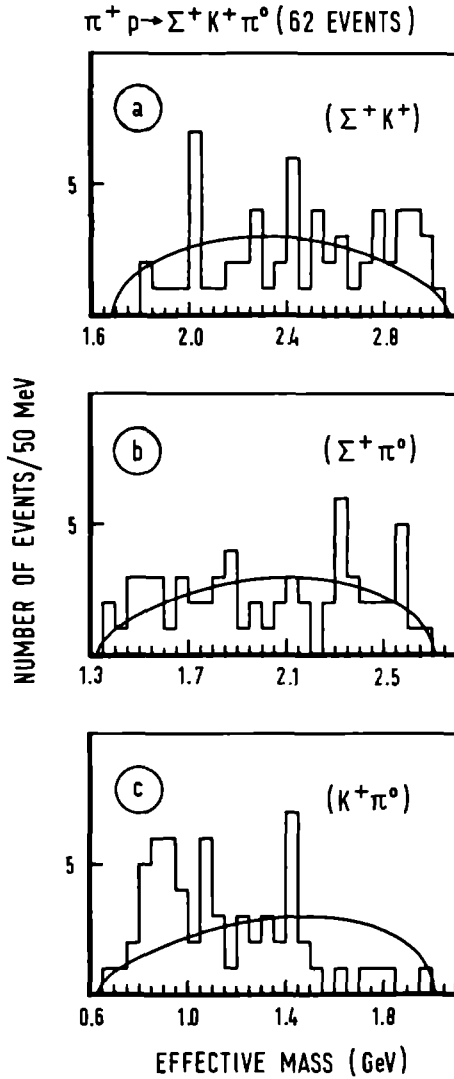


Fig. III.18. Two body mass spectra in the channel  $\Sigma^+ K^+ \pi^0$ . The curves are the phase space distributions normalized to the total number of events.

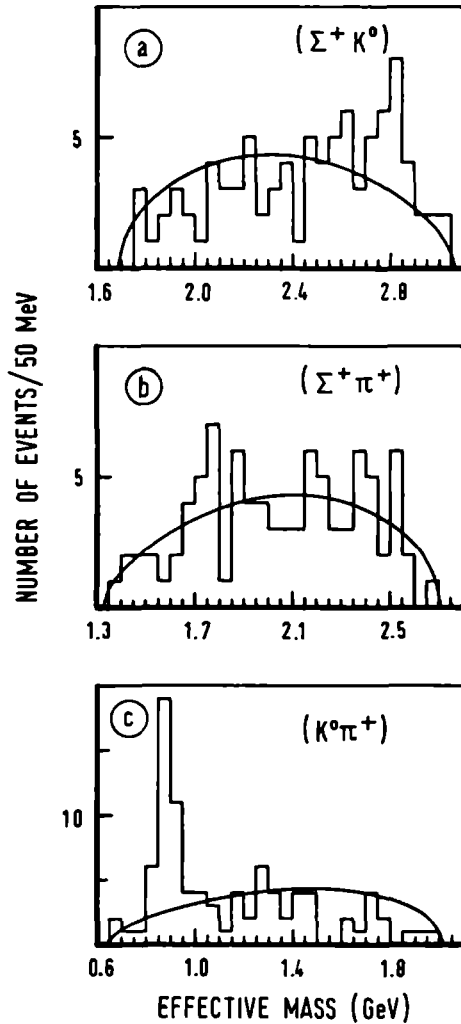
$\pi^+ p \rightarrow \Sigma^+ K^0 \pi^+$  (89 EVENTS)


Fig. III.19 Two body mass spectra in the channel  $\Sigma^+ K^0 \pi^+$ . The curves are the phase space distributions normalized to the total number of events.

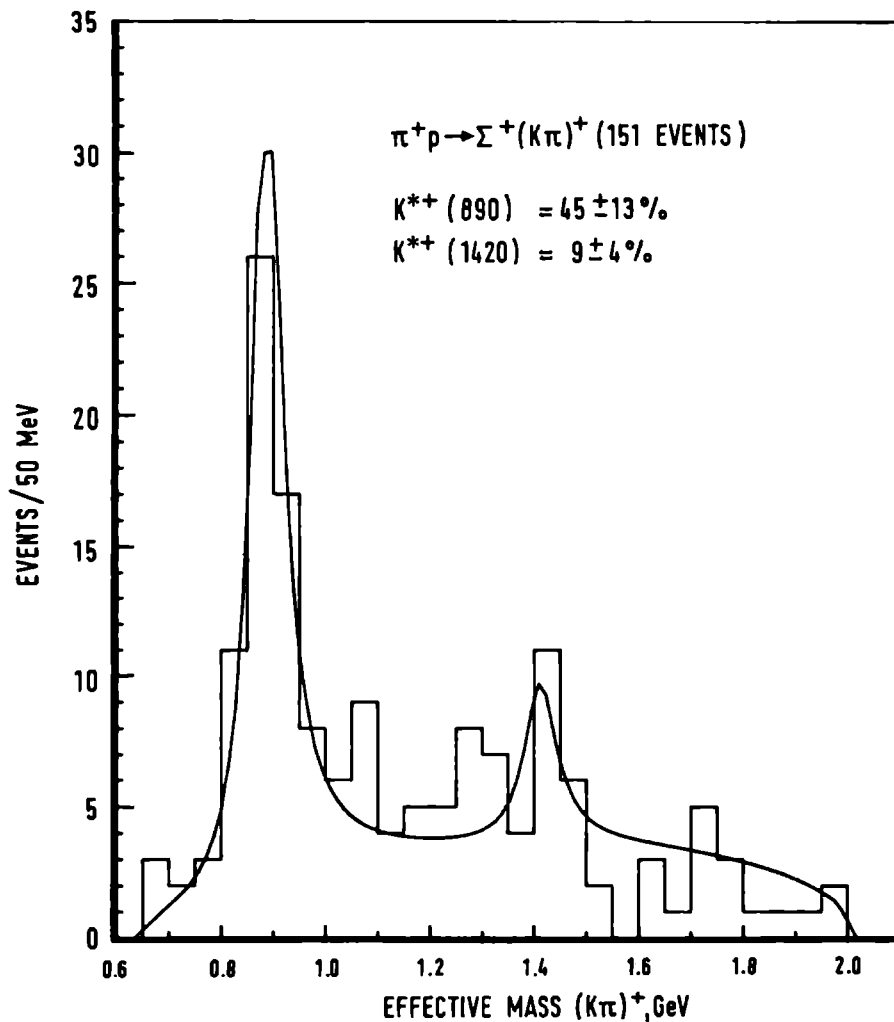


Fig. III.20  $(K\pi)^+$  mass spectrum from the combined channels  $\Sigma^+K^+\pi^0$  and  $\Sigma^+K^0\pi^+$ . The curve represents the result of fitting two Breit-Wigner distributions ( $K^*(890)$  and  $K^*(1420)$ ) and a phase space background.

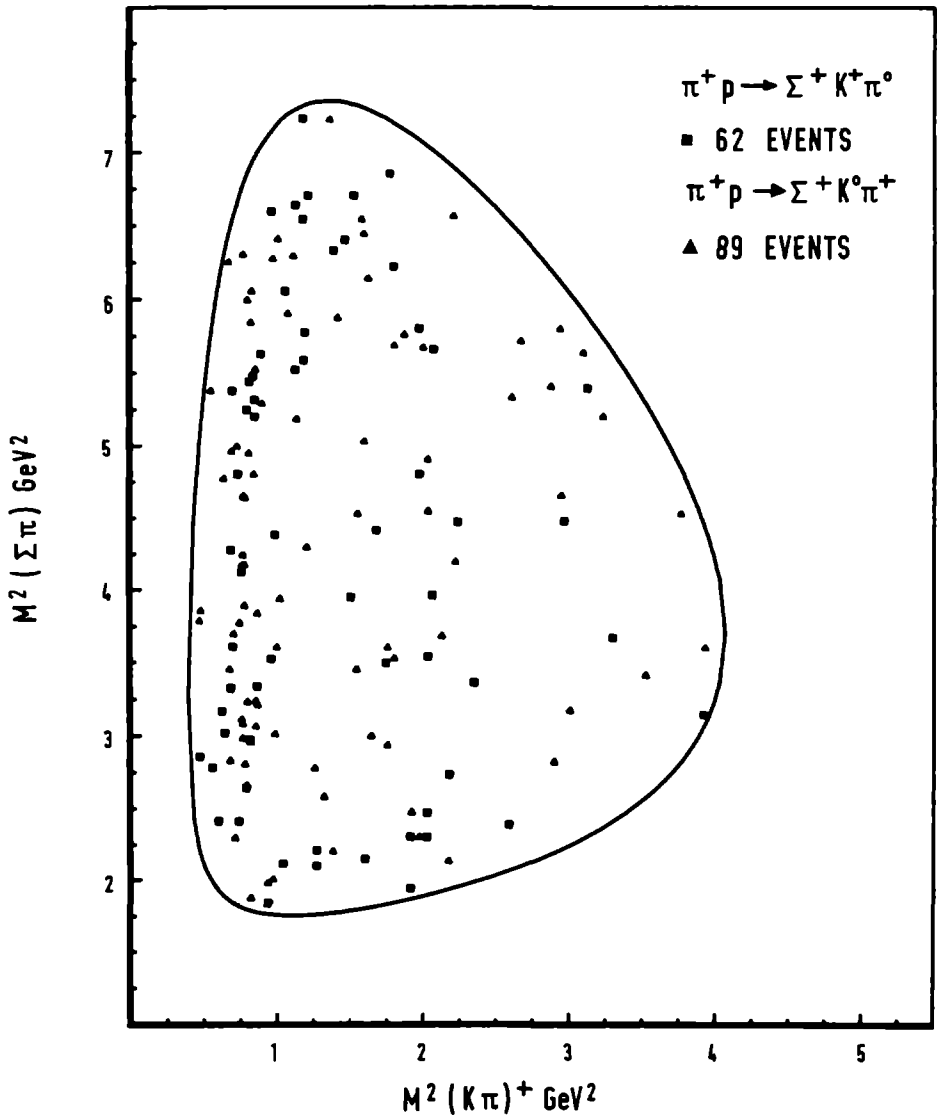


Fig. III.21 Dalitzplot  $M^2(\Sigma\pi)$  versus  $M^2(K\pi)^+$  for the combined channels  $\Sigma^+K^+\pi^0$  and  $\Sigma^+K^0\pi^+$ .

(fig. III.20) shows that  $K^{*+}$  (890) production is present in  $(45 \pm 13)\%$  of the events or:

$$\sigma(\Sigma^+ K^{*+} (890) \rightarrow \Sigma^+ (K\pi)^+) = (60 \pm 17) \mu\text{b}$$

of which approximately  $(22 \pm 6) \mu\text{b}$  is found in  $\Sigma^+ K^+ \pi^0$  and  $(38 \pm 16) \mu\text{b}$  in  $\Sigma^+ K^0 \pi^+$ . On the basis of the C.G. ratio of the  $K^{*+}$  decay modes involved, the ratio of these cross sections:

$$\frac{22 \pm 6}{38 \pm 16} = 0.6 \pm 0.3 \text{ is expected to be } 0.5.$$

The  $(K\pi)^+$  spectrum also shows a hint of  $K^{*+}$  (1420) production. The signal has  $s < 2$  and is too narrow. We estimate an upper limit (at a two standard deviations level) of:

$$\sigma(\Sigma^+ K^{*+} (1420) \rightarrow \Sigma^+ (K\pi)^+) < 19 \mu\text{b}.$$

The Dalitzplot  $M^2(\Sigma\pi)$  versus  $M^2(K\pi)^+$  is shown in fig. III.21.

### III.3.8 The channel $\Sigma^+ K^+ \pi^+ \pi^-$ (74 events)

. In the  $(K^+ \pi^-)$  distribution (fig. III.22e) we clearly observe  $K^{*0}$  (890) production ( $s \approx 3$ ) claiming  $(23 \pm 7)\%$  of the channel:

$$\sigma(\Sigma^+ \pi^+ K^{*0} (890) \rightarrow \Sigma^+ \pi^+ K^+ \pi^-) = (21 \pm 7) \mu\text{b}.$$

. Another hint of resonance production is given by the  $s \approx 2$  signal at the  $\rho^0$  (765) position in  $(\pi^+ \pi^-)$ -fig. III.22f. We estimate  $(19 \pm 8)\%$ :

$$\sigma(\Sigma^+ K^+ \rho^0 (765) \rightarrow \Sigma^+ K^+ \pi^+ \pi^-) = (17 \pm 8) \mu\text{b}$$

We find no evidence for correlation of this resonance with existing  $\Delta^{*+}$  resonances in  $(\Sigma^+ K^+)$ .

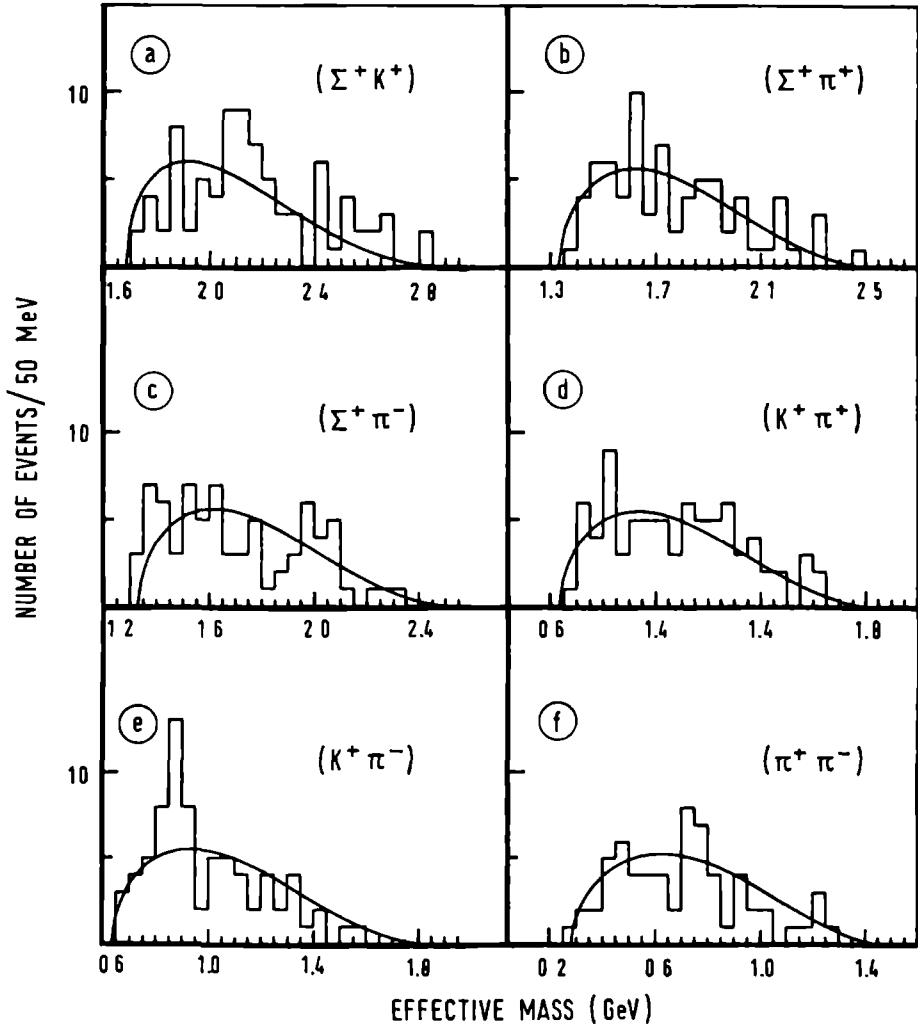
$\pi^+ p \rightarrow \Sigma^+ K^+ \pi^+ \pi^-$  (74 EVENTS)


Fig. III.22 Two body effective mass spectra in the channel  $\Sigma^+ K^+ \pi^+ \pi^-$ . The curves represent the phase space predictions normalized to the total number of events.



### III.3.9 Search for exotic baryon resonances

The existence of exotic (i.e.  $S = +1$ ) baryon resonances (symbol  $Z$ ) is still not definitely established. In the literature one finds references to  $Z$ -type bumps at mass values of 1780 and 1865 MeV ( $I=0$ ) and 1900, 2150 and 2500 MeV ( $I=1$ ).

Some of our  $S = +1$  ( $NK$ ) effective mass spectra show  $s > 2$  enhancements suggestive of resonance production:

(i) We observe an  $s \geq 3$  enhancement between 2050 and 2200 MeV in the  $(pK^+)$  spectrum from  $pK^+K^-\pi^+$  (fig. III.7a). This might be an indication for  $Z_1(2150)$  production. In the events with  $(p\pi^+)$  outside the  $\Delta^{++}(1236)$  band (1120-1320 MeV) an  $s \approx 2$  signal remains, indicating that the enhancement cannot be readily explained as a reflection caused by  $\Delta^{++}$  production. The relation with  $\bar{K}^{*0}(890)$  production in  $(K^-\pi^+)$  is unclear. The  $Z_1(2150)$  contribution corresponds to  $(8.5 \pm 4)\%$ .

(ii) In the  $(nK^+)$  spectrum from  $n\bar{K}^0K^+\pi^+$  (fig. III.12b) we observe an enhancement peaking between 1700 and 1850 MeV. Background estimation is difficult. The significance is  $\approx 2$  standard deviations. The central mass value seems too low to permit an association with the  $Z_1(1900)$ .

### III.3.10 The $(\bar{K}\bar{K}\pi)$ spectra

We investigated the doubly charged  $(\bar{K}\bar{K}\pi)^{++}$  spectrum of the channel  $n\bar{K}^0K^+\pi^+$  (not shown) and found no significant structure. The singly charged  $(\bar{K}\bar{K}\pi)^+$  spectrum from the combined channels  $p\bar{K}^0K^+\pi^0$ ,  $p\bar{K}^0K^0\pi^+$  and  $pK^+K^-\pi^+$  (fig. III.23) shows enhancements of approximately 2 standard deviations above background in the region

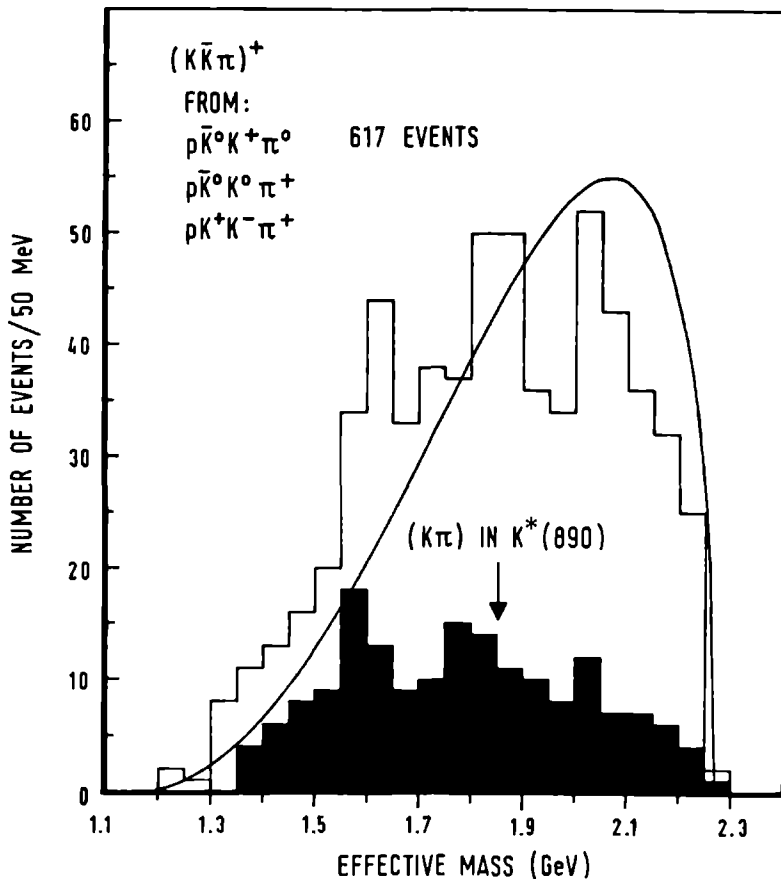


Fig. III.23  $(K\bar{K}\pi)^+$  effective mass spectrum from  $\rho\bar{K}^0K^+\pi^0$ ,  $\rho\bar{K}^0K^0\pi^+$  and  $\rho K^+K^-\pi^+$ . The shaded area corresponds to events with at least one combination  $(K^0\pi^0)$ ,  $(K^+\pi^0)$ ,  $(K^0\pi^+)$  or  $(K^-\pi^+)$  with an effective mass in the  $K^*(890)$  band (0.84 - 0.94 GeV). The curve represents the phase space distribution normalized to the total number of events.

between 1550 and 1650 MeV and between 1800 and 1900 MeV. If we require at least one  $(K\pi)$  combination to have an effective mass value within the  $K^*(890)$  band (840-940 MeV), the first signal maintains a significance of 2 whilst the second signal falls below this level. If we accept this to be an indication of a state decaying into  $K^*(890) \bar{K}$  and/or  $\bar{K}^*(890) K$ , the  $A_3^+$  (1640) is the nearest known candidate. Cooper et al.<sup>(13)</sup> claim to find no statistically compelling structure in  $(K\bar{K}\pi)^+$  at 5.4 GeV/c. Their spectrum shows a  $s \approx 1.5$  enhancement at approximately the same position (1550-1000 MeV) as ours. Aderholz et al.<sup>(14)</sup> at 8 GeV/c find an  $s \approx 4$  enhancement at  $(1490 \pm 20)$  MeV ( $F'(1540)$ ) and an  $s \approx 3.5$  signal at  $(1690 \pm 16)$  MeV ( $g(1680)$ ), both having  $K^*(890) \bar{K}$  and/or  $\bar{K}^*(890) K$  decay modes.

Neutral  $(\bar{K}\bar{K}\pi)$  spectra have been studied in several  $p\bar{p}$  experiments. Apart from the E-meson ( $I = 0$ ), several enhancements were reported in the region between 1625-1725 MeV<sup>(15)(16)</sup>.

## References - chapter III

- (1) O. Skjeggstad in Proceedings of the 1964 Easter School  
CERN 64-13 (1964).
- (2) G.F. Wolters in Kinematics and Multiparticle systems  
ed. M. Nikolić (Gordon and Breach, 1968),  
R.H. Dalitz, Ann. Rev. Nucl. Sci. 13, 339 (1963).  
See also ref. (9).
- (3) J.D. Jackson, Nuovo Cimento 34, 1644 (1964).
- (4) A. Barbaro-Galtieri in Advances in Particle Physics, vol. 2,  
ed. R.L. Cool and R.E. Marshak (Wiley, New York,  
1968),  
I. Pisūt and M. Roos, Nucl. Phys. B6, 325 (1968).
- (5) MINUIT, Long write-up D 506, Cern Program Library.
- (6) Bonn - Durham - Nijmegen - Paris (E.P.) - Torino Collabora-  
tion: K. Böckmann, M. Rost, B. Wagini, G. Winter, J.V. Major,  
C.L. Pols, D.J. Schotanus, D.Z. Toet, R.T. Van de Walle,  
E. Cirba, B. Quassiat, G. Rinaudo, M. Vigone, A. Werbrouck,  
Nucl. Phys. B16, 221 (1970).
- (7) W.R. Butler, D.G. Coyne, G. Goldhaber, J. MacNaughton and  
G.H. Trilling,  
Phys. Rev. D7, 3177 (1973).
- (8) C.L. Pols, D.J. Schotanus, D.Z. Toet, R.T. Van de Walle,  
K. Böckmann, K. Sternberger, B. Wagini, G. Winter, J.V. Major,  
E. Cirba, R. Vanderhaghen, G. Rinaudo, A. Werbrouck,  
Nucl. Phys. B25, 109 (1970).
- (9) H.J. Lipkin, Phys. Rev. 176, 1709 (1968).
- (10) P. Söding, J. Bartels, A. Barbaro-Galtieri, E. Enstrom, Th.  
A. Lasinski, A. Rittenberg, A.H. Rosenfeld, Th.G. Trippe,  
N. Barash-Schmidt, C. Bricman, V. Chaloupka and M. Roos,  
Phys. Lett. 39B, (1972).

*References - chapter III (cont.)*

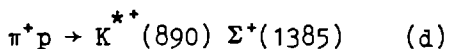
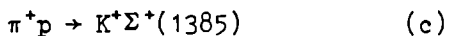
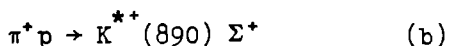
- (11) D.J. Schotanus, Ph.D. Thesis, Nijmegen (1971).
- (12) C.L.A. Pols, Ph.D. Thesis, Nijmegen (1972).
- (13) W.A. Cooper, W. Manner, B. Musgrave, D. Pollard and  
L. Voyvodič,  
Nucl. Phys. B23, 605 (1970).
- (14) M. Aderholz, J. Bartsch, R. Schulte, R. Speth,  
H.H. Kaufmann, S. Nowak, M. Bardadin-Otwinowska,  
V.T. Cocconi, J.D. Hansen, J. Loskiewicz, G. Kellner,  
A. Mihul, D.R.O. Morrison, H. Tøfte, A. Eskreys,  
K. Juszczak, D. Kisielewska, P. Malecki, W. Zielinski,  
H. Piotrowska and A. Wroblewski,  
Nucl. Phys. B11, 259 (1969).
- (15) B.R. French, J.B. Kinson, R. Rigopoulos, V. Simak,  
F. McDonald, G. Petmezas and L. Riddiford,  
N.C. 52A, 438 (1967).
- (16) C. Baltay, J. Lach, J. Sandweiss, H. Taft, N. Yeh,  
D.J. Crennell, Y. Oren, C.R. Richardson, D.L. Stonehill  
and R. Stump,  
Report to the International Conference on High  
Energy Physics, Dubna (1964).  
C. Baltay, J. Lach, J. Sandweiss, H.D. Taft, N. Yeh,  
D.L. Stonehill, and R. Stump,  
Phys. Rev. 142, 932 (1966).
- (17) G. Alexander, H.J. Lipkin and F. Scheck,  
Phys. Rev. Letters 17, 412 (1966).

*Chapter IV*

## CHARACTERISTICS OF SOME REACTIONS AND COMPARISON WITH MODELS

*IV.1 Introduction*

In this chapter we will discuss the following (quasi-) two body reactions:



A common feature of these reactions is, that within the framework of exchange model descriptions (see sect. IV.3) they need the exchange of objects with a strangeness quantum number different from zero.

For each of these reactions we study the experimental behaviour of the differential cross section as a function of four momentum transfer. For reactions (b), (c) and (d) we also examine the spin density matrix elements. Our results are compared with predictions from some models.

For the study of the reactions (b), (c) and (d) we used all events that satisfy the  $K^{*+} (890)$  and/or  $\Sigma^+(1385)$  mass band selections (840-940 MeV and 1330-1430 MeV respectively). We did not apply background corrections. Statistics rarely allow this and the methods commonly used are subject to criticism. Usually one predicts background behaviour in the resonance region by

interpolating from regions where the resonance contribution is believed to be negligible or small. As a consequence these regions are relatively far away from - and possibly no longer representative for - the region to be studied. Moreover one generally assumes that interference effects between the resonance and the background can be neglected, i.e. that the background is produced incoherently, an assumption which may or may not be justified (cf. ref. 2 chapter III).

We start this chapter with a definition of the variables used, a description of the quantities studied and an outline of the models discussed.

#### *IV.2 Mandelstam variables ; Differential cross section*

In fig. IV.1 we give a schematic representation of a (quasi-) two body reaction  $a+b \rightarrow c+d$  in the overall C.M.-system i.e. the system, where the total momentum is zero. In our case particle a (c) symbolizes the initial (final) state meson, while particle b (d) symbolizes the initial (final) state baryon. Kinematically the reaction can be described by variables:

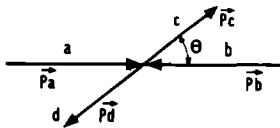


Fig. IV.1 Schematic representation of the kinematics of a 2-body reaction in the overall C.M.-system.

$p_i$  = the magnitude of the C.M. momentum of the initial state particles:  $p_i = |\vec{p}_a| = |\vec{p}_b|$

$p_f$  = the magnitude of the C.M. momentum of the final state particles:  $p_f = |\vec{p}_c| = |\vec{p}_d|$

$\theta$  = the C.M. production angle of one of the final state

particles; e.g.  $\cos \theta = \frac{\vec{p}_c \cdot \vec{p}_a}{|\vec{p}_c| |\vec{p}_a|}$

Because  $\theta$  and the momenta are not relativistically invariant, one often introduces the invariant variables  $s$ ,  $t$  and  $u$ :

$$s = - (P_a + P_b)^2 = - (P_c + P_d)^2 \quad (\text{IV.1})$$

$$t = - (P_a - P_c)^2 = - (P_b - P_d)^2 \quad (\text{IV.2})$$

$$u = - (P_a - P_d)^2 = - (P_b - P_c)^2 \quad (\text{IV.3})$$

In these expressions the symbol  $P_j$  denotes the four vector  $(p_j, iE_j)$  of particle  $j$ .  $s$ ,  $t$  and  $u$  are the so-called *Mandelstam variables*. They satisfy the relation:

$$s + t + u = m_a^2 + m_b^2 + m_c^2 + m_d^2$$

For our reaction  $a+b \rightarrow c+d$  the expressions ((IV.1)-(IV.3)) become:

$$s = E_{CM}^2 \quad (> 0) \quad (\text{IV.4})$$

$$\begin{aligned} t &= m_a^2 + m_c^2 - 2E_a E_c + 2p_a p_c \cos \theta \\ &= m_b^2 + m_d^2 - 2E_b E_d + 2p_b p_d \cos \theta \quad (< 0) \end{aligned} \quad (\text{IV.5})$$

$$\begin{aligned} u &= m_a^2 + m_d^2 - 2E_a E_d - 2p_a p_d \cos \theta \\ &= m_b^2 + m_c^2 - 2E_b E_c - 2p_b p_c \cos \theta \quad (< 0) \end{aligned} \quad (\text{IV.6})$$



In Eq. (IV.4)  $E_{CM}$  denotes the total energy in the C.M.-system. In this channel  $t$  and  $u$  are called *four momentum transfers*.

To obtain a symmetric description one replaces in fig. IV.1 the outgoing particles  $m$  with four momenta  $P_m$  by anti-particles  $\bar{m}$  with four momenta  $P_m^- = -P_m$  (fig. IV.2). We now can rewrite Eqs. (IV.1) - (IV.3) as follows:

$$s = - (P_a + P_b)^2 = - (P_c^- + P_d^-)^2 \quad (IV.1a)$$

$$t = - (P_a + P_c^-)^2 = - (P_b + P_d)^2 \quad (IV.2a)$$

$$u = - (P_a + P_d^-)^2 = - (P_b + P_c^-)^2 \quad (IV.3a)$$

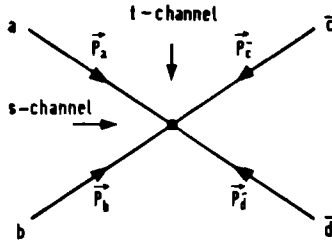


Fig. IV.2 Illustration of a symmetric description of two body reactions.

Fig. IV.2 can be interpreted as the representation of three different reactions. We list them here with their names and with some characteristics:

$$a+b \rightarrow c+d ; s\text{-channel reaction} ; s > 0, t < 0, u < 0$$

$$a+\bar{c} \rightarrow \bar{b}+d ; t\text{-channel reaction} ; s < 0, t > 0, u < 0$$

$$a+\bar{d} \rightarrow \bar{b}+c ; u\text{-channel reaction} ; s < 0, t < 0, u > 0.$$

We find:

$$E_{CM}^2(\text{t-channel reaction}) = - (p_a + p_c)^2 \equiv t$$

In this channel  $t$  has the meaning of an energy variable and is now  $> 0$ , while  $s$  and  $u$  are now four momentum transfers  $< 0$ . An analogous discussion can be given for the  $u$ -channel, where now  $u$  is the energy variable. The  $s$ ,  $t$  and  $u$  channel reactions are 'physical' in different regions of the  $(s, t, u)$  space. We will make use of the above symmetric description in section IV.3.

The *differential cross section* is defined as the cross section per unit of solid angle  $d\sigma/d\Omega$  or equivalently as  $d\sigma/[d(\cos \theta) d\varphi]$ , where  $\varphi$  is the azimuthal angle. In fig. (IV.1)  $\varphi$  is defined as the angle of rotation of the production plane around  $\vec{p}_a$ . If the beam and the target are unpolarized (as is the case in our experiment),  $\varphi$  is physically irrelevant and can be integrated over. As  $\cos \theta$  is linearly dependent on  $t$  (cf. Eq. (IV.5)), the differential cross section is often defined in terms of  $t$ , i.e. as  $d\sigma/dt$ .

The maximum (minimum) value of  $t$  is obtained by putting  $\cos \theta = +1(-1)$  in Eq. (IV.5) e.g.:

$$m_a^2 + m_c^2 - 2E_a E_c - 2p_a p_c \leq t \leq \tag{IV.7}$$

$$m_a^2 + m_c^2 - 2E_a E_c + 2p_a p_c$$

For a two body reaction involving stable particles only, ideally - in the limit of infinite measuring precision -  $|t|_{\min}$  ( $= -t_{\max}$ ) has the same value for all events. If however a resonance is produced (e.g. particle  $c$  in fig. IV.1),

$m_c$  has a distribution of finite width (cf. the Breit-Wigner distribution, sect. III.2.2) and the lowest  $|t|$  values reached correspond to the lowest possible  $m_c$  values, i.e. to the left tail of the resonance mass distribution. In addition, measuring errors will tend to wash out these limits.

In order to separate these effects from other - possibly dynamical - effects, one often uses the so-called *reduced* four-momentum transfer  $t'$ , defined as:

$$t' = t_{\max} - t = |t| - |t|_{\min}$$

where  $|t|_{\min}$  is a limit varying from event to event depending on the observed value of  $m_c$ . The differential cross section is then correspondingly defined as  $d\sigma/dt'$ .

### IV.3 Outline of models used

Interactions at energies in or above the region of our experiment are often characterized by a common feature: in the C.M. system of the interaction the produced particles can be grouped into two systems; in one the particles closely follow the original direction of the beam particle, while in the other system directions close to that of the target particle dominate. This forward-backward preference is generally the stronger the smaller the number of particles produced. One describes this situation by stating that the two initial state particles interact *peripherally* instead of head-on or, equivalently, that the interaction is dominated by long range forces.

These forces can be thought of as mediated by the exchange

of one or more (virtual) particles. Models based upon this idea are called *exchange models*.

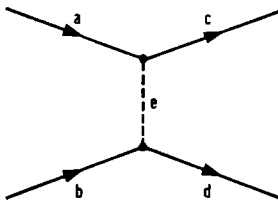


Fig. IV.3 Diagram of a two body reaction mediated by an exchange process.

For (quasi-) two body interactions one schematically depicts this situation by the diagram of fig. IV.3. The incident particles  $a$  and  $b$  interact by means of the exchange of one or more objects  $e$ ; the interaction produces the particles (or particle systems)  $c$  and  $d$ .

The strong interaction conserves the total isospin ( $I$ ),  $G$ -parity ( $G$ ), angular momentum ( $l$ ), parity ( $P$ ), baryon number ( $B$ ) and strangeness ( $S$ ) at each of the vertices ( $aec$ ) and ( $bed$ ). This puts restrictions on the quantum numbers of  $e$ : the conservation laws determine which 'particles'  $e$  can be exchanged. If  $a$  and  $c$  (fig. IV.3) are mesons and  $b$  and  $d$  are baryons ( $B=1$ ),  $e$  must have  $B = 0$  (meson exchange). If  $a$  and  $d$  are mesons and  $b$  and  $c$  are baryons,  $e$  has  $B = 1$  (baryon exchange). Because of peripherism the meson exchange reaction will mainly populate the low  $|t|$  region i.e. the secondary meson (baryon) will closely follow the direction of the primary mesons (baryon) ('forward peak'). On the other hand, in a

peripheral baryon exchange reaction the secondary meson (baryon) will approximately follow the direction of the primary baryon (meson) ('backward peak').

Calling  $\mu$  the 'mass' of  $e$ , one finds, e.g. at vertex (aec) in fig. IV.3):

$$\mu^2 = (E_a - E_c)^2 - (\vec{p}_a - \vec{p}_c)^2 = - (P_a + P_c)^2 = t \quad (\text{IV.8})$$

Since  $t < 0$  for our process, we find  $\mu^2 < 0$ . The exchanged object is called a 'virtual particle' ('off the mass shell');  $\mu^2$  is a linear function of the cosine of the scattering angle  $\theta$  (sect. IV.2).

The simplest exchange model is based upon the so-called *Born Term Model*<sup>(1)</sup>. In this model the transition probability (amplitude) between initial and final state is given by the sum of all possible Born terms, calculated by means of the Feynman rules in lowest order perturbation theory. These terms generally contain two vertex factors and a so-called propagator of the form  $(m_e^2 - t)^{-1}$ , where  $m_e$  is the mass of a physical particle ('on the mass shell') with the quantum numbers of  $e$ . The propagator has a pole at the unphysical value  $t = m_e^2$  and tends to make the amplitude large for physical  $t$  values close to the pole, i.e. for small negative  $t$  values or for small scattering angles. One often reduces the number of Born terms to one by considering only the dominating Feynman diagram. In terms of the propagator this usually means that only the term containing the *lightest* particle with the required quantum numbers is kept.

Of course in general also the effect of the vertex factors has to be taken into account.

Models of the above type are called *one-particle exchange (OPE) models*. Qualitatively the behaviour predicted for the differential cross section as a function of  $t$  agrees with the observations. Quantitatively however the predicted decrease of  $d\sigma/dt$  with  $|t|$  is much slower than experimentally observed. Moreover, the calculated absolute values of the cross sections are generally too high.

Among the models that try to remedy this situation are the so-called *absorption-models*. One introduces the idea, that at higher energies many inelastic channels compete with and suppress each other. This 'absorptive' effect is the stronger the closer the incident particles come together. Using the relation  $l(l+1) \sim (pb/\hbar)^2$  - where  $l$  is the relative angular momentum of the incident particles,  $p$  the C.M. momentum and  $b$  the impact parameter - one sees that small impact parameters correspond to low  $l$  values. This implies that the reduction of the differential cross section caused by the absorption effect will be strongest for collisions with low  $l$ -values or, correspondingly (because low impact-parameters also mean large scattering angles) strongest for collisions with large  $|t|$ -values.

In practice the idea of absorption is implemented by the introduction of an  $l$ -dependent factor which damps the amplitude contribution of partial waves with low angular momentum. The net effect is, that  $d\sigma/dt$  falls off sharper with  $|t|$  than in the simple OPE model.

Absorption models are successful in describing several aspects of a limited number of interactions; e.g. the Gottfried-

Jackson absorption model<sup>(2)</sup> for reactions with  $\pi$ -exchange and the Dar-Watts-Weisskopf absorption model<sup>(3)</sup> for exchange of mesons with  $J \leq 1$ . Several discrepancies however remain (e.g. the predictions for the s-dependence of cross sections).

A different class of models are the so-called *Regge-pole models*. The basic ideas behind these models stem from developments in low energy potential scattering theory. Regge has shown that the partial wave amplitudes, considered as complex functions not only of energy, but also of angular momentum, have poles for (complex) values  $l = \alpha(E)$ . For E-values where  $l = \text{integer} > 0$  ('physical'  $l$  values) the poles are associated with bound states ( $E < 0$ ) or resonances ( $E > 0$ ). The function  $\alpha(E)$ , interpolating between the positions of the poles, is called a *Regge trajectory*. One generally assumes that these Regge trajectories also exist in relativistic scattering processes and - for each specific family of particles with common internal quantum numbers (B, I, G, S and P, i.e. the quantum numbers conserved by strong interactions) - give the spin ( $J$ ) as a function of mass ( $M_0$ ):  $J = \text{Re}\alpha(M_0^2)$ .

The importance of Regge-pole theory for scattering processes results from its combination with the concept of *crossing symmetry*. Following this concept the amplitudes for related s-, t- and u-channel reactions (sect. IV.2) are given by the values of one single analytic function  $A(s, t, u)$  in the respective 'physical' s, t, and u regions. Consider for example the t-channel reaction  $a + \bar{c} \rightarrow \bar{b} + d$  (fig. IV.4b). Resonances  $R$ , formed according to the scheme  $a + \bar{c} \rightarrow R \rightarrow \bar{b} + d$  lie on the trajectory  $\alpha(t)$  and have spins  $J_R = \alpha(t = M_R^2)$  ( $M_R$  being a resonance mass). By crossing one now can relate this low energy behaviour in the t-channel ( $t$  small  $> 0$ ,  $s \rightarrow \infty$ ) to the high energy be-

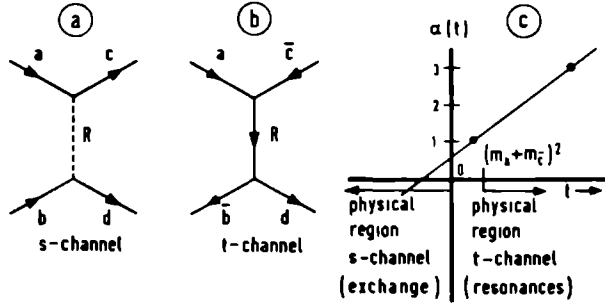


Fig. IV.4 An s-channel reaction (a) and a t-channel reaction (b) mediated by the same Regge trajectory  $R$ ; (c) Chew-Frautschi plot for an odd signature Regge trajectory.

haviour in the (crossed) s-channel ( $t < 0$ ,  $|t|$  small,  $s \rightarrow \infty$ )  $a+b \rightarrow c+d$  (fig. IV.4a). One thus describes the amplitude in the s-channel as a sum of terms involving t-channel Regge trajectories  $\alpha(t)$ .

The amplitude in the s-channel obtained has the general form:

$$A_{\lambda_t}^{(s)}(s, t) \xrightarrow{s \rightarrow \infty} \sum f_{\lambda_t}(t) \beta_{\lambda_t}(t) \xi(t) (s/s_0)^{\alpha(t)} \quad (\text{IV.9})$$

The sum runs over different Regge trajectories, each characterized by a different set of allowed internal quantum numbers. The *index*  $\lambda_t$  denotes the t-channel spin state of the incoming and outgoing particles. The *function*  $f_{\lambda_t}(t)$  contains kinematical factors and accounts for the conservation of total angular momentum in the s-channel.  $\beta_{\lambda_t}$  is the so-called *residue function*. The *signature factor*  $\xi(t)$  gives the phase of the amplitude and can be written as:



$$\xi(t) = \frac{1 + \tau \exp(-i\pi\alpha(t))}{\sin \pi\alpha(t)}$$

indicating that a Regge trajectory links together poles with  $J = \text{even}$  ( $\tau = +1$ ) or  $J = \text{odd}$  ( $\tau = -1$ ) only (e.g. resonances with spins separated by two units of angular momentum only). If two trajectories of opposite signature and parity coincide, one calls these trajectories *exchange degenerate*. The factor  $(s/s_0)^{\alpha(t)}$  gives the energy dependence of the amplitude ( $s_0$  is a scale factor). Often one approximates the amplitude by considering only the trajectory with the largest  $\alpha(t)$  (leading trajectory).

One generally assumes that  $\alpha(t)$  depends linearly on  $t$  (fig. IV.4c). For  $t > 0$  this assumption is born out by the experimentally observed  $J$  versus  $M^2$  dependence. By analyzing high energy processes one also finds that the functions  $\alpha(t)$  ( $t < 0$ ) are compatible with linear extrapolation of their positive  $t$  branches.

For more detailed descriptions of the above and further aspects of Regge pole theory we refer to literature<sup>(4)</sup>.

To test a model one usually compares its predictions for the differential cross sections, the energy dependence of the cross sections etc. with the data. In the case of a decaying product one can in principle also compare the decay angular distribution and spin density matrix elements. This subject is shortly described in the next section.

#### IV.4 The decay angular distribution; spin density matrix elements

In exchange processes the mixture of spin substates of the reaction products depends on the spin and parity of the particle(s) exchanged. If in addition one or more of produced particles decays, one can obtain information on this mixture by studying the decay angular distribution(s).

In this thesis we will study decay angular distributions in the so-called Gottfried-Jackson system (see fig. IV.5). In this system the resonance  $d$  is at rest and the spin-quantization axis is in the direction of the initial state particle at the production vertex ( $bed$ ). The resonance decay products are called  $\alpha$  and  $\beta$  (two body decay). If  $d$  is a meson- (baryon-) resonance,  $b$  is the initial state meson (baryon);

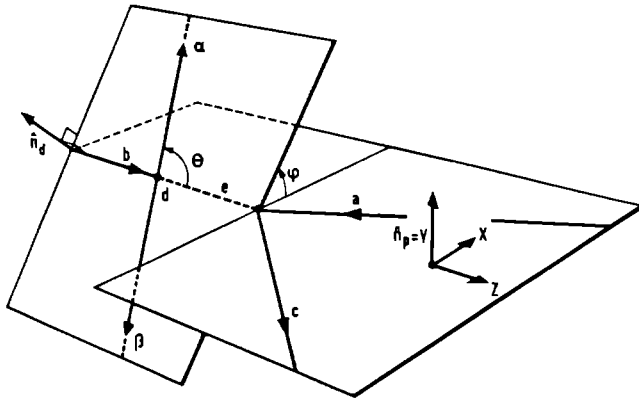


Fig. IV.5 Gottfried-Jackson frame for the study of the decay of a resonance  $d$  produced in an interaction  $a+b \rightarrow c+d$ . For details we refer to the text.

a and c are the initial and final state particles at the other vertex (aec); e represents the exchanged particle. We now define (fig. IV.5):

$$\begin{aligned}
 \text{the normal to the production plane: } \hat{n}_p &= \vec{a} \times \vec{c} / |\vec{a} \times \vec{c}| \\
 \text{the normal to the decay plane} &: \hat{n}_d = \vec{b} \times \vec{\alpha} / |\vec{b} \times \vec{\alpha}| \\
 \text{the Gottfried-Jackson frame} &: \hat{z} = \hat{b} \\
 &: \hat{y} = \hat{n}_p \\
 &: \hat{x} = \hat{y} \times \hat{z}
 \end{aligned}$$

the Gottfried-Jackson frame decay angles:

$$\begin{aligned}
 \theta &= \text{arc cos } (\hat{z} \cdot \hat{\alpha}) \\
 \psi &= \text{arc cos } (\hat{y} \cdot \hat{n}_d) \\
 &= \text{arc sin } (\hat{x} \cdot \hat{n}_d)
 \end{aligned}$$

The statistical mixture of spin states of a resonance d, produced in a reaction  $a+b \rightarrow c+d$  is usually described by means of the spin density matrix formalism.

We symbolize the orientation (e.g. the z-component) of the spins of a, b, c and d (if any) by k, l, m and n respectively. By  $M_m^c(\hat{\alpha}, q)$  we denote the amplitude for decay of c from a state with 'orientation' m into a two body final state with angular vector  $\hat{\alpha}$  ( $= \cos \theta, \varphi$ ) and with spin orientations of the decay products symbolized by q. In the most general case we can write an analogous expression for the decay amplitude of d:  $M_n^d(\hat{\beta}, r)$ . The transition amplitude between the initial state and the final state can thus be written as:

$$M_m^c(\hat{\alpha}, q) M_n^d(\hat{\beta}, r) \langle m, n | T | k, l \rangle$$

The joint decay distribution  $W(\hat{\alpha}, \hat{\beta})$  is now given by<sup>\*</sup>:

<sup>\*</sup>) *Note.* General expressions for decay angular distributions can be found in ref. (6).

$$\begin{aligned}
W(\hat{\alpha}, \hat{\beta}) &= \\
&= \sum_{mm'} [\sum_q M_m^c(\hat{\alpha}, q) M_m^{c*}(\hat{\alpha}, q)] [\sum_r M_n^d(\hat{\beta}, r) M_n^{d*}(\hat{\beta}, r)] \rho_{nn'}^{mm'}
\end{aligned} \tag{IV.10}$$

where:

$$\rho_{nn'}^{mm'} = \sum_{k,l} \langle m, n | T | k, l \rangle \langle m', n' | T | k, l \rangle^* \tag{IV.11}$$

are the joint *spin density matrix elements*.

The functions  $M_m^c$ ,  $M_n^d$  are generalized spherical harmonics. Integration over  $\hat{\alpha}$  resp.  $\hat{\beta}$  gives the decay distributions of d resp. c alone. Because of orthonormality:

$$\int \sum_q M_m^c(\hat{\alpha}, q) M_m^{c*}(\hat{\alpha}, q) d\Omega_\alpha = \delta_{mm}$$

and we obtain for  $W(\hat{\beta})$ :

$$W(\hat{\beta}) = \sum_{nn'} [\sum_r M_n^d(\hat{\beta}, r) M_n^{d*}(\hat{\beta}, r)] \rho_{nn'} \tag{IV.12}$$

with:

$$\rho_{nn'} = \sum_m \rho_{n,n'}^{m,m} \tag{IV.13}$$

An analogous expression can be obtained for  $W(\hat{\alpha})$  and  $\rho_{mm'}$ .

In general the spin density matrix elements depend on t (or the production angle). General properties are:

$$0 \leq \rho_{m,m} \leq 1 \tag{IV.14}$$

$$\sum_m \rho_{m,m} = 1 \tag{IV.15}$$

$$\rho_{m,m'} = \rho_{m',m}^* \text{ (hermiticity)} \tag{IV.16}$$

Moreover, for parity conserving reactions between unpolarized particles, the following relation holds in any system with the quantization axis (z) in the production plane: \*)

$$\rho_{m,m'} = (-1)^{m-m'} \rho_{-m,-m'} \quad (\text{IV.17})$$

Using the properties given above, one can write the density matrix for  $K^*(890)$  ( $J=1$ ) as:

$$\rho(J=1) = \begin{bmatrix} \frac{1}{2}(1 - \rho_{0,0}) & \rho_{1,0} & \rho_{1,-1} \\ \rho_{1,0}^* & \rho_{0,0} & -\rho_{1,0}^* \\ \rho_{1,-1} & -\rho_{1,0} & \frac{1}{2}(1 + \rho_{0,0}) \end{bmatrix} \quad (\text{IV.18})$$

This matrix depends on 4 independent parameters, as  $\rho_{00}$  and  $\rho_{1,-1}$  are real (see Eqs. (IV.16) and (IV.17)).

For the decay  $K^*(890) \rightarrow K\pi$  ( $J_c = 1$ ,  $J_\alpha = J_\beta = 0$ ) one derives the following decay distribution:

$$W^{(1,0,0)}(\cos \theta, \varphi) = \frac{3}{4\pi} \left\{ \frac{1}{2}(1 - \rho_{0,0}) + \frac{1}{2}(3\rho_{0,0} - 1) \cos^2 \theta - \right. \quad (\text{IV.19})$$

$$\left. - \rho_{1,-1} \sin^2 \theta \cos 2\varphi - \sqrt{2} \text{Re } \rho_{1,0} \sin 2\theta \cos \varphi \right\}$$

with the projected distributions:

$$W^{(1,0,0)}(\cos \theta) = \frac{3}{4} \left\{ (1 - \rho_{0,0}) + (3\rho_{0,0} - 1) \cos^2 \theta \right\} \quad (\text{IV.19a})$$

$$W^{(1,0,0)}(\varphi) = \frac{1}{2\pi} \left\{ 1 + 2\rho_{1,-1} - 4\rho_{1,-1} \cos^2 \varphi \right\} \quad (\text{IV.19b})$$

\*) *Note.* For further details on the density matrix formalism we refer to ref. 5 and 6.

The spin density matrix for  $\Sigma^+(1385)$  ( $J=3/2$ ) - writing  $\rho_{n,m}$  for  $\rho_{\frac{n}{2}, \frac{m}{2}}$  - has the form:

$$\rho(J=3/2) = \begin{bmatrix} \rho_{3,3} & \rho_{3,1} & \rho_{3,-1} & \rho_{3,-3} \\ * & \frac{1}{2}\rho_{3,3} & \rho_{1,-1} & * \\ \rho_{3,1} & -\rho_{1,-1} & \frac{1}{2}\rho_{3,3} & \rho_{3,-1} \\ * & -\rho_{3,-1} & * & * \\ \rho_{3,-1} & -\rho_{3,-1} & \frac{1}{2}\rho_{3,3} & -\rho_{3,1} \\ -\rho_{3,-3} & \rho_{3,-1} & -\rho_{3,1} & \rho_{3,3} \end{bmatrix} \quad (\text{IV.20})$$

This matrix depends on 7 independent parameters:  $\rho_{3,3}$ ,  $\rho_{3,-3}$  and  $\rho_{1,-1}$  are real;  $\rho_{3,1}$  and  $\rho_{3,-1}$  are complex.

For  $\Sigma^+(1385)$  decaying into  $\Lambda$  and  $\pi^+$  ( $J_d = \frac{3}{2}$ ,  $J_\alpha = \frac{1}{2}$ ,  $J_\beta = 0$ ) the decay distribution takes the form:

$$W\left(\frac{3}{2}, \frac{1}{2}, 0\right)(\cos \theta, \varphi) = \frac{3}{4\pi} \left\{ \frac{1}{6}(1+4\rho_{3,3}) + \frac{1}{2}(1-4\rho_{3,3}) \cos^2 \theta \right. \\ \left. - \frac{2}{\sqrt{3}} \text{Re } \rho_{3,-1} \sin^2 \theta \cos 2\varphi - \frac{2}{\sqrt{3}} \text{Re } \rho_{3,1} \sin 2\theta \cos \varphi \right\} \quad (\text{IV.21})$$

with the projected distributions:

$$W\left(\frac{3}{2}, \frac{1}{2}, 0\right)(\cos \theta) = \frac{1}{4} \left\{ (1+4\rho_{3,3}) + (3-12\rho_{3,3}) \cos^2 \theta \right\} \quad (\text{IV.21a})$$

$$W\left(\frac{3}{2}, \frac{1}{2}, 0\right)(\varphi) = \frac{1}{2\pi} \left\{ \left(1 + \frac{4}{\sqrt{3}} \text{Re } \rho_{3,-1}\right) - \frac{8}{\sqrt{3}} \text{Re } \rho_{3,-1} \cos^2 \varphi \right\} \quad (\text{IV.21b})$$

The experimental values of the matrix elements are obtained by fitting the appropriate expression to the experimental distribution (e.g. by using a maximum likelihood method) or by using the so-called method of moments.

The latter method uses the fact that the average values of the different functions  $f(\cos \theta, \varphi)$  building up  $W(\cos \theta, \varphi)$  i.e.:

$$\bar{f} = \int d \cos \theta d\varphi f(\cos \theta, \varphi) W(\cos \theta, \varphi)$$

become particularly simple expressions of co-factors of  $f$  if  $W(\cos \theta, \varphi)$  is written in terms of orthogonal functions. The averages relevant for  $K^*$  decay are given by:

$$\begin{aligned} \overline{\cos^2 \theta} &= \frac{1}{5}(1 + 2\rho_{0,0}) \\ \overline{\sin^2 \theta \cos 2\varphi} &= -\frac{4}{5} \rho_{1,-1} \\ \overline{\sin 2\theta \cos \varphi} &= -\frac{4\sqrt{2}}{5} \operatorname{Re} \rho_{1,0} \end{aligned} \quad (\text{IV.22})$$

and for  $\Sigma^*(1385)$  decay by:

$$\begin{aligned} \overline{\cos^2 \theta} &= \frac{1}{15}(7 - 8\rho_{3,3}) \\ \overline{\sin^2 \theta \cos 2\varphi} &= -\frac{8}{5\sqrt{3}} \operatorname{Re} \rho_{3,-1} \\ \overline{\sin 2\theta \cos \varphi} &= -\frac{8}{5\sqrt{3}} \operatorname{Re} \rho_{3,1} \end{aligned} \quad (\text{IV.23})$$

In the method of moments the r.h.s. spin density matrix elements are obtained from approximate l.h.s. *average* values derived from the experimental sample by putting e.g.:

$$\overline{\cos^2 \theta} \approx \frac{1}{N} \sum_K^N \cos^2 \theta_K \quad (\text{IV.24})$$

where  $\theta_K$  is the value of  $\theta$  for the K-th event and where the K-sum runs over the total experimental sample consisting of N events.

Minnaert<sup>(7)</sup> has shown, that - because the eigenvalues of the spin density matrix are all positive - the elements of this matrix have to satisfy certain conditions. For frames with the quantization axis in the production plane (such as the Gottfried-Jackson frame used here) the following positivity conditions hold:

for spin 1 ( $K^*$ ):

$$|\rho_{1,-1}| \leq \frac{1}{2}(1-\rho_{0,0}) \quad (\text{IV.25})$$

$$|\text{Re } \rho_{1,0}| \leq \frac{1}{2} [\rho_{0,0}(1-\rho_{0,0}-2\rho_{1,-1})]^{1/2} \quad (\text{IV.26})$$

for spin  $\frac{3}{2}$  ( $\Sigma^+(1385)$ ):

$$(\rho_{3,3}^{-1/4})^2 + (\text{Re } \rho_{3,1})^2 + (\text{Re } \rho_{3,-1})^2 \leq \frac{1}{16} \quad (\text{IV.27})$$

#### IV.5 The reaction $\pi^+p \rightarrow K^+\Sigma^+$

##### IV.5.1 Experimental Results

The cross section for  $\pi^+p \rightarrow K^+\Sigma^+$  was found to be  $(59 \pm 10) \mu\text{b}$  (see table II.26 and fig. II.2j).

In fig. (IV.6) we show the differential cross section for this reaction as a function of  $t'$ . Only events with  $\Sigma^+ \rightarrow \pi\pi^+$  decay were used. Each individual event has been weighted for



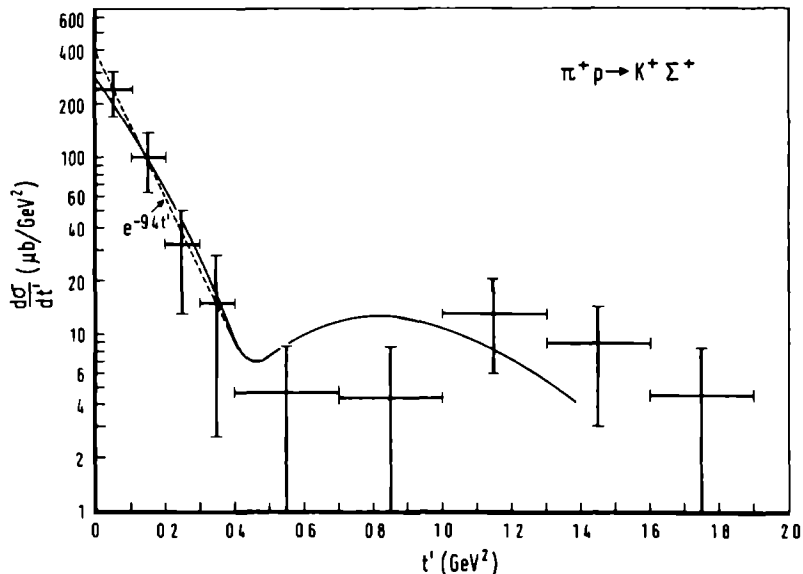


Fig. IV.6 Differential cross section as a function of  $t'$  for the reaction  $\pi^+ p \rightarrow K^+ \Sigma^+$ . The solid curve represents the prediction of the model of Reeder and Sarma<sup>(10)</sup>. The dashed line represents the result of a fit to an expression of the form  $\frac{d\sigma}{dt} = A \exp(-\lambda t)$ .

geometrical and angular losses. We find that the forward  $t'$  distribution ( $0 \leq t' \leq 0.4$ ) can be approximated by an expression of the form  $\frac{d\sigma}{dt} = A \exp(-\lambda t)$ . The symbol  $\lambda$  is often called the 'slope' (parameter) of the differential cross section. Its numerical value can be found in table IV.1.

Data for this reaction are available at several beam momenta and were obtained using different measurement techniques (9a-d, f-j). We especially mention the high statistics wire spark chamber results published by the Argonne-Michigan group (9f-i) and the Stony Brook - Wisconsin results<sup>(9j)</sup>. Some of

TABLE IV.1

Parameters in $d\sigma/dt = Ae^{-\lambda t}$ for $\pi^+p \rightarrow K^+\Sigma^+$				
$P_{\text{beam}}$ (GeV/c)	t-region (GeV <sup>2</sup> )	A ( $\mu\text{b}/\text{GeV}^2$ )	$\lambda$ (slope) (GeV <sup>-2</sup> )	ref.
3.0	$\lesssim 0.1$	$1037 \pm 34$ *)	$14.68 \pm 0.92$	9 h
3.0	0.1 - 0.4	$466 \pm 16$ *)	$6.06 \pm 0.20$	9 h
3.0	$\lesssim 0.45$	$500 \pm 40$	$6.4 \pm 0.4$	9 f
3.23	$\lesssim 0.5$	-	9.6	9 a
3.25	$\lesssim 0.4$	$540 \pm 40$	$7.2 \pm 0.4$	9 f
3.7	$\lesssim 0.4$	$690 \pm 160$	$8.4 \pm 1.4$	9 b
4.0	$\lesssim 0.4$	$430 \pm 30$	$8.8 \pm 0.5$	9 f
4.0	$\leq 0.44$	$248 \pm 28$	$4.6 \pm 0.5$	9 e
5.0	$\leq 0.41$	$455 \pm 160$	$9.4 \pm 1.9$	This expt.
5.0	$\leq 0.35$	$473 \pm 14$ *)	$9.37 \pm 0.16$	9 h
5.05	$\lesssim 0.45$	$360 \pm 40$	$8.8 \pm 0.5$	9 f
5.4	$\leq 0.48$	$162 \pm 40$ *)	$6.7 \pm 1.2$	9 d
6.0	$\leq 0.4$	$564 \pm 25$	$9.7 \pm 0.5$	9 j
7.0	$\leq 0.35$	$302 \pm 9$ *)	$9.01 \pm 0.21$	9 h
7.0	$\leq 0.45$	$320 \pm 50$	$9.3 \pm 0.6$	9 f
10.0	$\leq 0.4$	$265 \pm 12$	$9.7 \pm 0.5$	9 j
14.0	$\leq 0.4$	$223 \pm 11$	$10.5 \pm 0.5$	9 j

\*) Extrapolated from the published values for  $t' = 0$

these results are also presented in table IV.1. Our values are found to be in good agreement. In a bubble chamber experiment at 5.4 GeV/c, Cooper et al. <sup>(9d)</sup> found appreciably lower values for A and the slope parameter.

Another feature of the  $K^+\Sigma^+$  differential cross section is the evidence for a dip or break in the  $t'$  region between 0.5 and 0.8  $\text{GeV}^2$ . This feature has been the subject of a detailed experimental investigation by Han et al.<sup>(9g)</sup>, who also find a break at  $t' \approx 0.5 \text{ GeV}^2$ , followed by a secondary maximum at  $t' \approx 0.85 \text{ GeV}^2$ . The secondary maximum disappears at higher energies.

The polarization of the  $\Sigma^+$  was determined from the  $\Sigma^+ \rightarrow p\pi^0$  decay<sup>\*</sup>). The distribution of the proton in the  $\Sigma^+$  rest frame can be written as:

$$\frac{dN}{d\Omega} = \frac{N}{4\pi} (1 + \alpha P(\hat{q} \cdot \hat{n})) \quad (\text{IV.28})$$

where  $N$  = the number of events in the  $t'$  interval considered

$\Omega$  = a solid angle

$P$  = the polarization

$\hat{q}$  = a unit vector along the decay proton direction

$\hat{n}$  = a unit vector along the normal to the production plane:  $\hat{n} = (\vec{p}_{\pi^+} \times \vec{p}_{K^+}) / |\vec{p}_{\pi^+} \times \vec{p}_{K^+}|$ ;  $p_{\pi^+}$  and  $p_{K^+}$  are the momenta of the beam and  $K^+$  respectively

$\alpha$  = the asymmetry parameter; for the decay  $\Sigma^+ \rightarrow p\pi^0$  the experimentally known value of  $\alpha$  is  $(-0.991 \pm 0.019)$ .

The polarization can thus be obtained from:

$$P = \frac{3}{\alpha N} \sum_i (\hat{q}_i \cdot \hat{n}_i) \quad (\text{IV.29})$$

or from

$$P = \frac{2}{\alpha N} (N_u - N_D) \quad (\text{IV.30})$$

<sup>\*</sup>) Note. The  $\Sigma^+ \rightarrow n\pi^+$  decays were not used because of the well-known smallness of the decay - asymmetry parameter.

where  $N_u$  and  $N_D$  are the number of events with decay protons emitted at angles above (i.e. with  $\hat{q}_i \cdot \hat{n}_i > 0$ ) and below the production plane respectively.

Part of the events with  $\hat{q}_i \cdot \hat{n}_i \sim 0$  have a small decay angle in the laboratory and are likely to be lost (section II.5.5). In formula (IV.29) this effect reduces  $N$ , but leaves the sum virtually unchanged. We will therefore prefer to use Eq. (IV.30) where the bias drops out as we expect  $N_u$  and  $N_D$  to be reduced by approximately the same factor as  $N$ .

For the average value of the polarization in the interval  $0 \leq t'(\text{GeV}^2) \leq 1$  we found:

$$P = 0.17 \pm 0.37$$

#### IV.5.2 Exchange model predictions

From the conservation laws at the meson and baryon vertices of the reaction  $\pi^+ p \rightarrow K^+ \Sigma^+$  one deduces that only objects with the following quantum numbers can be exchanged:

$$I = \frac{1}{2}, \frac{3}{2}, J^P = 0^+, 1^-, 2^+, \dots \text{ (natural spin parity);}$$

$$|S| = 1; B = 0$$

Well established resonances with these quantum numbers are the  $K^*(890)$  ( $I = \frac{1}{2}; J^P = 1^-$ ) and the  $K^*(1420)$  ( $I = \frac{1}{2}; J^P = 2^+$ ), also called  $K^{**}$ . We can thus have both  $K^*$  and  $K^{**}$  (trajectory) exchange.

One of the earlier Regge pole models applied to this reaction is the 'hypercharge' <sup>\*)</sup> exchange model of Reeder and

\*) Note. Hypercharge (symbol  $Y$ ) is essentially an alternative quantum number for 'strangeness'. It is defined as the sum of the strangeness  $S$  and the baryon number  $B$ .

Sarma<sup>(10)</sup>, a phenomenological model based on nondegenerate  $K^*$  and  $K^{**}$  exchange. The model contains a large number of free parameters fitted to experimental data at several energies. Using the parameters given by the authors, we calculated the  $d\sigma/dt'$  behaviour at our energy. As shown by the solid curve in fig. IV.6, the general trend of our data is reasonably well reproduced, especially in the forward direction. The predicted value for the cross section in the forward peak is

$$\int_0^{0.4} \frac{d\sigma}{dt'} dt' = 37.6 \mu\text{b}$$

Experimentally we find  $(38.9 \pm 8.4) \mu\text{b}$ . The dip and second maximum seem to occur at higher  $t'$  values than predicted, although statistics in this region are too meagre to allow firm conclusions.

Simple Regge exchange models are known to run into difficulties in explaining several features of the data<sup>(11)</sup>. As shown by Han et al.<sup>(3g)</sup> the model of Reeder and Sarma fails in explaining the large  $t'$  behaviour. It predicts a dip in  $d\sigma/dt$  and a change of sign of the polarization at  $t \approx 1.8 (\text{GeV}/c)^2$ . Observations do not confirm this behaviour.

To remedy this and other shortcomings more sophisticated models have been developed, such as the models of Meyers, Noirot, Rimpault and Salin<sup>(12)</sup>; Ringland, Roberts, Roy and Tran Thanh Van<sup>(13)</sup>; Thews, Goldstein and Owens<sup>(14)</sup> and Loos and Matthews<sup>(15)</sup>. Most of these models rely on absorption corrections to improve the agreement with the data. In the  $t'$ -regions where we have some statistics, the discrepancies between the predictions of these models are not very dramatic.

## IV.5.3 SU(3) predictions

For the reactions

$$\pi^+ p \rightarrow K^+ \Sigma^+ \quad (a)$$

$$\pi^+ p \rightarrow \pi^+ p \quad (e)$$

$$K^+ p \rightarrow K^+ p \quad (f)$$

exact SU(3) symmetry predicts the following amplitude relation at equal  $s$  and  $t$  <sup>(16)</sup>:

$$A_a + A_e = A_f$$

which implies:

$$|A_a| \geq ||A_e| - |A_f|| \quad (IV.31)$$

$A_k$  is defined such that:

$$\begin{aligned} |A_k|^2 &= \frac{64\pi^2}{\alpha^2} \frac{s_k p_{i,k}}{p_{f,k}} \frac{d\sigma_k}{d\Omega} \\ &= \frac{64\pi}{\alpha^2} s_k p_{i,k}^2 \frac{d\sigma_k}{dt} \end{aligned} \quad (IV.32)$$

where  $s_k$  is the squared C.M. energy,  $p_{i,k}(p_{f,k})$  is the magnitude of the initial (final) C.M. momentum in reaction  $k$  and  $\alpha$  is a units conversion factor.

We make use of the optical theorem

$$\sigma_{T,k} = \text{Im } A_{el,k}(t=0) \quad \alpha^2 / (2p_{i,k} \sqrt{s_k}) \quad (IV.33)$$

for the r.h.s. of the triangular inequality. In this formula  $\sigma_{T,k}$  denotes the *total* cross section (meson + baryon + all channels) of the initial state and  $A_{el,k}$  is the amplitude for *elastic* scattering. From Eqs. (IV.32) and (IV.33) we derive for *elastic scattering*:

$$\left( \frac{d\sigma_{el,k}}{dt} \right)_{t=0} = \frac{\sigma_{T,k}^2}{16 \pi \alpha^2} (1 + \rho_k^2) \quad (IV.34)$$

where:

$$\rho_k = \left( \frac{\text{Re } A_{el,k}}{\text{Im } A_{el,k}} \right)_{t=0} \quad (IV.35)$$

If  $d\sigma/dt$  is expressed in  $\text{mb}/\text{GeV}^2$  and  $\sigma_T$  in  $\text{mb}$ ,  $\alpha$  takes the value  $0.624 \text{ GeVmb}^{\frac{1}{2}}$  ( $= \hbar c$ ).

The triangular inequality (IV.31) can now be written as:

$$\left( \frac{d\sigma_a}{dt'} \right)_{t'=0} \geq \frac{[\sqrt{s_e(1+\rho_e^2)} p_{i,e} \sigma_{T,e} - \sqrt{s_f(1+\rho_f^2)} p_{i,f} \sigma_{T,f}]^2}{16 \bar{\pi} \alpha^2 s_a p_{i,a}^2} \quad (IV.36)$$

In a previous analysis<sup>(17)</sup> of our  $\pi^+p$  elastic scattering data we have found:

$$\sigma_{T,e} = 26.60 \pm 0.01 \text{ mb}; |\rho_e| = 0.30 \pm 0.08$$

In our energy region the total  $K^+p$  section is<sup>(18)</sup>:

$$\sigma_{T,f} = (17.1 \pm 0.2) \text{ mb.}$$

For  $|\rho_f|$  we find<sup>(22)</sup>:

$$|\rho_f| = 0.41 \pm 0.03$$

a value which agrees well with the result of a Regge pole analysis of Dass, Michael and Phillips<sup>(19)</sup>. Experimentally,

the value of  $\rho_f$  does not seem to depend strongly on energy. Using the appropriate values for the momenta at our C.M. energy, we obtain:

$$\left( \frac{d\sigma_a}{dt'} \right)_{t'=0} > 0.056 [ \sigma_{T,e} - \sigma_{T,f} ]^2 \quad (\text{IV.37})$$

For the l.h.s. we derive from our data  $\left( \frac{d\sigma_a}{dt'} \right)_{t'=0} = (0.40 \pm 0.16) \text{ mb/GeV}^2$  (see sect. IV.5.2). For the r.h.s. we find  $(4.5 \pm 0.9) \text{ mb/GeV}^2$ , indicating a gross violation of the inequality. This presumably is partly caused by SU(3) symmetry breaking effects associated with the mass differences.

To remove these mass-effects in an approximate way Meshkov et.al.<sup>(21)</sup> suggested that the comparison (IV.31) be made at the *equal Q-value* ( $Q = \sqrt{s}$  - sum of final state masses). In several cases this method is known to fail<sup>(20)</sup>. We tested this method using the Q-value of reaction (a) at our beam momentum: 1.524 GeV. This implied that we had to compare the reaction (a) at 5 GeV/c with reaction (e) at 3.1 GeV/c and reaction (f) at 4.0 GeV/c.

First we made the comparison for the integrated cross sections. By interpolation of published data we found:

$$\sigma_e = 5.0 \pm 1.5 \text{ mb}^{(24)}; \quad \sigma_f = 4.0 \pm 0.3 \text{ mb}^{(25)}.$$

Comparison of the values  $M = (\sigma \cdot sp_i / p_f)^{\frac{1}{2}}$  following (IV.31) gives

$$(0.816 \pm 0.69) \gg | (5.8 \pm 0.9) - (5.91 \pm 0.22) | = 0.11 \pm 0.93$$

(all values are  $\text{mb}^{\frac{1}{2}} \cdot \text{GeV}$ ), which is satisfactory.

We now do the comparison for forward cross sections: we use the following values<sup>\*</sup>):

\* ) *Note.* These values were calculated from the total cross sections through the optical theorem (Eq.(IV.34)).



$$\left(\frac{d\sigma_e}{dt}\right)_{t=0} = (48 \pm 6) \text{ mb/GeV}^2 \text{ and}$$

$$\left(\frac{d\sigma_f}{dt}\right)_{t=0} = (18.5 \pm 1.9) \text{ mb/GeV}^2$$

Comparison of the values  $M = \left\{ \frac{sp_i^2}{\pi} \left(\frac{d\sigma}{dt}\right)_{t=0} \right\}^{\frac{1}{2}}$  following (IV.31) gives

$$(1.67 \pm 0.34) \geq (11.4 \pm 0.7) - (9.1 \pm 0.5) = (2.3 \pm 0.9)$$

(all values in  $\text{mb}^{\frac{1}{2}} \cdot \text{GeV}$ ). We see that within the errors also this inequality is satisfied.

Trilling<sup>(20)</sup> has pointed out that this procedure does not make much sense, because it can e.g. result in comparing reactions (a) and (e) near the resonance regions of  $\Delta^{**}(1950)$  and  $\Delta^{**}(1236)$  respectively. Instead he proposes to compare the reactions (a) and (e) at *equal C.M. energy* and to compensate for mass difference effects in (f) by a slight shift in energy scale. A correction for centrifugal barrier effects should be made by multiplying the amplitudes with a factor  $(1/p_f)^1$  (see below). The  $\sigma_{T,f}$  value is corrected for  $\pi$ -K mass difference effects by adding 4.4 mb, i.e. the difference  $\sigma_T(\pi^-p) - \sigma_T(K^-p)$ <sup>\*</sup>).

\*) *Note.* The fact, that the difference  $\sigma_T(\pi^-p) - \sigma_T(K^-p)$  changes very little between 3 and 60 GeV is taken as an indication that in the limit of exact SU(3) symmetry these cross sections would be equal. The experimentally observed remaining difference can be considered as a measure for the effect of mass-breaking.

In principle each partial wave should be corrected separately, but it is possible to determine an effective  $l$ -value for the whole amplitude using a method similar to the one described by Davier and Harari<sup>(23) \*</sup>. The inequality then reads:

$$\left(\frac{d\sigma_a}{dt'}\right)_{t'=0} \geq 0.051 \left(\frac{p_{f,a}}{p_{f,e}}\right)^{2l_{\text{eff}}} [\sigma_{T,e} - (\sigma_{T,f} + 4.4)]^2 \quad (\text{IV.38})$$

where  $p_{f,a} = 1.33 \text{ GeV}/c$ ;  $p_{f,e} = 1.46 \text{ GeV}/c$ .

For the r.h.s. we find  $(0.39 \pm 0.09) \text{ mb}/\text{GeV}^2$  which is in very good agreement with our experimental result:  $(0.40 \pm 0.16) \text{ mb}/\text{GeV}^2$ .

Another SU(3) prediction:

$$A(\pi^- p \rightarrow \pi^- p) + A(K^- p \rightarrow \pi^- \Sigma^+) = A(K^- p \rightarrow K^- p)$$

leads to a triangular inequality analogous to Eq. (IV.37), involving the difference between  $\sigma_T(\pi^- p)$  and  $\sigma_T(K^- p)$ . As already has been stated, this difference is zero in the limit of exact SU(3).

\*) *Note.* Davier and Harari have shown that the  $t$ -behaviour of difference of the differential cross sections for  $K^- p$  and  $K^+ p$  elastic scattering can be compared to a Bessel function  $J_0(r\sqrt{-t})$ . The experimentally observed cross-over then corresponds to the first zero ( $r\sqrt{-t} = 2.4048$ ) and determines the effective interaction radius  $r$ . In our case we determine  $r$  from the cross-over between the  $\pi^+ p$  and  $K^+ p$  elastic scattering differential cross sections. Experimentally this cross-over is observed for  $t = -0.3 \text{ GeV}^2$ , giving  $l_{\text{eff}} = p r = 6.41$ .

Using Eq.(IV.33) one arrives at the conclusion that  $A(K^-p \rightarrow \pi^- \Sigma^+)$  is real at  $t'=0$ . For the line-reversed reaction  $\pi^+p \rightarrow K^+ \Sigma^+$  we then expect an imaginary forward amplitude<sup>\*</sup>). This has the interesting consequence, that relation (IV.38) changes into an *equality*. We see, that also this equality is very well satisfied.

#### IV.6 The reaction $\pi^+p \rightarrow K^{**} (890) \Sigma^+$

##### IV.6.1 Experimental results

The reaction  $\pi^+p \rightarrow K^{**} (890) \Sigma^+$  was shown to be present in the channels  $\pi^+p \rightarrow \Sigma^+ K^+ \pi^0$  and  $\pi^+p \rightarrow \Sigma^+ K^0 \pi^+$  (sect. III.3.7).

The value of the cross section was determined to be  $(60 \pm 17)$   $\mu\text{b}$ . At  $4.0 \text{ GeV}/c$ <sup>(9c)</sup> and  $5.4 \text{ GeV}/c$ <sup>(9d)</sup> the cross sections found were  $(23 \pm 7)$   $\mu\text{b}$  and  $(42.9 \pm 6.2)$   $\mu\text{b}$  respectively.

\*) *Note.* The reality of the forward amplitude  $A(t=0)$  in the reaction  $K^-p \rightarrow \pi^- \Sigma^+$  follows from strong degeneracy of the exchanged  $K^*$  and  $K^{**}$  trajectories (i.e. not only the trajectories, but also the residue functions are assumed to coincide). Going to the line reversed reaction  $\pi^+p \rightarrow K^+ \Sigma^+$  (i.e. going from the s- to the u-channel reaction) involves a change of sign of the  $K^*$  contribution (odd signature) relative to the  $K^{**}$  contribution (even signature). We then obtain an imaginary amplitude  $\bar{A}(t=0) = A(t=0) e^{-i\pi\alpha(t=0)}$  with the intercept  $\alpha(t=0) \approx 0.5$  in the approximation considered.

The production angular distribution for the events in the  $K^*(890)$  mass band ( $0.84 \leq M(K\pi)^* (\text{GeV}) \leq 0.94$ ) is shown in fig. IV.7. We find a marked dip of at least 4 standard deviations in the forward direction, in disagreement with the observations of Cooper et al.<sup>(9d)</sup> at 5.4 GeV/c. Between  $t'$  values of 0.1 and 1.0  $(\text{GeV}/c)^2$  the behaviour of the differential cross section can be characterized by an exponential with a slope

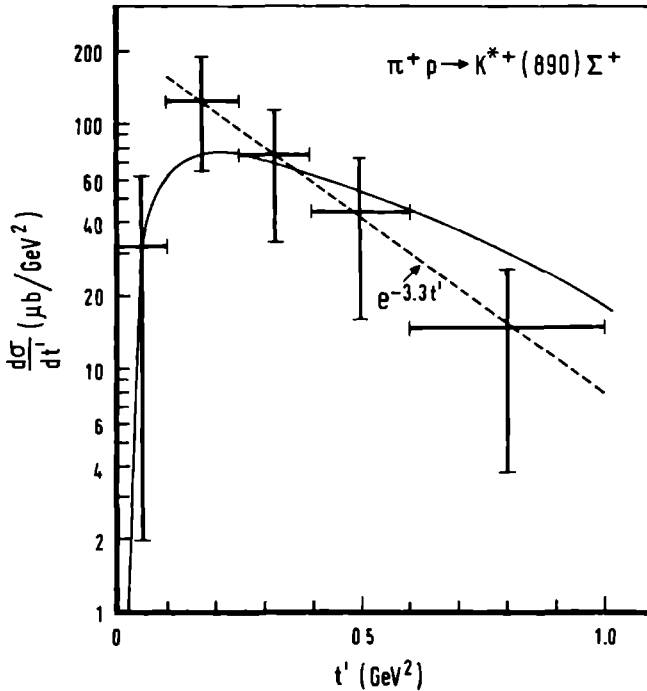


Fig. IV.7 Differential cross section versus  $t'$  for the reaction  $\pi^+ p \rightarrow K^{*+}(890)\Sigma^+$ . The dashed line represents an expression  $\frac{d\sigma}{dt'} = Ae^{-\lambda t'}$  fitted to the data ( $0.1 < t'(\text{GeV}^2) < 1.0$ ). The solid curve represents a (normalized) prediction from the model of Chilton et al.<sup>(26)</sup>.

parameter  $\lambda = (3.3 \pm 1.0) \text{ GeV}^{-2}$  (dashed line in fig. IV.7). From fig. 3a of ref. (9d) we estimate  $\lambda \approx 2.4 \text{ GeV}^{-2}$  at 5.4 GeV/c.

In table IV.2 we give the average values of the spin density matrix elements in the region  $0 \leq t'(\text{GeV}^2) \leq 1.0$  as determined from the  $K^{**}$  decay angular distribution (A) using the method of moments and (B) using a maximum likelihood fit (Eq. IV.19). The solutions obtained with method (B) were forced to obey the positivity conditions. The values obtained using method (A) do not obey these conditions. This could be due to the background or contaminations. Approximately 75% of the sample of  $\Sigma^+ K^{**}$  candidates consists of ambiguous events. The main difference between the two solutions is in the values for  $\text{Re} \rho_{1,0}$ , which differ by more than 2 standard deviations.

In table IV.2 we also give the  $\rho$ -values obtained by Bartsch et al. <sup>(9c)</sup> at 4.0 GeV/c and our own estimate (using fig. 3 in ref.(9d)) of the values obtained by Cooper et al. at 5.4 GeV/c.

In fig. IV.8 we show the projected decay angular distributions in  $\cos \theta$  and  $\varphi$  (Gottfried-Jackson system). The curves represent the projections of the maximum likelihood fit results.

#### IV.6.2 Comparisons with theory

The conservations laws at the baryon and meson vertices allow the exchange of objects with:

$$I = \frac{1}{2}, \frac{3}{2}; J^P = 0^-, 1^+, 1^-, 2^+, 2^-, \dots; |S| = 1; B = 0$$

In terms of known particles this means that the  $K(I=\frac{1}{2}; J^P=0^-)$ , the  $K^*(I=\frac{1}{2}; J^P=1^-)$  and the  $K^{**}(I=\frac{1}{2}; J^P=2^+)$  are candidates.

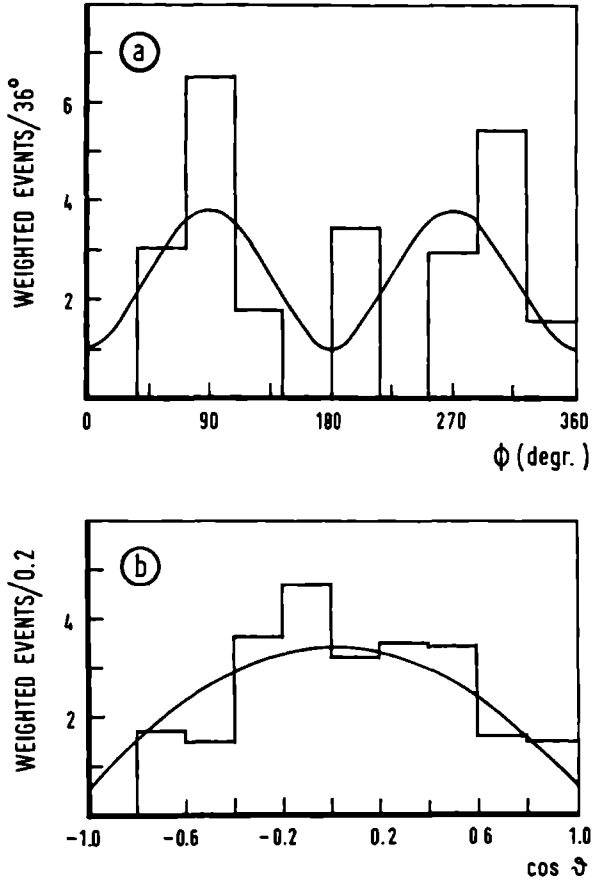


Fig. IV.8 Decay angular distributions (in the Gottfried-Jackson system) of the  $K^{**}$  produced in the reaction  $\pi^+ p \rightarrow K^{**} (890) \Sigma^+$ . (a)  $\phi$ -distribution; (b)  $\cos \theta$ -distribution. The solid curves are the results of the fit described in the text.

The solid curve in fig. IV.7 represents the prediction for the  $t'$  dependence of the differential cross section at 5.4 GeV/c.,

obtained from an absorptive one-particle-exchange model due to Chilton et al. (26,9d). The curve is normalized to the total experimental cross section below  $t' = 1.0 \text{ GeV}^2$ . The model assumes mixed K and  $K^*$  exchange. Above  $t' \sim 0.2 \text{ GeV}^2$  the cross section falls steeper than predicted. The observed dip is in agreement with the model.

The  $\rho$ -values expected on the basis of the above model are also presented in table IV.2.

TABLE IV.2					
Spin density matrix elements for $\pi^+p \rightarrow K^{*+}(890)\Sigma^+$ ( $0 \leq t'(\text{GeV}^2) \leq 1.0$ )					
$P_{\text{beam}}$ (GeV/c)	method*)	$\rho_{0,0}$	$\rho_{1,-1}$	Re $\rho_{1,0}$	reference
4	A	$0.27 \pm 0.16$	$0.26 \pm 0.12$	$0.02 \pm 0.02$	9c
5	A	$-0.08 \pm 0.10$	$0.41 \pm 0.15$	$-0.23 \pm 0.05$	this exp.
	B	$0.07 \pm 0.10$	$0.29 \pm 0.09$	$-0.08 \pm 0.04$	this exp.
5.4	C	$0.17 \pm 0.07$	$0.35 \pm 0.06$	$0.06 \pm 0.03$	9d
	Chilton model (26)	0.09	0.42	0.02	9d
*) method A: method of moments B: maximum likelihood fit (with positivity conditions imposed) C: estimated from fig. 3.b in ref. (9d)					

## IV.7 The reaction $\pi^+p \rightarrow K^+\Sigma^+(1385)$

### IV.7.1 Experimental results

This reaction has been observed in the channel  $\Lambda K^+\pi^+$  (sect. III.3.5). The cross section found was:

$$\sigma(\pi^+p \rightarrow K^+\Sigma^+(1385) \rightarrow K^+\pi^+\Lambda) = (16 \pm 4) \text{ } \mu\text{b, in agreement}$$

with the value obtained by Cooper et al.<sup>(9d)</sup> at 5.4 GeV/c. In a spark chamber experiment, Ying et al.<sup>(27)</sup> obtain a value of approximately 13  $\mu\text{b}$  at 5.05 GeV/c. As the branching ratio for  $\Sigma^+(1385) \rightarrow \Lambda\pi^+ = 89 \pm 5\%$ , we obtain for the total cross section at 5 GeV/c:

$$\sigma(\pi^+p \rightarrow K^+\Sigma^+(1385)) = (18 \pm 5) \text{ } \mu\text{b}$$

In fig. IV.9 we plot the experimental cross sections versus the beam momentum. The data are taken from refs. (24), (9 b-e) and (27). The values indicated by open circles are normalized (partly by us) to include all decay modes using the branching ratio given above. For the values indicated by black dots it was not clear whether or not the authors had performed this normalization themselves. The crosses indicate results of the spark chamber experiment, mentioned above (published without errors).

The  $t'$  behaviour of the differential cross section for events with  $1.334 \leq M(\Lambda\pi^+) \text{ GeV} \leq 1.430$  is presented in fig. IV.10. We observe some indication for a dip or plateau in the forward direction. This effect has also been observed in other experiments (see e.g. refs. 9b, d, h, j). In the region  $0.1 < t'(\text{GeV}^2) \leq 1.1$  we fitted an expression of the form  $d\sigma/dt' = A e^{-\lambda t'}$  to the experimental data. The result is given



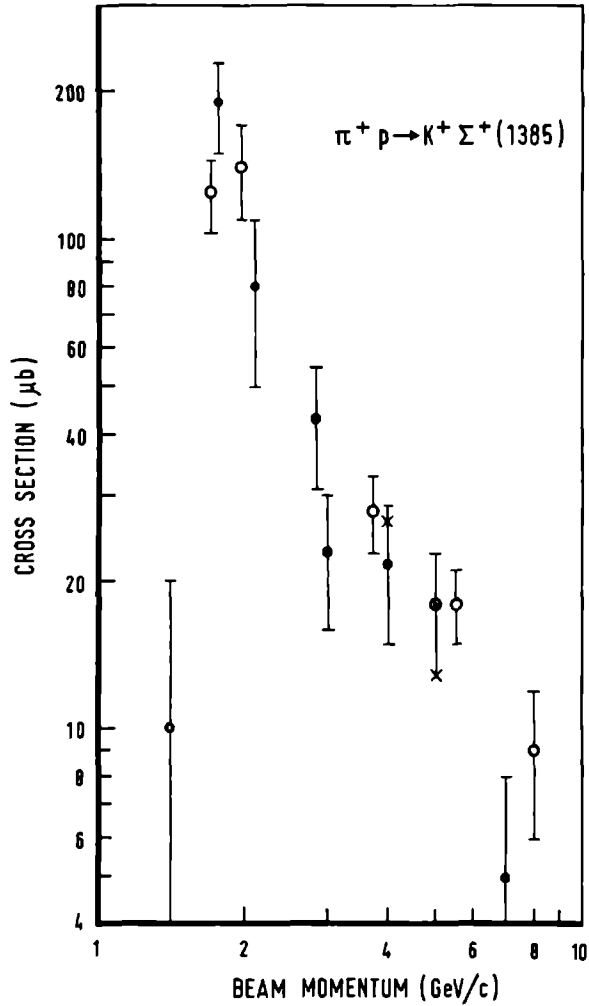


Fig. IV.9 Total cross section versus beam momentum for the reaction  $\pi^+ p \rightarrow K^+ \Sigma^+(1385)$ .

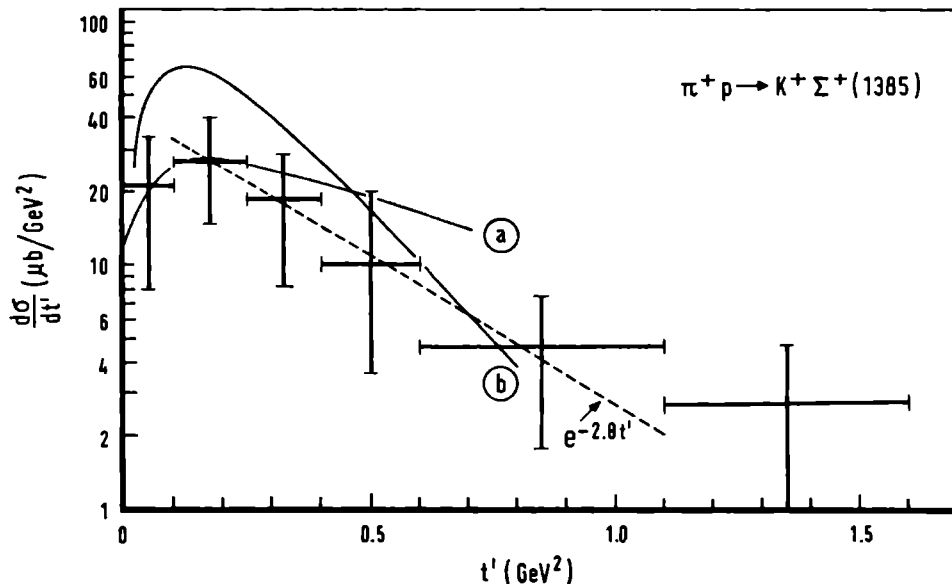


Fig. IV.10 Differential cross section versus  $t'$  for the reaction  $\pi^+ p \rightarrow K^+ \Sigma^+(1385)$ . The dashed line gives the result of an exponential fit to the data. Curve (a) and (b) represent the predictions of an absorption and a Regge model respectively.

in table IV.3 together with the parameters obtained at other energies.

The average spin density matrix elements for the interval  $0 \leq t'(\text{GeV}^2) \leq 1.1$  are presented in table IV.4, again together with values obtained at other energies. They have been derived from the  $\Sigma^+(1385)$  decay angular distribution (A) using the method of moments and (B) performing a maximum likelihood fit of the expression (IV.21) to this distribution. The result of

TABLE IV.3			
SLOPE PARAMETER FOR THE DIFFERENTIAL CROSS SECTION OF $\pi^+p \rightarrow K^*\Sigma^+(1385)$			
$P_{\text{beam}}$ (GeV/c)	$t'$ -region (GeV <sup>2</sup> )	$\lambda$ (slope) (GeV <sup>-2</sup> )	ref.
3.7	0.12-1.5	3.0±0.6	9b
4.0	~ 0.05-1.0	2.3±0.3	27
5.0	0.10-1.1	2.8±1.0	this expt.
5.05	~ 0.05-1.0	2.6±0.4	27
6.0	0.18-0.70	5.0±0.5	9j
8.0	0. -1.2	1.9±0.9	9e

TABLE IV.4						
SPIN DENSITY MATRIX ELEMENTS for $\pi^+p \rightarrow K^*\Sigma^+(1385)$						
$P_{\text{beam}}$ (GeV/c)	$t'$ interval (GeV <sup>2</sup> )	method	$\rho_{3,3}$	Re $\rho_{3,-1}$	Re $\rho_{3,1}$	ref.
3.7	0 - 1.0	-	0.24±0.08	0.19±0.08	0.07±0.06	9b
4.0	0 - 0.8	A	0.16±0.16	0.0 ±0.15	0.40±0.14	9c
5.0	0 - 1.1	A	0.31±0.12	0.27±0.11	0.26±0.10	this exp.
		B	0.30±0.11	0.19±0.18	-0.12±0.25	this exp.
5.5		A	0.29±0.10	0.24±0.10	-0.02±0.10	9d
8.0		A	0.26±0.11			9e
Predictions		K* exchange	0.375	0.216	0.	8
		K* exchange + absorption	0.16	0.19	0.02	30
		K* exchange Reggeized	0.17	0.19	-0.07	30
method A : method of moments B : maximum likelihood fit						

this fit is shown on the projected distributions in fig. IV.11. The  $\rho$ -values obtained by method A violate the positivity condition (IV.27) by approximately one standard deviation, while the fit results do not. In fig. IV.12 we present the spin density matrix elements as a function of  $t'$ . They have been obtained using the method of moments in each  $t'$  interval separately.

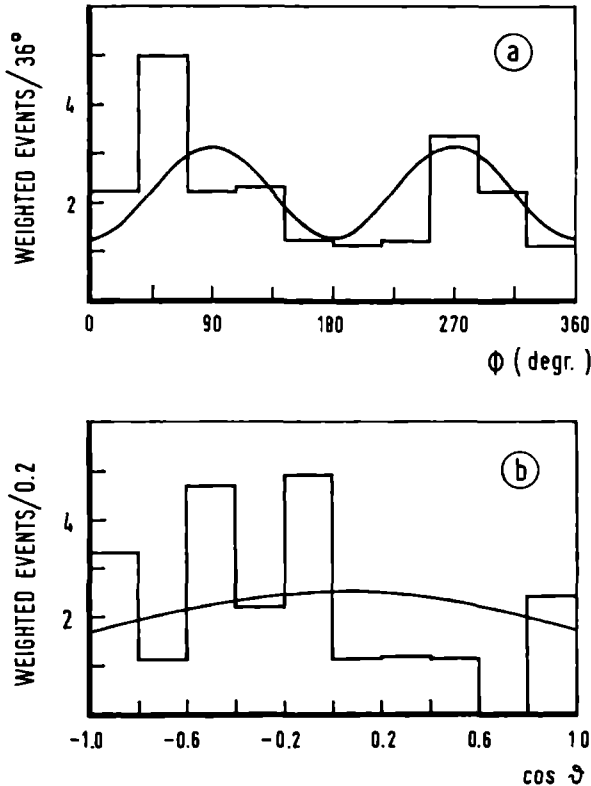


Fig. IV.11 Decay angular distribution in the Gottfried-Jackson system for the  $\Sigma^*(1385)$  produced in the reaction  $\pi^+p \rightarrow K^+\Sigma^*(1385)$ : (a)  $\phi$ -distribution; (b)  $\cos \theta$  distribution. The solid lines represent the results of the fit described in the text.

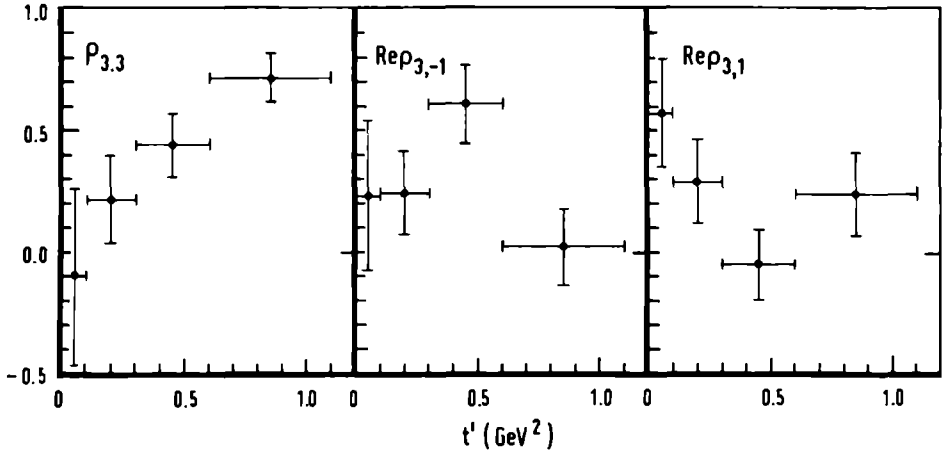


Fig. IV.12 Spin density matrix elements as a function of  $t'$  in the reaction  $\pi^+ p \rightarrow K^+ \Sigma^+(1385)$ .

#### IV.7.2 Comparison with exchange models

In case of mesonic exchange, the exchanged object(s) can have the following quantum numbers:

$$I = \frac{1}{2}, \frac{3}{2}; J^P = 0^+, 1^-, 2^+, \dots \text{ (natural spin parity);}$$

$$|S| = 1; B = 0$$

Among the established resonances the  $K^*$  ( $IJ^P = \frac{1}{2}, 1^-$ ) and  $K^{**}$  ( $IJ^P = \frac{1}{2}, 2^+$ ) satisfy these requirements.

Calculations on the basis of an absorptive  $K^*$  exchange model for this reaction have been done by Eysel, Locher and Wessel<sup>(28)</sup>, Mott<sup>(29)</sup> and Griffiths and Jabbur<sup>(30)</sup>. On the basis of the latter model we obtained at 5 GeV/c the curve (a) shown in fig. IV.10. In view of the large uncertainties in the coupling constants we normalized the prediction to our data.

We notice, that the experimental  $d\sigma/dt'$  slope is steeper than predicted, a common defect of vector exchange models.

Renninger and Sarma<sup>(31)</sup> have recently performed a Regge model-calculation involving both  $K^*$  and  $K^{**}$  exchange. The trajectory parameters were fitted with the help of  $\pi^+p \rightarrow K^+\Sigma^+(1385)$  and  $K^-p \rightarrow \pi^-\Sigma^+(1385)$  data obtained at several energies. Using this model at 5 GeV/c, we found the result represented by curve (b) (absolute prediction). The slope is in good agreement with the data, the absolute values however are a factor 2-2.5 higher than the experimental data.

All models predict a dip in the forward direction, in agreement with our observations and indicating the dominance of spin flip amplitudes in the low  $t'$  region.

In table IV.4 some model predictions for the spin density matrix elements can be found. The uncertainty in the experimental values does not allow a discrimination between these models, although the  $K^*$  exchange prediction is somewhat favoured.

### IV.7.3 $SU(3)$ relations

Between the reactions:

$$\pi^+p \rightarrow K^+\Sigma^+(1385) \quad (c)$$

$$\pi^+p \rightarrow \eta^0\Delta^{++} \quad (g)$$

$$\pi^+p \rightarrow \pi^0\Delta^{++} \quad (h)$$

$$K^-n \rightarrow \bar{K}^0\Delta^- \quad (i)$$

$$K^-n \rightarrow K^0\Xi^{*-}(1530) \quad (j)$$

$$K^+p \rightarrow K^0\Delta^{++} \quad (k)$$

there exist the following SU(3) relations<sup>(20,32)</sup>:

$$3 \frac{d\sigma(c)}{dt} = \frac{d\sigma(i)}{dt} + 3 \frac{d\sigma(j)}{dt} \quad (\text{IV.39})$$

$$- 3 \frac{d\sigma(c)}{dt} + 3 \frac{d\sigma(g)}{dt} + \frac{d\sigma(h)}{dt} = \frac{d\sigma(k)}{dt} \quad (\text{IV.40})$$

(a) Reaction (j) involves the exchange of object(s) with the exotic quantum number  $S = 2$ . Above  $3\text{--}4$  GeV/c and at low  $|t|$  values the amplitudes for such reactions are known to be negligible with respect to the non-exotic exchange amplitudes. In this limit, relation (IV.39) becomes:

$$\left[ 3 \frac{d\sigma(c)}{dt} = \frac{d\sigma(i)}{dt} \right]_{\text{high } s, \text{ low } |t|} \quad (\text{IV.41})$$

For reaction (c) we calculated a forward cross section<sup>\*</sup> of  $(9.0 \pm 2.1)$   $\mu\text{b}$ .

Data on reaction (i) are very scarce. From a fit to data obtained at beam momenta of 3.0, 3.6, 3.9 and 4.5 GeV/c performed by Kwan-Wu Lai and Louie<sup>(35)</sup> we estimated a forward cross section for reaction (i) at 5 GeV/c of approximately 65  $\mu\text{b}$ . From the differential cross section behaviour found by Carmony et al.<sup>(33)</sup> at 4.5 GeV/c and by Burdick et al.<sup>(34)</sup> at 4.9 GeV/c we derive forward cross sections of  $(83 \pm 6)$   $\mu\text{b}$  and  $(116 \pm 20)$   $\mu\text{b}$  respectively. All three values indicate a strong violation of relation (IV.41).

\* ) *Note.* Here and in the following we define the forward

$$\text{cross section as } \int_0^{0.4} \frac{d\sigma}{dt'} dt'.$$

To make this violation disappear, Meshkov et al.<sup>(32)</sup> prescribe a comparison of  $|M|^2 = sp_1^2 \frac{d\sigma}{dt}$  at the same Q-value (sect. IV.5.3) i.e.  $p_{\text{beam}}(i) = 4.4 \text{ GeV}/c$ . This procedure produces an effective increase of (c) by a factor 1.3, which is insufficient to remove the violation.

The angular momentum barrier corrections described by Trilling<sup>(20)</sup> (sect. IV.5.3) can provide a boosting factor for e of approximately the required magnitude ( $\approx 3$ ) when reactions are compared at  $5.0 \text{ GeV}/c$ . However, in view of mass difference effects, it is not clear whether it is justified to make the comparison at exactly the same beam momentum.

(b) Relation (IV.40) involves three reactions<sup>(c,g,h)</sup> observed in our experiment (l.h.s.) and a  $K^+p$  reaction (k; r.h.s.). The forward cross sections found for (c), (g) and (h) are  $(9.0 \pm 2.1)$ ,  $(72 \pm 15)$ <sup>(36)</sup> and  $(176 \pm 10) \mu\text{b}$ <sup>(36)</sup> respectively. For reaction (k) we use the data of Goldschmidt-Clermont at  $5.0 \text{ GeV}/c$ <sup>(37)</sup> giving a forward cross section of  $(278 \pm 72) \mu\text{b}$ . The angular momentum barrier factors attenuate the contributions of (g), (h) and (k) with respect to (c) by factors of approximately 0.60, 0.33 and 0.34 respectively. From the l.h.s. we then predict a forward cross section for (k) of  $(475 \pm 80) \mu\text{b}$  which is  $\sim 2$  standard deviations above the experimentally obtained value.

The general conclusion is, that the SU(3) predictions - after phase space and angular momentum barrier corrections - are in reasonable agreement with the experimental data.



#### IV.8 The reaction $\pi^+p \rightarrow K^{*+}(890) \Sigma^+(1385)$

##### IV.8.1 Experimental results

This reaction is present in the channels  $\Lambda K^+ \pi^+ \pi^0$  and  $\Lambda K^0 \pi^+ \pi^+$ . In section III.3.6 we obtained the cross sections:

$$\sigma(\pi^+p \rightarrow K^{*+}(890) \Sigma^+(1385) \rightarrow K^+ \pi^0 \Lambda \pi^+) = (13 \pm 4) \mu\text{b}$$

$$\text{and } \sigma(\pi^+p \rightarrow K^{*+}(890) \Sigma^+(1385) \rightarrow K^0 \pi^+ \Lambda \pi^+) = (11 \pm 3) \mu\text{b}$$

The ratio between these cross sections ( $(13 \pm 4)/(11 \pm 3) = 1.2 \pm 0.5$ ) is approximately 1.5 standard deviations higher than the expected C.G. ratio ( $= 0.5$ ).

Averaging the total cross section values calculated independently from the above partial cross sections, using the C.G. ratios for  $K^{*+}(890)$  decay and the branching fraction for  $\Sigma^+(1385) \rightarrow \Lambda \pi^+$  decay ( $0.89 \pm 0.05$ ), we arrived at:

$$\sigma(\pi^+p \rightarrow K^{*+}(890) \Sigma^+(1385) \rightarrow \text{all channels}) = (22 \pm 5) \mu\text{b}.$$

The values for the above partial cross sections determined by Cooper et al. <sup>(9a)</sup> at 5.5 GeV/c were  $(13 \pm 2) \mu\text{b}$  and  $(6 \pm 3) \mu\text{b}$  respectively; the ratio between these cross sections is approximately the inverse of the expected C.G. ratio. For the total cross section calculated using the same procedure as described above we then find a value of  $(21 \pm 5) \mu\text{b}$ . At 3.7 <sup>(9b)</sup> and 8 GeV/c <sup>(9e)</sup> the sum of the above partial cross sections was reported to be  $(31 \pm 12) \mu\text{b}$  and  $(10 \pm 5) \mu\text{b}$  respectively.

The  $d\sigma/dt'$  distribution for events with  $1.334 \leq M(\Lambda \pi^+)(\text{GeV}) \leq 1.430$  and  $0.84 \leq M(K\pi)^+(\text{GeV}) \leq 0.94$  is plotted in fig. IV.13. In the region  $0 \leq t'(\text{GeV}^2) \leq 1.1$  the  $d\sigma/dt'$  behaviour can be described with the expression  $d\sigma/dt' = (47 \pm 9) \exp(-2.2 \pm 0.8)t' \mu\text{b}/\text{GeV}^2$ . In table IV.5 the slopes obtained in some other experiments are compared with our result.

The averaged spin density matrix elements extracted from the  $\Sigma^+(1385)$  and  $K^{*+}(890)$  decay angular distributions are given in table IV.6. They have been obtained both using the method of moments and a maximum likelihood fit to the  $(\cos \theta, \varphi)$  distribution. The result of this fit is shown on the projected distributions in fig. IV.14. The two methods of determination give reasonably compatible results. The positivity conditions are satisfied for both sets of values. The table also contains some results obtained at other energies. The  $t'$  dependence of the  $\rho$ 's is given in fig. IV.15.

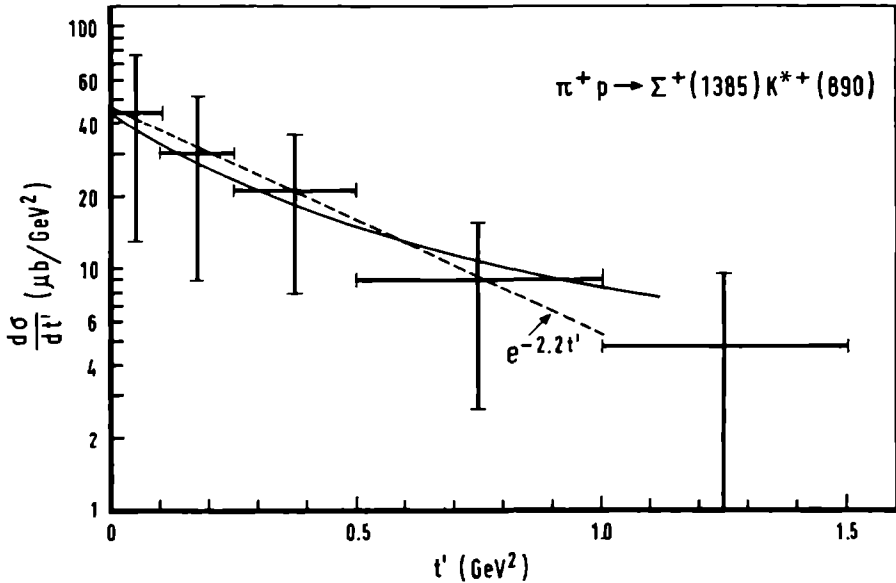


Fig. IV.13 Differential cross section versus  $t'$  for the reaction  $\pi^+ p \rightarrow K^{*+}(890) \Sigma^+(1385)$ . The dashed line gives the result of an exponential fit to the data. The curve represents the prediction of an absorption model<sup>(28)</sup>.

TABLE IV.5			
SLOPE PARAMETER OF THE DIFFERENTIAL CROSS SECTION FOR $\pi^+p \rightarrow K^{*+}(890)\Sigma^+(1385)$			
$P_{\text{beam}}$ GeV/c	$t'$ region GeV <sup>2</sup>	$\lambda$ (slope) GeV <sup>-2</sup>	ref.
4.0	< 2.0	$1.7 \pm 0.5$	9c
5.0	< 1.0	$2.2 \pm 0.8$	this exp.
8.0	< 1.2	$1.6 \pm 0.8$	9e

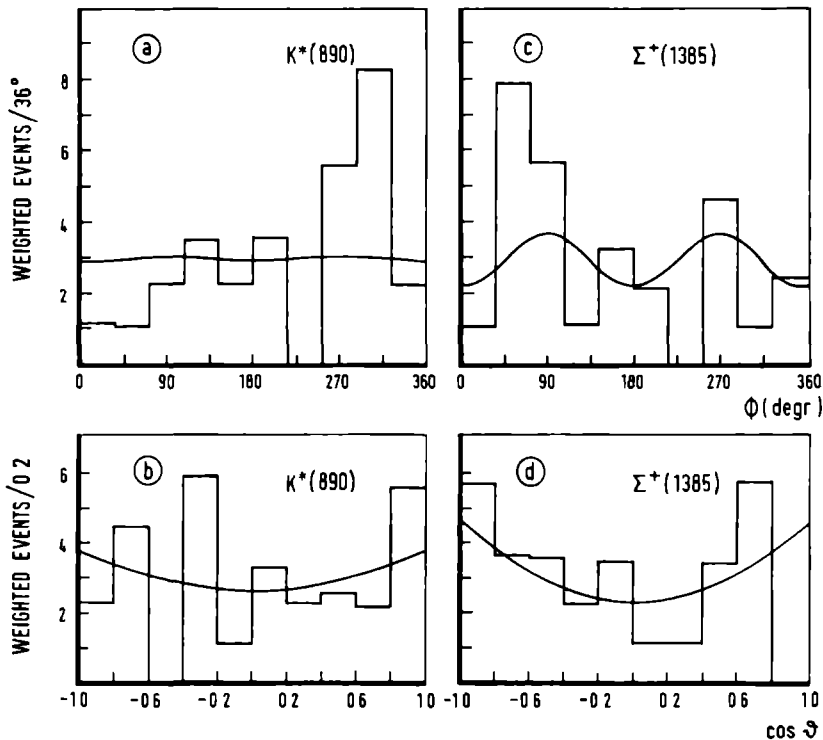


Fig. IV.14 Decay angular distributions (in the Gottfried-Jackson system) of the  $K^{*+}(890)$  and the  $\Sigma^+(1385)$  produced in the reaction  $\pi^+p \rightarrow K^{*+}(890)\Sigma^+(1385)$ .

TABLE IV.6

SPIN DENSITY MATRIX ELEMENTS FOR  $\pi^+ p \rightarrow K^{*+} (890) \Sigma^+ (1385)$ 

$E_{\text{beam}}$ (GeV/c)	method	$\rho_{00}$	$\rho_{1,-1}$	Re $\rho_{1,0}$	$\rho_{3,3}$	Re $\rho_{3,-1}$	Re $\rho_{3,1}$	ref.
3.7	-	0.32±0.08	0.08±0.06	- 0.09±0.05	0.20±0.06	- 0.04±0.06	- 0.12±0.07	9b *)
5.0	A	0.40±0.14	0.02±0.11	0.02±0.07	0.18±0.09	0.09±0.10	0.01±0.11	this exp.
	B	0.42±0.07	0.01±0.12	- 0.05±0.14	0.14±0.08	0.10±0.12	0.01±0.10	this exp.
5.5	-	0.18±0.10	- 0.11±0.09	- 0.06±0.06	0.19±0.09	0.12±0.07	- 0.09±0.08	9d
8.0	-	0.28±0.13	-	-	0.30±0.08	-	-	9e
Pre- dictions	K exchange	1	0	0	0	0	0	-
	K exchange with absorption	0.50	- 0.01	- 0.14	0.17	- 0.12	- 0.01	39
	$K^{*}$ exchange	0	0	0	0.375	0.216	0.	8

A : results of the method of moments

 $t' < 1.0 \text{ GeV}^2$ 

B : results of a maximum likelihood fit to the angular distribution

 $t' < 1.0 \text{ GeV}^2$ \*)  $t' < 1.0 \text{ GeV}^2$

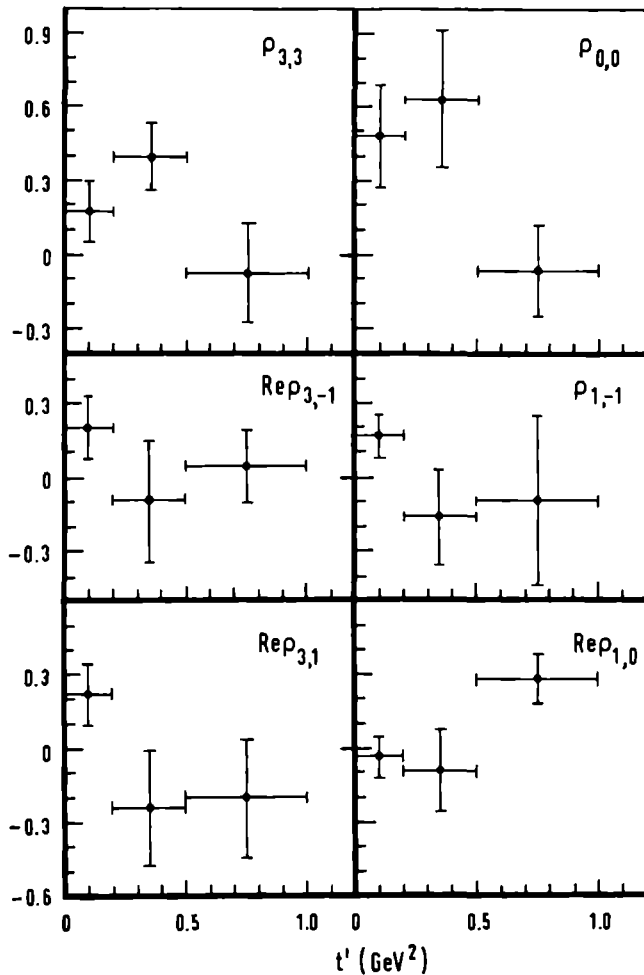


Fig. IV.15 Spin density matrix elements as a function of  $t'$  in the reaction  $\pi^+ p \rightarrow K^{*+} \Sigma^+$  (890)  $\Sigma^+$  (1385).

### IV.8.2 Absorption model calculations

The exchanged mesons can have the following quantum numbers:

$$I = \frac{1}{2}, \frac{3}{2}; J^P = 0^-, 1^+, 1^-, 2^+, 2^-, \dots;$$

$$|S| = 1; B = 0$$

i.e. K, K\* and K\*\* exchange are possible.

Absorption model calculations for K-exchange have been performed by Eysel, Locher and Wessel<sup>(28)</sup>. Their result, normalized to our data is represented by the curve in fig. IV.13. The agreement with our data is reasonable.

In table IV.6 the average experimental spin density matrix elements are compared with different model predictions. Agreement with the predictions from K-exchange with absorption is somewhat better than with the other model predictions.

### IV.8.3 Quark model predictions for the spin-density matrix elements

On the basis of the quark model, Bialas and Zalewski<sup>(40)</sup> have predicted the following relations between the baryon and the boson density matrix elements for reactions of this type:

$$\rho_{1,1} = (4/3) \rho_{3,3} \quad (\text{IV.42})$$

$$\text{Re } \rho_{1,-1} = (4/\sqrt{3}) \text{Re } \rho_{3,-1} \quad (\text{IV.43})$$

$$\text{Re } \rho_{1,0} = (4/\sqrt{6}) \text{Re } \rho_{3,1} \quad (\text{IV.44})$$

In table IV.7 we give the observed and predicted ratios

of the related spin density matrix elements. Within the large errors relations IV.42 and IV.44 are satisfied. Relation IV.43 shows a discrepancy of approximately 2 standard deviations. Kotański and Zalewski<sup>(38)</sup> have pointed out, that the above relations can be obtained without involving the quark model. It is enough to make the assumption that the spins of the incident and outgoing baryons are coupled to a resultant spin  $\leq 1$ .

TABLE IV.7

TEST OF QUARK-MODEL PREDICTIONS		
ratio	observed	predicted
$\rho_{1,1}/\rho_{3,3}$	$1.7 \pm 0.9$	1.33
$\text{Re } \rho_{1,-1}/\text{Re } \rho_{3,-1}$	$0.2 \pm 1.1$	2.31
$\text{Re } \rho_{1,0}/\text{Re } \rho_{3,1}$	$2 \pm 7$	1.63

#### IV.8.4 $SU(3)$ relations

For the reactions:

$$\pi^+ p \rightarrow K^{*+}(890)\Sigma^+(1385) \quad (d)$$

$$\pi^+ p \rightarrow \rho^0(765)\Delta^{++}(1236) \quad (l)$$

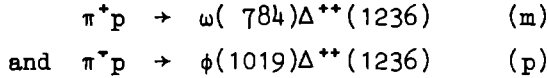
$$\pi^+ p \rightarrow \phi_0 \Delta^{++}(1236) \quad (m')$$

$$K^+ p \rightarrow K^{*0}(890)\Delta^{++}(1236) \quad (n)$$

we can check the  $SU(3)$  amplitude relation<sup>(32)</sup>:

$$-3|A_d|^2 + |A_l|^2 + 3|A_{m'}|^2 - |A_n|^2 = 0 \quad (\text{IV.45})$$

$\phi_0$  denotes the isosinglet member of the vector meson octet. Because of the phenomenon of  $\omega$ - $\phi$  mixing we have to consider both the reactions:



where now  $\omega(784)$  and  $\phi(1019)$  are the physically observed particles.

Neglecting dynamical effects of  $\omega$ - $\phi$  mixing, we can write the amplitude for reaction (m') as a function of the 'physical' amplitudes for (m) and (p):

$$A_{m'} = \cos \lambda A_p - \sin \lambda A_m \quad (\text{IV.46})$$

where  $\lambda$  is the  $\omega$ - $\phi$  mixing angle ( $39 \pm 1^\circ$ ). We already know from section III.3.3 that the cross section for reaction (p) is very small compared to that for reaction (m). We can therefore approximate

$$A_{m'} \approx -\sin \lambda A_m.$$

Relation (IV.45) can now be rewritten as:

$$-3|A_d|^2 + |A_1|^2 + 3 \sin^2 \lambda |A_m|^2 = |A_n|^2$$

We test this relation for the total cross sections at 5 GeV/c, including phase space and angular momentum barrier factors as described in section IV.5.3 by replacing  $|A|^2$  by  $\sigma_{p_1/(p_f)}^{2l_{\text{eff}}+1}$ . For the three terms at the l.h.s. of the relation we use the results obtained in our experiment<sup>(41)</sup> and for reaction (n) we use the results of Ciapetti et al.<sup>(42)</sup> at 5.0 GeV/c:



$$\begin{aligned}\sigma_d &= (23 \pm 8)\mu\text{b} \\ \sigma_1 &= (870 \pm 80)\mu\text{b} \\ \sigma_m &= (280 \pm 10)\mu\text{b} \\ \sigma_n &= (707 \pm 65)\mu\text{b}^*\end{aligned}$$

For the relative phase space and angular momentum barrier factors we obtain 1, 0.24, 0.26 and 0.25 respectively. From the l.h.s. we predict for reaction (n) a cross section of  $(920 \pm 130)\mu\text{b}$ . The difference with the measured value is 1.5 standard deviations. However, all reactions considered are so-called double resonance processes. It is well known, that the estimation of cross sections for such processes is subject to large systematic errors. Results of different experiments often show fluctuations well outside the range of the quoted statistical errors. In view of this fact the agreement with the SU(3) prediction can be considered satisfactory.

(\* ) *Note:* Corrected to include all decaymodes

*References - Chapter IV*

- (1) H. Pilkuhn, *The Interactions of Hadrons*, North Holland Publ. Co., Amsterdam (1967).
- (2) K. Gottfried and J.D. Jackson, *Nuovo Cimento* 34, 735 (1964)  
J.D. Jackson, J.T. Donohue, K. Gottfried, R. Keyser and B.E.Y. Svensson,  
*Phys. Rev.* 139, B 428 (1965).
- (3) A. Dar, T.L. Watts and V.F. Weisskopf,  
*Nucl. Phys.* B 13 477, (1969).
- (4) P.D.B. Collins and E.J. Squires,  
*Regge poles in Particle Physics*,  
Springer Verlag, Berlin (1968).  
V.D. Barger and D.B. Cline,  
*Phenomenological Theories of High Energy  
Scattering*, W.A. Benjamin, New York (1969).  
G.E. Hite, *Rev. Mod. Phys.* 41, 669 (1969).  
B.E.Y. Svensson, *Proceedings of the 1967 CERN School of  
Physics*, CERN 67-24 (1967).  
J.J.J. Kokkedee, *Regge pole theory*, *Lectures at the Dutch-  
Belgian Summer School for High-Energy Physics*  
(1969).  
J.J.J. Kokkedee, *Lectures given for the Experimental High-  
Energy Physics Groups of Nijmegen and Amsterdam*  
(1970).
- (5) W. Koch, *Proceedings of the 1964 Easter School at Herceg-  
Novi*, CERN 64-13, Vol II (1964).
- (6) K. Gottfried and J.D. Jackson, *Nuovo Cimento* 33, 309 (1964).  
H. Pilkuhn and B.E.Y. Svensson, *Nuovo Cimento* 38, 518 (1965).

- (7) P. Minnaert, Phys. Rev. Letters 16, 672 (1966).  
 P. Minnaert, Phys. Rev. 151, 1306 (1966).
- (8) J.J. Sakurai and R. Stodolsky,  
 Phys. Rev. Letters 11, 90 (1963).
- (9) We here list some references concerning experiments with  
 a beam momentum  $> 3$  GeV/c. For lower momenta we refer to  
 the CERN-HERA tables (see ref. 24).

*Bubble chamber technique:*

- (a) 3.23 GeV/c: R.R. Kofler, R.W. Hartung and D.D. Reeder,  
 Phys. Rev. 163, 1479 (1967).
- (b) 3.7 GeV/c: W.R. Butler, D.G. Coyne, G. Goldhaber,  
 J. MacNaughton and G.H. Trilling,  
 Phys. Rev. D7, 3177 (1973).
- (c) 4.0 GeV/c: J. Bartsch, L. Bondar, R. Speth, G. Hotop,  
 G. Knies, F. Storim, J.M. Brownlee,  
 N.N. Biswas, D. Lüers, N. Schmitz,  
 R. Seeliger and G.R. Wolf  
 Nuovo Cimento 43, 1010 (1966).  
 F. Storim, Diplomarbeit, Hamburg (1966).
- (d) 5.5 GeV/c: W.A. Cooper, W. Manner, B. Musgrave and  
 L. Voyvodic, Phys. Rev. Letters 20, 472  
 (1968).  
 W.A. Cooper, W. Manner, B. Musgrave,  
 D. Pollard and L. Voyvodic,  
 Nucl. Phys. B23, 605 (1970).
- (e) 8.0 GeV/c: M. Aderholz, J. Bartsch, R. Schulte,  
 R. Speth, H.H. Kaufmann, S. Nowak,  
 M. Barbadin-Otwinowska, V.T. Cocconi,  
 J.D. Hansen, J. Loskiewicz, G. Kellner,

A. Mihul, D.R.O. Morrison, H. Tøfte,  
 A. Eskreys, K. Juszcak, D. Kisielewska,  
 P. Malecki, W. Zielinski, H. Piotrowska  
 and A. Wroblewski,

Nucl. Phys. B11, 259 (1969).

*Other techniques*

(f) 3.0, 3.25, 4.0, 5.0 and 7.0 GeV/c:

S.M. Pruss, C.W. Akerlof, D.I. Meyer,  
 S.P. Ying, J. Lales, R.A. Lundy,  
 C.E.W. Ward and D.D. Yovanovitch,

Phys. Rev. Letters 23,  
 189 (1969).

(g) 3.0, 4.0 and 5.0 GeV/c:

K.S. Han, C.W. Akerlof, P. Schmueser,  
 P.N. Kirk, D.R. Rust, C.E.W. Ward,  
 D.D. Yovanovitch and S.M. Pruss,

Phys. Rev. Letters 24,  
 1333 (1970).

(h) 3.0, 5.0 and 7.0 GeV/c:

P. Kalbaci, C.W. Akerlof, P.K. Caldwell,  
 C.T. Coffin, D.I. Meyer, P. Schmueser  
 and K.C. Stanfield,

Phys. Rev. Letters 27,  
 74 (1971).

(i) 5.0 GeV/c : C.W. Akerlof, P.K. Caldwell, P. Kalbaci,  
 D.I. Meyer, K.C. Stanfield, P.N. Kirk,  
 A. Lesnik, D.R. Rust, C.E.W. Ward and  
 D.D. Yovanovitch,

Phys. Rev. Letters 27,  
 219 (1971).

- (j) 3.5, 3.75, 4.0, 4.25, 4.5, 4.75, 5.0, 6.0, 10.0 and 14.0 GeV/c: A. Bashian, G. Finocchiaro, M.L. Good, P.D. Grannis, O. Guisan, J. Kirz, Y.Y. Lee, R. Pittman, G.C. Fisher and D.D. Reeder, Phys. Rev. D4, 2667 (1971).
- (10) D.D. Reeder and K.V.L. Sarma, Phys. Rev. 172, 1566 (1968).
- (11) For a review see:  
H. Harari, Phys. Rev. Letters 26, 1400 (1971).
- (12) C. Meyers, Y. Noirod, M. Rimpault and Ph. Salin, Nucl. Phys. B23, 99 (1970).
- (13) G.A. Ringland, R.G. Roberts, D.P. Roy and J. Tran Thanh Van, Nucl. Phys. B44, 395 (1972).
- (14) R.L. Thews, G.L. Goldstein and J.F. Owens III, Nucl. Phys. B46, 557 (1972).
- (15) J.S. Loos and J.A.J. Matthews, Phys. Rev. D6, 2463 (1972).
- (16) H. Harari and H.J. Lipkin, Phys. Rev. Letters 13, 208 (1964).  
P.G.O. Freund, H. Ruegg, D. Speiser and A. Morales, Nuovo Cimento 25, 307 (1962).
- (17) D.J. Schotanus, Ph. D. thesis, Nijmegen (1971).
- (18) Particle Data Group, UCRL - 20000 K<sup>+</sup>N (1969).
- (19) G.V. Dass, C. Michael and R.J.N. Phillips, Nucl. Phys. B9, 549 (1966).
- (20) G.H. Trilling, Nucl. Phys. B40 (1972) 13.
- (21) S. Meshkov and G.B. Yodh, Phys. Rev. Letters 18 (1967) 474.
- (22) G. Giacomelli, CERN-HERA 69-3 (1969).

- (23) M. Davier and H. Harari,  
Phys. Letters 35B (1971) 239.
- (24) E. Bracci, J.P. Droulez, E. Flaminio, J.D. Hansen and  
D.R.O. Morrison, CERN/HERA 72-1 (1972).
- (25) E. Bracci, J.P. Droulez, E. Flaminio, J.D. Hansen and  
D.R.O. Morrison, CERN/HERA 72-2 (1972).
- (26) F. Chilton, D. Griffiths and R.J. Jabbur,  
Phys. Rev. 153, 1610 (1967).
- (27) S.P. Ying, C.W. Akerlof, D.I. Meyer, S.M. Pruss, J. Lales,  
R.A. Lundy, D.R. Rust, C.E.W. Ward and D.D. Yovanovitch,  
Phys. Letters 30B, 289 (1969).
- (28) F. Eysel, M.P. Locher and H. Wessel,  
Zeitschrift für Physik 199, 411 (1967).
- (29) J. Mott,  
Nucl. Phys. B13, 565 (1969).
- (30) D. Griffiths and R.J. Jabbur,  
Nucl. Phys. B11, 7 (1969)
- (31) G.H. Renninger and K.V.L. Sarma,  
Phys. Rev. D2, 1281 (1970).
- (32) S. Meshkov, G.A. Snow and G.B. Yodh,  
Phys. Rev. Letters 12, 87 (1964).
- (33) D.D. Carmony, R.L. Eisner, A.C. Ammann, A.F. Garfinkel,  
L.J. Gutay, D.H. Miller, L.K. Rangan and W.L. Yen,  
Phys. Rev. D2, 30 (1970).
- (34) B.J. Burdick, W.A. Carnahan, W.J. Fickinger, S.A. Gourevitch,  
T. Kikuchi, J.L. Korpi and D.K. Robinson,  
Nucl. Phys. B41, 45 (1972).
- (35) Kwan-Wu Lai and J. Louie,  
Nucl. Phys. B19, 205 (1970).
- (36) D.J. Schotanus, C.L. Pols, D.Z. Toet, R.T. Van De Walle,  
J.V. Major, G.E. Pearson, B. Chaurand, R. Vanderhaghen,  
G. Rinaudo and A.E. Werbrouck,  
Nucl. Phys. B22, 45 (1970).

- (37) Y. Goldschmidt-Clermont, V.P. Henri, B. Jongejans,  
A. Moiseev, F. Muller, J.-M. Perreau, A. Prokes, V. Yarba,  
W. De Baere, J. Debaisieux, P. Dufour, F. Grard,  
J. Heughebaert, L. Pape, P. Peeters, F. Verbeure and  
R. Windmolders,  
Nuovo Cimento 46A, 539 (1966).
- (38) A. Kotański and K. Zalewski,  
Nucl. Phys. B13, 119 (1969).
- (39) N.B. Durusoy, M. Goldberg, G. de Rosny and G. Kayas,  
Lettere al Nuovo Cimento 6, 381 (1973).
- (40) A. Bialas and K. Zalewski,  
Nucl. Phys. B6, 465 (1968).  
A. Kotański and K. Zalewski,  
Nucl. Phys. B13, 119 (1969).
- (41) C.L. Pols, D.J. Schotanus, D.Z. Toet, R.T. Van de Walle,  
K. Böckmann, K. Sternberger, B. Wagini, G. Winter,  
J.V. Major, E. Cirba, R. Vanderhaghen, G. Rinaudo and  
A. Werbrouck, Nucl. Phys. B25, 109 (1970).
- (42) G. Ciapetti, R.L. Eisner, A.C. Irving, W. Dunwoodie,  
Y. Goldschmidt-Clermont, A. Grant, F. Muller, L. Pape,  
J. Quinquard, Z. Sekera, N. Yamdagni, D.C. Watkins,  
J.B. Kinson, J.N. Carney, M. Yobes, G.T. Jones, K.M. Storr,  
E. de Wolf, P. Peeters, F. Verbeure, F. Grard, V.P. Henri,  
P. Herquet, R. Windmolders, C. Bonnel, J. Ginestet,  
D. Manesse, Tran Ha Ahn, D. Vignaud and M. Sene,  
Nucl. Phys. B64, 58 (1973).

## Appendix A

## KINEMATIC SOLUTIONS FOR SHORT CHARGED PARTICLE DECAYS

Consider the decay  $M \rightarrow m+n$ , where  $M$  and  $m$  are charged (visible) particles,  $M$  leaves a short straight track of which the curvature cannot be determined, and  $n$  is neutral.

We first list the quantities used in the calculation (see fig. A.1).

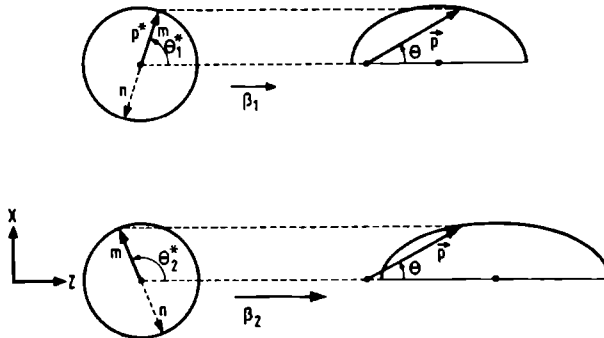


Fig. A.1 Example of two different rest system decay situations which transform to the same apparent lab configuration.

The *known* quantities are:

the masses  $M$ ,  $m$  and  $n$

in the laboratory system:

the direction of the momentum of  $M$ :

$$\hat{P}_M = \hat{z} \text{ (definition of } z\text{-axis)}$$



the momentum vector of m:

$$\vec{P}_m = (P_x, 0, P_z) = (P \sin \theta, 0, P \cos \theta)$$

in the rest system of M:

the magnitude of the momenta of the decay products:

$$P^* = \frac{[M^2 - (m+n)^2]^{\frac{1}{2}} [M^2 - (m-n)^2]^{\frac{1}{2}}}{2M}$$

The *unknown* quantities are:

in the laboratory system:

the magnitude of the momentum of M:

$$P_M$$

in the rest system of M:

the decay angle of m with respect to the z-axis:

$$\theta^*$$

From the Lorentz-transformation we know:

$$P_x = P_x^* = P^* \sin \theta^* \quad (\text{A.1})$$

$$P_z = \gamma(P_z^* + \beta E^*) = \gamma(P^* \cos \theta^* + \beta E^*) \quad (\text{A.2})$$

with

$$\gamma = (1 - \beta^2)^{-\frac{1}{2}} \quad \text{and} \quad \beta = v_M/c$$

where:

$v_M$  is the velocity of M in the laboratory

and  $E^* = (P^{*2} + m^2)^{\frac{1}{2}}$

From Eq. (A.1) we find

$$\sin \theta^* = P_x / P^* \quad \text{or:}$$

$$\cos \theta_{1,2}^* = \pm (P^{*2} - P^2 \sin^2 \theta)^{\frac{1}{2}} / P^* \quad (\text{A.3})$$

which apart from the sign fixes  $\cos \theta^*$ .

For  $\beta$  we derive from A(2):

$$\beta_{1,2} = \frac{-E^* P^* \cos \theta_{1,2}^* + P_z^* (E^{*2} + P_z^2 - P^{*2} \cos^2 \theta_{1,2}^*)^{\frac{1}{2}}}{E^{*2} + P_z^2} \quad (\text{A.4})$$

In the above expression we eliminated the minus sign possibility in front of the square root, using the fact that the (absolute) minimum value of  $P_z^*$  ( $= -P^*$ ) is reached for  $\beta = 0$ .

The two corresponding solutions for  $\vec{P}_M$  are thus:

$$\vec{P}_{M,1} = \vec{\beta}_1 \gamma_1^M \quad \text{and} \quad \vec{P}_{M,2} = \vec{\beta}_2 \gamma_2^M$$

Fig. A.1 shows an example. The left half of the figure gives the two rest system situations from which the observed lab configuration (right half of the figure) may follow. It should be remembered, that the neutral particle  $n$  in these two situations undergoes the Lorentz-transformations given in formula (A.2) with the same  $\beta_{1,2}$ , but in general with a different  $E^* = (P^{*2} + n^2)^{\frac{1}{2}}$ .

## Appendix B

## DETERMINATION OF ANGULAR LOSSES

The determination of and correction for small angle losses in *kink* samples forms the main subject of this appendix. In the kink events ( $\Sigma^+ \rightarrow p\pi^0$ ;  $\Sigma^\pm \rightarrow n\pi^\pm$ ; etc.) this loss is very prominent, because decays with a small angle between the tracks of the (charged) decaying particle and the charged decay product are hard to distinguish from straight tracks.

A different type of loss occurs in  $V^0$  samples ( $\Lambda \rightarrow p\pi^-$ ;  $K^0 \rightarrow \pi^+\pi^-$ ) for events with a small decay *opening* angle (here the 'small laboratory angle' is the angle between the charged decay products themselves, rather than between the decaying primary and the charged decay product). This loss can be corrected by basically the same method as explained further on for kink events (see end of the appendix). The correction factors found are however generally considerably smaller than the ones required for kink events, because the geometrical features of  $V^0$ -decay allow detection even for small opening angles.

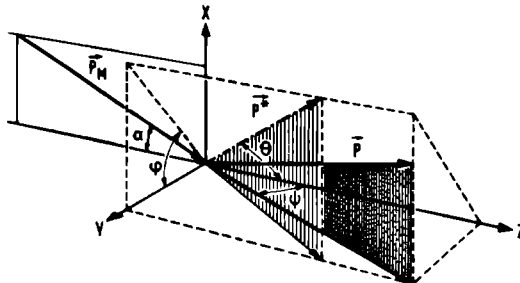


Fig. B.1 Schematic picture of a charged strange particle decay. The kinematic quantities are defined in the text.

Returning to the problem of kink losses we begin with a definition of the reference frame and the quantities used (see fig. B.1):

Decay considered	: $M \rightarrow m+n$
Lab momenta	: $\vec{p}_M, \vec{p}, \vec{p}_n$
energies	: $E_M, E, E_n$
C.M. *) momenta	: $0, \vec{p}^*, -\vec{p}^*$
energies	: $M, E^*, E_n^*$

Lab frame of reference:

x-axis	: parallel to the optical axes of - and directed towards - the cameras
y-axis	: $\hat{y} = \hat{p}_M \times \hat{x} /  \vec{p}_M \times \hat{x} $
z-axis	: $\hat{z} = \hat{x} \times \hat{y}$

Angles:

$\alpha$  = lab dip angle of  $\vec{p}_M$ :

$$\alpha = \arcsin(\hat{x} \cdot \hat{p}_M) \quad (-\frac{\pi}{2} \leq \alpha \leq \frac{\pi}{2})$$

$\theta$  = angle between  $\vec{p}^*$  and the z-axis:

$$\theta = \arccos(\hat{z} \cdot \hat{p}^*) \quad (0 \leq \theta \leq \pi)$$

$\varphi$  = angle between  $(\vec{p}^*-z)$ -plane and  $(y-z)$ -plane:

$$\varphi = \arcsin[\hat{x} \cdot (\vec{p}^* \times \hat{z}) / |\vec{p}^* \times \hat{z}|] \\ (-\frac{\pi}{2} \leq \varphi \leq \frac{\pi}{2})$$

$\psi$  = projected lab decay angle:

$$\psi = \arccos[\hat{y} \cdot (\vec{p} \times \hat{x}) / |\vec{p} \times \hat{x}|] \\ (0 \leq \psi \leq \pi)$$

\*) Note. C.M. here denotes the rest system of M.

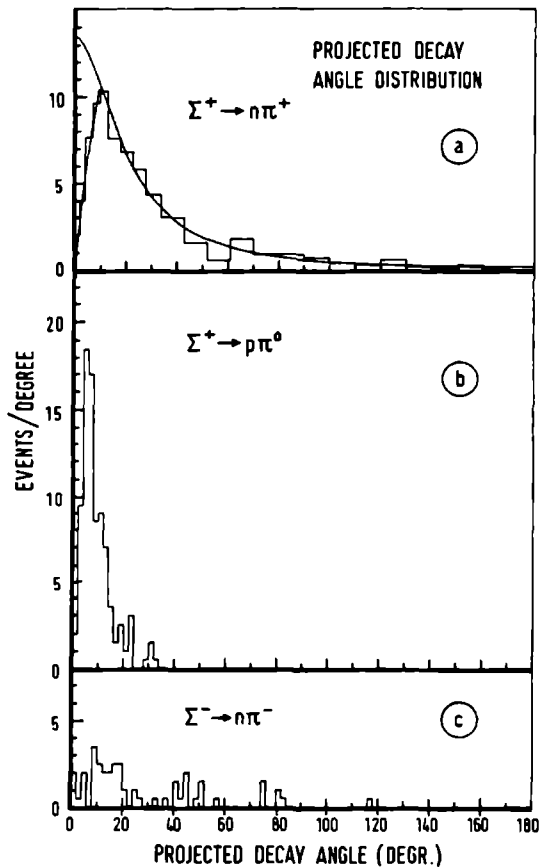


Fig. B.2 Distribution of the projected decay angle in the kink samples  $\Sigma^+ \rightarrow n\pi^+$  (a),  $\Sigma^+ \rightarrow p\pi^0$  (b),  $\Sigma^- \rightarrow n\pi^-$  (c). The curves in (a) represent the theoretical (loss-free) and the fitted (predicted) distribution.

Transformation quantities:  $\vec{\beta} = \vec{p}_M / E_M$

$$\gamma = (1 - \beta^2)^{-\frac{1}{2}}$$

Because of reflection symmetry with respect to the (x-z) plane we only consider half the allowed intervals for  $\varphi$  and  $\psi$ .

The angular loss correction method discussed starts from the observed  $\psi$ -distributions (see fig. B.2). The magnitude of  $\psi$  is directly related to the detection probability. The use of other variables, such as e.g. the C.M. decay angle, has the disadvantage that the loss effect is more or less blurred by the transformation.

From fig. B.1 we derive:

$$\tan \psi = \frac{p_y}{p_z} = \frac{p_y^*}{p_z^* + \beta_z \gamma \left( \frac{\gamma}{\gamma+1} \vec{\beta} \cdot \vec{p}^* + E^* \right)}$$

or:

(B.1)

$$\text{tg } \psi = \frac{p^* \sin \theta \cos \varphi}{p^* \cos \theta + \beta_z \gamma \left[ \frac{\gamma}{\gamma+1} (\beta_x p^* \sin \theta \sin \varphi + \beta_z p^* \cos \theta) + E^* \right]}$$

In the C.M. system of M we expect no anisotropy in the decay distribution of M because in our experiment neither the beam nor the target were polarized. The probability for a decay with  $p^*$  lying within a solid angle  $d\Omega = d\varphi d \cos \theta$  is thus equal to  $(4\pi)^{-1} d\varphi d \cos \theta$ .

From (Eq. B.1) we derive for constant  $\psi = \psi'$ :

$$\sin \theta_{1,2}(\psi', \varphi) = \frac{-Cq(\psi', \varphi) \pm A\sqrt{[q(\psi', \varphi)]^2 + A^2 - C^2}}{[q(\psi', \varphi)]^2 + A^2} \quad (\text{B.2})$$

$$\cos \theta_{1,2}(\psi', \varphi) = \frac{-AC \pm q(\psi', \varphi) \sqrt{[q(\psi', \varphi)]^2 + A^2 - C^2}}{[q(\psi', \varphi)]^2 + A^2} \quad (\text{B.3})$$

$$\text{where } q(\psi', \varphi) = B \sin \varphi - \cotg \psi' \cos \varphi \quad (\text{B.4})$$

$$A = 1 + \frac{\beta_z^2 \gamma^2}{\gamma + 1} \quad (\geq 1)$$

$$B = \frac{\beta_x \beta_z \gamma^2}{\gamma + 1}$$

$$C = \beta_z \gamma \frac{E^*}{p^*} \quad (\geq 0)$$

If we know the curves  $\cos \theta_{1,2}(\psi', \varphi)$  as a function of  $\varphi^*$ , the probability for a decay with  $\psi \geq \psi'$  can be expressed as

$$P(\psi \geq \psi') = \frac{1}{4\pi} \int_L |\cos \theta_1 - \cos \theta_2| d\varphi, \quad (\text{B.5})$$

where L stands for the allowed integration region.

The integration limits  $\varphi_L(\psi')$  of  $\varphi$  can be found from the arguments of the square roots in Eqs. (B.2) and (B.3) because for  $\varphi = \varphi_L(\psi')$  we should have  $\cos \theta_1 = \cos \theta_2$  etc. Using the condition  $q^2 = C^2 - A^2$  in Eq. (B.2) we find  $\sin \theta(\psi', \varphi_L) = -q/C$ . In the  $\theta$ -interval considered we must have  $\sin \theta \geq 0$ , which requires  $q < 0$ . Thus for  $\varphi = \varphi_L(\psi')$ :

$$q(\psi', \varphi_L) = -|\sqrt{C^2 - A^2}| \quad (\text{B.6})$$

$$\cos \theta(\psi', \varphi_L) = -A/C \quad (\text{B.7})$$

\*) *Note.* Examples of these curves can be found in fig. B.5. They are discussed at the end of this chapter.

From Eqs. (B.4) and (B.6) we now find:

$$\varphi_{L_{1,2}}(\psi') = \arcsin \left[ \frac{-B|\sqrt{C^2-A^2}| \pm \cotg \psi' \sqrt{\cotg^2 \psi' + A^2 + B^2 - C^2}}{\cotg^2 \psi' + B^2} \right] \quad (\text{B.8})$$

We distinguish the following cases:

- (i)  $A > C$ . There are no integration limits, because one of the square roots in Eq. (B.8) is imaginary.  $\cos \theta$  (Eq. B.3) exists for any  $x$ ; i.e. for any  $\psi$  and  $\varphi$ .

Thus:

$$-\frac{\pi}{2} < \varphi \leq \frac{\pi}{2}; \quad ; 0 \leq \psi' \leq \pi$$

- (ii)  $C \geq A$  and  $C^2 - A^2 < B^2$ . Integration limits exist for all  $\psi'$ .

Thus:

$$\varphi_{L_1} \leq \varphi \leq \varphi_{L_2} \quad (\text{Eq. B.8}); \quad 0 \leq \psi' \leq \pi$$

- (iii)  $C \geq A$  and  $C^2 - A^2 \geq B^2$ . Integration limits exist only for those  $\psi'$  for which:

$$\cotg^2 \psi' \geq C^2 - A^2 - B^2 \quad (\text{B.9})$$

For other  $\psi'$  values now  $\cos \theta$  is imaginary. Calling  $\psi_L$  the limiting value of  $\psi'$ , we find using Eq.(B.8):

$$\sin \varphi_L(\psi_L) = -B / |\sqrt{C^2 - A^2}|$$

In the same way we find from Eqs. (B.4) and (B.6)

$$\cos \varphi_L(\psi_L) = \cotg \psi_L / |\sqrt{C^2 - A^2}|$$

Because we have chosen a  $\varphi$  interval where  $\cos \varphi \geq 0$ ,



we have the condition  $\cotg \psi_L > 0$ . We can now rewrite Eq. (B.9) as:

$$\cotg \psi' \geq |\sqrt{C^2 - A^2 - B^2}| \quad (\text{B.9a})$$

Resuming we thus have for situation (iii):

$$\begin{aligned} \varphi_{L,1} &\leq \varphi \leq \varphi_{L,2} \quad (\text{Eq. B.8}); \\ 0 &\leq \psi' \leq \arctan |(C^2 - A^2 - B^2)^{-\frac{1}{2}}| \end{aligned}$$

With these formulae at hand we can perform the numerical integrations implied by Eq. (B.5). For *each event* we derive a theoretical distribution over the projected decay angle in the laboratory system:

$$n'(\psi') \Delta \psi' = P(\psi \geq \psi') - P(\psi \geq \psi' + \Delta \psi') \quad (\text{B.10})$$

with:

$$\sum_{\Delta \psi'} n'(\psi') \Delta \psi' = 1$$

We then introduce a trial function  $f(\psi)$  for the *angular detection efficiency* to simulate the observed loss at small angles:

$$n''(\psi) = f(\psi) n'(\psi) \quad (\text{B.11})$$

Because:

$$\sum_{\Delta \psi} n''(\psi) \Delta \psi = S'' < 1$$

we have to weight the distribution of each event by its inverse. The *theoretical (loss-free) distribution* reconstructed from each observed event is thus:

$$n_{\text{TH}}(\psi) \Delta \psi = \frac{n'(\psi)}{S''} \Delta \psi \quad (\text{B.12})$$

where:

$$\sum_{\Delta \psi} n_{\text{TH}}(\psi) \Delta \psi > 1$$

The *predicted* probability distribution for the *detection* of this event is then given by:

$$n_{PR}(\psi)\Delta\psi = f(\psi)n_{TH}(\psi)\Delta\psi = f(\psi)n'(\psi)\Delta\psi/S'' \quad (\text{B.13})$$

The experimentally observed projected decay angle does not play any role in these predictions; the only input information used is the vector  $\vec{p}_M$ .

The efficiency functions  $f(\psi)$  chosen have the following general form:

$\psi$ interval:	$f(\psi)$ :
$0 - \psi_1$	$K$ (constant)
$\psi_1 - \psi_2$	$F(\psi)$
$\psi_2 - \pi$	$1$

We varied  $\psi_1$ ,  $\psi_2$ ,  $K$  and chose different forms of  $F(\psi)$ ;

such as: a linear form :  $F(\psi) = \frac{\psi - \psi_1}{\psi_2 - \psi_1}$   
 a parabolic form:  $F(\psi) = \sqrt{(\psi - \psi_1)(\psi_2 - \psi_1)}$   
 an elliptic form:  $F(\psi) = \sqrt{2(\psi - \psi_1)(\psi_2 - \psi_1 - 1)}/(\psi_2 - \psi_1)$   
 etc.

We used these forms with  $K = 0$  and  $\psi_1 = 0$ , determining the cutoff angle  $\psi_2$  by fitting with a maximum likelihood method the *total* predicted distribution to the observed experimental distribution. This procedure was applied to the  $\Sigma^+ \rightarrow n\pi^+$  and  $\Sigma^- \rightarrow n\pi^-$  distributions. The three  $F(\psi)$  forms give comparable results for the angular loss.

Before we get to the fit results we want to draw attention to an interesting simplification. In our situation a good ap-

proximation can be found by neglecting the x-component of the momentum of the decaying particle ( $p_{M_x}$ ). Formally this involves putting in the foregoing expressions:

$$\beta_x = 0; \beta = \beta_z; \gamma = (1 - \beta_z^2)^{-\frac{1}{2}} \text{ or: } A = \gamma_z, B = 0, C = \beta_z \gamma_z E^* / p^*$$

The integrals  $\int \cos \theta \, d\varphi$  (Eq. B.5) can then be evaluated analytically. The following closed expressions are obtained:

(a)  $A > C$ :

$$\psi' \leq \frac{\pi}{2} : P(\psi \geq \psi') = Q \left[ -\frac{3}{2} + \frac{1}{\pi} \arcsin R \right] + \frac{1}{\pi} \arcsin S + \frac{1}{2} \quad (\text{B.14})$$

$$\psi' \geq \frac{\pi}{2} : P(\psi \geq \psi') = Q \left[ -\frac{1}{2} - \frac{1}{\pi} \arcsin R \right] - \frac{1}{\pi} \arcsin S + \frac{1}{2} \quad (\text{B.15})$$

(b)  $A \leq C$ :

$$P(\psi \geq \psi') = |1 - 2Q|; \psi_{\max} = \arcsin \frac{1}{\sqrt{C^2 - A^2}} \quad (\text{B.16})$$

where:

$$Q = \left| \frac{C}{2\sqrt{A^2 + \cot^2 \psi'}} \right|$$

$$R = \frac{(A^2 - 2C^2) + A^2 \operatorname{tg}^2 \psi' (A^2 - C^2)}{A^2 [1 + \operatorname{tg}^2 \psi' (A^2 - C^2)]}$$

$$S = [(A^2 - C^2) \operatorname{tg}^2 \psi' + 1]^{-\frac{1}{2}}$$

This approximation succeeds well because kinematics and dynamics limit the value of  $\beta_x$  to small values. For instance, in the reaction  $\pi^+p \rightarrow \Sigma^+K^+$ , the maximum lab angle  $\alpha$  (fig. B.1) allowed by kinematics is 0.8 radians. Dynamics pushes this limit down because the  $\Sigma$ 's are preferentially produced forward in the overall C.M. system. The  $(\beta, \cos \alpha)$  distribution for all  $\Sigma^+$  ( $\rightarrow n\pi^-$ ) is given in fig. B.3.

Both methods (neglecting and keeping  $\beta_x$ ) have been tried and give differences for the whole sample in the order of 1%, which is well within the errors.

The  $\Sigma$  decay distributions are given in fig. (B.2). The fit results are given in table B.1. The curve in fig. B.2a represents the fit to the  $\Sigma^+ \rightarrow n\pi^+$  sample. The  $\Sigma^+ \rightarrow p\pi^0$  mode was not fitted for reasons discussed in sect. II.5.5.

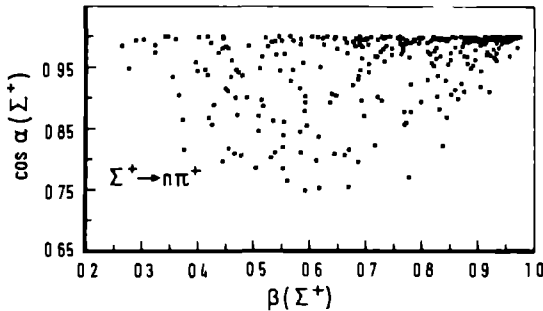


Fig. B.3 Scatter plot ( $\cos \alpha$  versus  $\beta$ ) for  $\Sigma^+$  particles with  $n\pi^+$  decays.

A few examples of the shape of  $\cos \theta$  ( $\psi$ ) curves for constant  $\psi$  are given in fig. B.4. The curves are for  $\Sigma^+ \rightarrow n\pi^+$  decay in the case that  $\alpha = 34.5^\circ$  and  $\beta = 0.875$  (an extreme case).

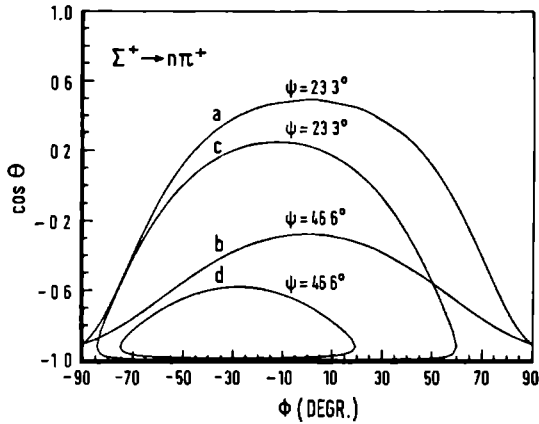


Fig. B.4 Examples of  $\cos \theta$  ( $\psi$ ) curves for  $\Sigma^+ \rightarrow n\pi^+$  decay.  
For explanations see text.

TABLE B.1

Angular loss fit results for kinks			
Decay	$\psi_2$ *	loss(%)	$\chi^2$ /ND
$\Sigma^+ \rightarrow n\pi^+$	$10^\circ$	$20 \pm 3$	163/179
$\Sigma^+ \rightarrow n\pi^-$	$8^\circ$	$16 \pm 5$	278/179
*) $F(\psi)$ linear			

The figure demonstrates several features. The curves a and b are symmetric around  $\phi = 0^\circ$  because  $\beta_x$  was neglected. They also demonstrate the 'open' form obtained when  $A > C$  (case (a) - see above). The curves c and d show asymmetry around  $\phi = 0^\circ$ . These curves are 'closed' because they represent a case mentioned under (iii).

The opening angle distributions of the  $\Lambda$  and  $K^0$  decays are given in fig. B.5a and fig. B.5b respectively. The theoretical distributions have been obtained by transforming 'each'

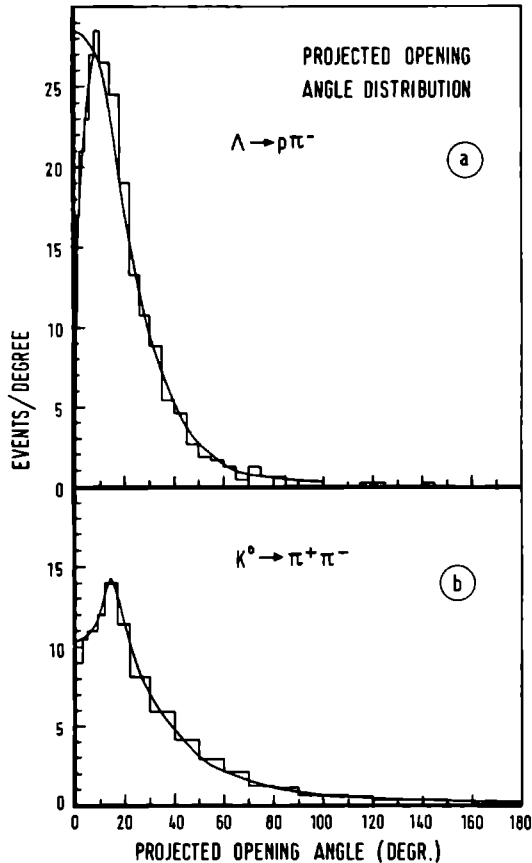


Fig. B.5 Distribution of the projected opening angle in the  $V^0$  samples  $\Lambda \rightarrow \rho\pi^-$  (a) and  $K^0 \rightarrow \pi^+\pi^-$  (b). The curves in (a) represent the loss-free distribution and the fitted (predicted) distribution. The curve in (b) represents the loss free distribution.

possible C.M. configuration ( $\Delta\theta = \Delta\phi = 2^\circ$ ) separately to the laboratory frame for all  $\Lambda$ 's and  $K^0$ 's and by applying an analogous weighting procedure as described for the kinks. The fit results are given in table B.2 and presented by the curves in fig. B.5.

TABLE B.2

Angular loss fit results for $V^0$ 's			
Decay	$\psi_2$ *)	Loss(%)	$\chi^2/ND$
$K^0 \rightarrow \pi^+ \pi^-$	$1^\circ$	$1 \pm 1$	185/179
$\Lambda \rightarrow p \pi^-$	$2^\circ$	$3 \pm 2$	114/179
*) $F(\psi)$ linear			

*References - Appendix B*

(1) See for example:

W.W.M. Allison, D. Phil. Thesis, Oxford, 1967.

R.J. Hemmingway and H. Whiteside

, Maryland University Technical Report  
70-065 (1969).

G.C. Mason , Oxford Bubble Chamber Group Physics  
Notes 19 (1971).

## Appendix C

## LIST OF PARTICLE PROPERTIES

This appendix gives an abbreviated list of properties of the particles mentioned in this thesis. The values are taken from the Review of Particle Properties from the Particle Data Group (ref. 10 Chapter III). We use the following abbreviations:

I=isospin, G=G-parity, J=spin, P=parity, S=strangeness, M=mass,  $\Gamma$ =width. Some decay modes are presented in Table II.22 of Chapter II.

Particle	I	G	J	P	M(MeV)	$\Gamma$ (MeV)
<i>Mesons (B=0)</i>						
a. S=0						
$\pi^{\pm}$	1	-	0	-	140	0
$\pi^0$					135	$\sim 0$
$\eta$	0	+	0	-	549	$\sim 0$
$\rho$ (765)	1	+	1	-	770	146
$\omega$ (784)	0	-	1	-	784	10
$S^*$	0	+	0	+	997	50-150
$\phi$ (1019)	0	-	1	-	1020	4
$f$ (1260)	0	+	2	+	1270	163
$A_2$ (1310)	1	-	2	+	1310	100
b. $ S =1$						
$K^{\pm}$	$\frac{1}{2}$		0	-	494	0
$K^0$					498	0
$K^*$ (890)	$\frac{1}{2}$		1	-	892	50
$K^*$ (1420)	$\frac{1}{2}$		2	+	1421	100



Particle	I	G	J	P	M(GeV)	$\Gamma$ (MeV)
<i>Baryons</i> (B=1)						
a. S=0						
p	$\frac{1}{2}$		$\frac{1}{2}$	+	938	0
n					940	0
$\Delta$ (1236)	$\frac{3}{2}$		$\frac{3}{2}$	+	1233	110-122
b.  S =1						
$\Lambda$	0		$\frac{1}{2}$	+	1116	0
$\Lambda$ (1520)	0		$\frac{3}{2}$	-	1518	16
$\Sigma^+$	1		$\frac{1}{2}$	+	1189	0
$\Sigma^-$					1197	0
$\Sigma^0$					1192	0
$\Sigma$ (1385)	1		$\frac{3}{2}$	+	1383	34
$\Sigma$ (1670)	1		$\frac{3}{2}$	-	1670	35-65



## SUMMARY

The subject of this thesis is an experimental study by means of the bubble chamber technique of reactions between  $\pi^+$  mesons with a laboratory momentum of 5 GeV/c and protons. The reactions analyzed in this thesis are all characterized by the fact that so-called "strange particles", i.e. particles with a strangeness quantum number different from zero, occur among their end-products.

The exposure of the bubble chamber film was performed at the 28 GeV/c Proton Synchrotron of the European Organization for Nuclear Research (CERN). The bubble chamber used was the British 1.5 metre chamber, the so-called British National Hydrogen Bubble Chamber. Some 125.000 pictures were analyzed by a collaboration of five European laboratories (at Bonn, Durham, Nijmegen, Paris and Turin). The handling of the strange particle events was mainly done at Bonn ( $V^0$ -events) and Nijmegen ( $V^0$  and kink events).

The first chapter gives various experimental details. It contains a description of:

- the experimental conditions during the exposure,
- the scanning,
- the geometrical and kinematical reconstruction techniques, and finally
- the methods used for the resolution of kinematical ambiguities.

The second chapter is devoted to the methods used in the determination of the cross sections of the strange particle channels and the results obtained.

In these methods, the corrections for the various types of losses characteristic of strange particle physics, play a central rôle.

Chapter III deals with resonance production in the statistically more significant three and four body channels. An introduction to the methods used for quantitative determination of resonance production is followed by a channel-by-channel discussion of the results. In the treatment of the  $p\pi^+(K\bar{K})^0$  channels a method is discussed to eliminate interference effects between the  $A_2^0$  and  $f$  resonances.

The main subject of the fourth and last chapter is an examination of the four reactions  $\pi^+p \rightarrow K^+\Sigma^+$ ,  $\pi^+p \rightarrow K^{*+}(890)\Sigma^+$ ,  $\pi^+p \rightarrow K^+\Sigma^+(1385)$  and  $\pi^+p \rightarrow K^{*+}(890)\Sigma^+(1385)$ . The total and differential cross sections and the spin-density matrix elements are determined and compared with predictions of some exchange models (absorption- and Regge models) as well as with results from other experiments. In general the agreement is reasonable to good. In  $K^{*+}(890)\Sigma^+$ , the dip in the forward differential cross section, predicted by the model of Chilton et al., is confirmed by our observations, in contrast with the experimental results obtained at 5.4 GeV/c. SU(3) predictions, relating the cross sections of our reactions to those of other  $\pi^+p$  and KN reactions are in general reasonably well satisfied.

## Р Е З Ю М Е

Эта диссертация касается экспериментального изучения реакций  $\pi^+$  мезонов при 5 GeV/c в жидководородной пузырьковой камере. Эта диссертация касается реакций, в которых рождаются так называемые "странные частицы", т.е. частицы, имеющие квантовое число странностей, различающееся от нуля.

Фильм снят при 28 GeV/c протон-синхротроне европейской организации для ядерного исследования/CERN/. Использовалась английская пузырьковая камера 1.5 метра, так называемая английская национальная водородная пузырьковая камера. Коллаборация пяти европейских лабораторий/в Бонне, в Дургаме, в Неймегене, в Париже и в Турино/ изучала 125.000 снимков. События странных частиц исследовались главным образом в Бонне/ $V^0$  события/ и в Неймегене/ $V^0$  и  $V^\pm$  события/.

Экспериментальные особенности описываются в первой главе, включая описание экспериментальных условий во время съёмки фильма, сканирования, геометрической и кинематической реконструкции и методов отделения различных кинематических гипотез.

Вторая глава касается методов определения

сечения каналов со странными частицами и его результатов. При этом поправки для различных потерь событий играют важную роль.

Третья глава касается рождения резонансов в каналах трёх и четырёх частиц со сравнительно большим числом событий. Дается введение к методам количественного описания рождения резонансов и обсуждения результатов для каждого канала. Обсуждается метод исключения эффектов помех между  $A_2^0$  и  $f$  резонансами.

Четвертая, последняя глава касается изучения четырёх реакций  $\pi^+p \rightarrow K^+\Sigma^+$ ,  $\pi^+p \rightarrow K^{*+}(890)\Sigma^+$ ,  $\pi^+p \rightarrow K^+\Sigma^+(1385)$  и  $\pi^+p \rightarrow K^{*+}(890)\Sigma^+(1385)$ . Всеобщее и дифференциальное сечение и спин-матрикс-элементы определены и сравниваются с предсказаниями некоторых обобщенных моделей/абсорбированных и моделей "Редже", а также с результатами других экспериментов. Согласие, можно сказать, вообще: от "довольно" до "хорошо". При  $K^{*+}(890)\Sigma^+$  спускание дифференциального сечения вперед, предсказанного моделью Чилтона и др., наблюдается в данной работе в противоречии с результатами при 5.4 GeV/c. Сравнения сечений реакций в данной работе с другими  $\pi^+p$  и  $kn$  реакциями обычно хорошо совпадают с  $SU(3)$  предсказаниями.

## SAMENVATTING

Het onderwerp van dit proefschrift is een experimentele studie, m.b.v. de bellenvat techniek, van reacties tussen  $\pi^+$  mesonen met een laboratorium impuls van 5 GeV/c en protonen. De reacties, die in dit proefschrift onderzocht worden, zijn alle gekenmerkt door het feit, dat tot hun eindproducten zgn. "vreemde deeltjes" behoren, d.w.z. deeltjes met een vreemdheids-quantum getal verschillend van nul.

De belichting van de bellenvat opnamen vond plaats te Genève bij het 28 GeV/c Proton Synchrotron van de Organisation Européenne pour Recherches Nucléaires (C.E.R.N.). Het gebruikte bellenvat was het Britse 1.5 meter vat, de zgn. British National Hydrogen Bubble Chamber. De ongeveer 125.000 opnamen werden geanalyseerd door een samenwerkingsverband van vijf Europese laboratoria (te Bonn, Durham, Nijmegen, Parijs en Turijs). De bewerking van de vreemde deeltjes-reacties vond voornamelijk plaats te Bonn ( $V^0$  verschijnselen) en Nijmegen ( $V^0$  en kink verschijnselen).

Het eerste hoofdstuk geeft allerlei experimentele bijzonderheden. Het bevat een beschrijving van:

- de experimentele omstandigheden waaronder de bellenvat-opnamen zijn gemaakt,
- de scanning,
- de geometrische en kinematische reconstructie technieken, en tenslotte
- de methoden, die zijn gebruikt om kinematische ambiguiteiten op te lossen.

Het tweede hoofdstuk is gewijd aan de bespreking van de methoden, gebruikt bij de bepaling van de werkzame doorsneden

van de vreemde deeltjes-kanalen en de resultaten daarvan. Bij deze methoden nemen de correcties voor de verschillende soorten verliezen, die speciaal bij vreemde deeltjes een belangrijke rol spelen, de voornaamste plaats in.

Hoofdstuk III behandelt de productie van resonanties in de statistische meestbeduidende drie en vier deeltjes-kanalen. Na een inleiding betreffende de methoden, gebruikt bij de quantitative bepaling van resonantie productie, volgt een bespreking van de resultaten per kanaal. Bij de behandelingen van de  $p\pi^+ (K\bar{K})^0$ -kanalen wordt een methode beschreven om inter-ferentie-effecten tussen  $A_2^0$  en  $f$  resonanties te elimineren.

De kern van het vierde en laatste hoofdstuk wordt gevormd door een nadere studie van vier reacties, te weten:  $\pi^+p \rightarrow K^+\Sigma^+$ ,  $\pi^+p \rightarrow K^{*+}(890)\Sigma^+$ ,  $\pi^+p \rightarrow K^+\Sigma^+(1385)$  en  $\pi^+p \rightarrow K^{*+}(890)\Sigma^+(1385)$ . De totale en differentiële werkzame doorsneden en de spin-dichtheids matrix elementen worden bepaald en vergeleken zowel met de voorspellingen van enige uitwisselingsmodellen (absorptie- en Reggmodellen) als met de resultaten van andere experimenten. De overeenstemming is over het algemeen redelijk tot goed te noemen. In  $K^{*+}(890)\Sigma^+$  wordt het door het model van Chilton et al. voorspelde minimum in de differentiële werkzame doorsnede voor de voorwaartse richting bevestigd door onze waarnemingen, in tegenstelling tot de meetresultaten verkregen bij 5.4 GeV/c. Aan de SU(3) voorspellingen, die een verband leggen tussen de werkzame doorsneden van de bovenstaande reacties en die van andere  $\pi p$  en  $KN$  reacties, wordt in het algemeen redelijk goed voldaan.



## CURRICULUM VITAE

Na twee jaar M.U.L.O. genoot ik gedurende de periode 1946-1951 onderwijs aan het Christelijk Lyceum "Zandvliet" te 's-Gravenhage, waar ik het diploma Gymnasium- $\beta$  behaalde. Na het vervullen van de militaire dienstplicht en na een korte periode als employé op de wiskundige afdeling van een verzekeringsmaatschappij werkzaam te zijn geweest, begon ik in 1953 mijn studie in de natuurkunde aan de Rijksuniversiteit te Leiden. In december 1958 werd het kandidaatsexamen afgelegd, waarna in december 1962 het doctoraalexamen met als hoofdvak experimentele natuurkunde en als bijvakken wiskunde en sterrenkunde volgde. Gedurende de periode 1959-1964 was ik als F.O.M.-medewerker werkzaam op het Kamerlingh Onnes Laboratorium te Leiden. Onder supervisie van Prof.dr. K.W. Taconis en onder dagelijkse leiding van Dr. J. Reuss was ik van 1959-1962 medewerker bij het ontwerpen en bedrijfsklaar maken van een waterstofbellenvat. Nadat deze groep zijn werkzaamheden had beëindigd werkte ik onder supervisie van Prof.dr. C.J. Gorter aan enige paramagnetische relaxatie-experimenten.

In september 1964 opende zich de mogelijkheid de lijn van de hoge energiefysika, begonnen bij het bellenvat, wederom op te vatten door medewerker te worden van Prof.Dr. R.T. Van de Walle. Gedurende de daarop volgende jaren nam ik naast mijn onderwijstaak deel aan de opbouw van de groep en aan de analyse van verscheidene experimenten waaronder voornamelijk het 720 MeV  $\pi^+p$  experiment en het 5 GeV/c  $\pi^+p$  experiment (dit laatste in samenwerking met enkele andere Europese instituten). Het onderwerp van mijn proefschrift heeft betrekking op het laatstgenoemde experiment.

Nijmegen, januari 1974

D.Z. Toet











# STELLINGEN

## I

De door Bockmann et al gebruikte grafische methode om aan te tonen, dat de spin-dichtheids matrixelementen voldoen aan de positiviteitseisen, is onjuist

K Bockmann et al Proceedings of the Topical Conference on High Energy Collisions of Hadrons, CLRN, January 1968 Vol II, p 150

## II

De aanname van Allison, dat bij een gegeven vervalswijze de waarschijnlijkheidsverdeling van de geprojecteerde vervalshoek kinematisch slechts bepaald wordt door de geprojecteerde impuls van het vervallende deeltje, is onjuist.

W W M Allison D Phil Thesis, Oxford 1967 Appendix A  
Dit proefschrift, Appendix B

## III

De door Kofler et al gebezigde berekeningswijze van de  $\Sigma$ -polarisatie is ongeschikt om de invloed van het selectieve verlies, dat optreedt bij kleine vervalshoeken, te elimineren

R R Kofler et al Phys Rev 163, 1479 (1967)  
Dit proefschrift, Sectie IV 5 1

## IV

Het feit, dat Cooper et al. in een bellenvat-experiment bij 5.4 GeV/c een ongecorrigeerde vertakkingsverhouding voor  $\Sigma^+$  verval vond, die overeenkomt met de theoretisch verwachte verhouding, is vanuit experimenteel oogpunt onbegrijpelijk

W A Cooper et al , Phys Rev Letters 20, 472 (1968)

## V

De wijze, waarop sommige auteurs resultaten betreffende werkzame doorsneden presenteren, laat meerduidige interpretatie toe

S Dagan et al , Phys Rev 161, 1384 (1967)

## VI

In tegenspraak met de o a door Luna geuite veronderstelling bestaat er geen 'law of physics' volgens welke alle objecten streven naar hun laagste energietoestand

S E Luna, 'Life, the Unfinished Experiment', Charles Scribner's Sons, New York 1973, p 88

## VII

De methode, volgens welke Miller de glory undulation by botsing van diatomische moleculen op atomen berekent, impliceert een onfysische veronderstelling en leidt daardoor reeds bij een eerste orde benadering van de asymmetrie-parameters tot onjuiste resultaten.

W H. Miller, J. Chem Phys 50, 3124 (1969).

## VIII

Bij de bepaling van het alpha-gemiddelde uit electro- encephalogrammen is het bipolare afleiding te prefereren boven een referentie afleiding

Handbook of Electroencephalography and Clinical Neurophysiology, vol 5, part B, Editors A. Remond, H. Petsche, Elsevier 1972, p. 48 e.v.

## IX

Het sociaal gevoel en het aanpassingsvermogen van jonge kinderen worden in het algemeen gunstig beïnvloed door deelname aan groepen met een gevarieerde samenstelling naar leeftijd en capaciteiten

## X

De Nijmeegse promotieregeling, die o m. kan vergen, dat tussen de bestuursorganen en personen, betrokken bij één enkele promotie, tot circa 30 brieven worden uitgewisseld, geeft aanleiding tot een niet geringe mate van milieuverontreiniging, tijdverlies en grondstoffenverspiling

Promotieregeling vastgesteld door het College en Decanen bij besluit van 9 april 1973.



